6 Effective Hamiltonians for FCNC Processes

6.1 Overture: General View of FCNC Processes

6.1.1 General Remarks

The pattern of flavor violation in the SM is governed by the $V-A$ structure of $W^{\pm}$ interactions with quarks and leptons and equally importantly by the natural suppression of flavor-changing neutral current processes with the help of the GIM mechanism that we introduced briefly in Chapter 2. The flavor diagonal structure of the basic vertices involving γ, Z, and G in the SM forbids the appearance of FCNC processes at the tree level. With the help of the flavor-changing $W^{\pm}$-vertex one can, however, construct one-loop and higher-order diagrams that mediate FCNC processes. Our next goal is then to describe first the general structure of these processes within the SM and subsequently to cast the gained knowledge into effective Hamiltonians given in the form of various OPEs. This will allow us to include QCD effects by means of the technology developed in the last chapters in a straightforward manner. We will soon see that the structure of these processes is much richer than the one of tree-level decays considered so far, which involved only the current-current operators Q_1 and Q_2.

The fact that FCNCs take place in the SM only as loop effects makes them particularly useful for testing the quantum structure of the theory and the search for NP beyond the SM. There they can enter in principle already at treelevel being suppressed by propagators of very heavy new particles. But in the SM at the one-loop level they can be described by a set of basic triple and quartic effective vertices. In the literature they appear under the names of penguin and box diagrams, respectively. These vertices depend on electroweak parameters like G_F, α and $\sin\vartheta_W$, the CKM parameters, and very importantly on the masses of quarks that appear virtually in these diagrams together with $W^{\pm}$. Therefore, once these parameters are determined in other processes, the rate for FCNC decays in the SM can be predicted.

The description of this class of processes in terms of effective vertices is useful as it allows to exhibit very strong correlations between various decays within the SM, which provide a number of excellent tests of this model. Let us then discuss the structure of FCNCs in the SM in explicit terms. In the next section we will calculate some of these vertices in detail and then move to include QCD corrections to FCNCs. These considerations will be generalized to extensions of the SM in the last part of this book.

Downloaded from https://www.cambridge.org/core. UNIVERSIDAD AUTONOMA METROPOLITANA, on 18 Nov 2026 at 18:06:35, subject to the Cambridge Core terms of use, available at https://www.cambridge.org/core/terms. https://doi.org/10.1017/9781139524100.011

6.1.2 Effective Vertices

Penguin Vertices

These vertices involve only quarks and can be depicted as in Figure 6.1, where i and j have the same charge but different flavor, and k denotes the internal quark whose charge is different from that of i and j. These effective vertices can be calculated by using the Feynman rules for elementary vertices and propagators in the SM. Important examples are given in Figure 6.2. The diagrams with Goldstone boson exchanges in place of $W^{\pm}$ have not been shown. They have to be included to obtain a gauge independent result, where gauge refers to the $W^{\pm}$ propagator. Only in the unitary gauge the diagrams with Goldstone bosons are absent but then the loop calculations are more difficult because the $W^{\pm}$ propagator in this gauge is more complicated than in the Feynman gauge used for most calculations in this book. Strictly speaking, also self-energy corrections on external lines have to be included to make the effective vertices finite. These technicalities are discussed explicitly in Section 6.2.

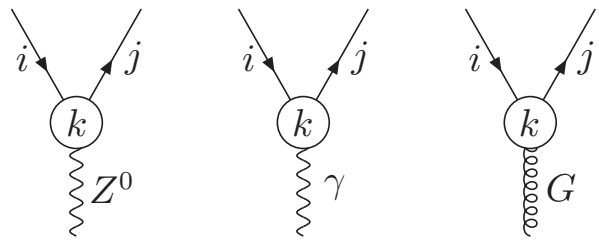


Figure 6.1 Penguin vertices. From [29].

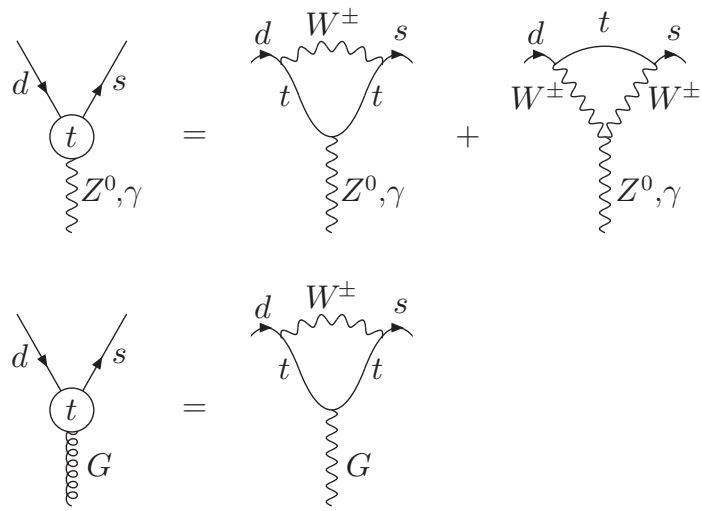


Figure 6.2 Penguin vertices resolved in terms of basic vertices. From [29].

Downloaded from https://www.cambridge.org/core. UNIVERSIDAD AUTONOMA METROPOLITANA, on 18 Nov 2026 at 18:06:35, subject to the Cambridge Core terms of use, available at https://www.cambridge.org/core/terms. https://doi.org/10.1017/9781139524100.011

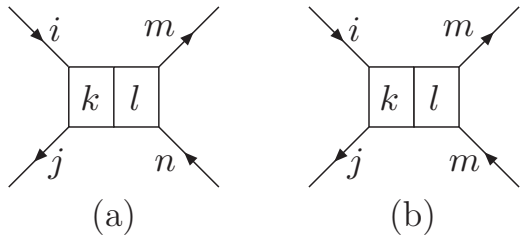


Figure 6.3 Box vertices. From [29].

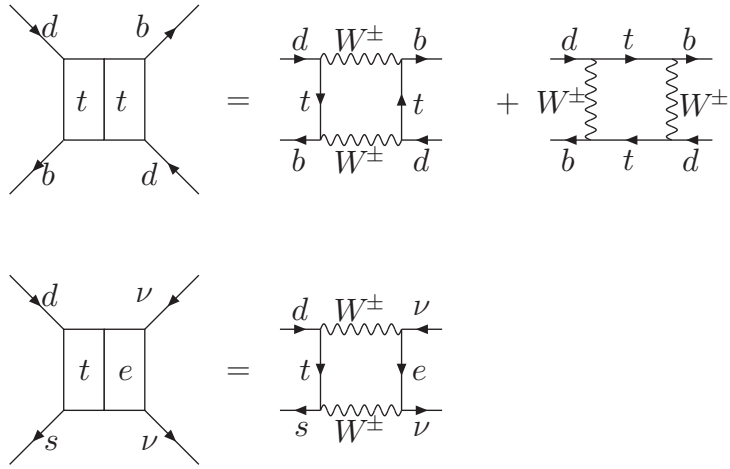


Figure 6.4 Box vertices resolved in terms of elementary vertices. From [29].

Box Vertices

These vertices involve in general both quarks and leptons and can be depicted as in Figure 6.3, where again i, j, m, and n stand for external quarks or leptons and k and l denote the internal quarks and leptons. In the vertex (a) the flavor violation takes place on both sides (left and right) of the box, whereas in (b) the right-hand side is flavor conserving. These effective quartic vertices can also be calculated using the Feynman rules for elementary vertices and propagators in the SM. We have, for instance, the vertices in Figure 6.4, which contribute to $B_d^0 - \bar{B}_d^0$ mixing and $K^+ \to \pi^+ \nu \bar{\nu}$, respectively. Other interesting examples will be discussed later. Again, the explicit calculation of these vertices in the SM is performed in Section 6.2.

Effective Feynman Rules

Using the Feynman rules for elementary vertices and propagators in the SM, one can derive "Feynman rules" for the effective vertices in question. This derivation is obtained by simply calculating the diagrams on the r.h.s. of the equations in Figures 6.2 and 6.4 and similar for other vertices. In Figure 6.2 the Z^0, γ, and *gluon* are off-shell. In the case of inclusive decays $B \to X\gamma$ and $B \to XG$, with G standing for gluons, we need also

Downloaded from https://www.cambridge.org/core. UNIVERSIDAD AUTONOMA METROPOLITANA, on 18 Nov 2026 at 18:06:35, subject to the Cambridge Core terms of use, available at https://www.cambridge.org/core/terms. https://doi.org/10.1017/9781139524100.011

corresponding vertices with on-shell photons and gluons. For these two cases it is essential to keep the masses of the external quarks, as otherwise the corresponding vertices would vanish. Moreover, momentum flowing through gluons and the photon propagator cannot be set to zero because these particles are massless. This means that also external momenta of quarks have to be kept, which makes the calculations more difficult than in the case of Z-penguin diagrams and box diagrams. We will return to these technicalities in Section 6.2. Here we just present the results so that readers not interested in spending days and nights in going through the calculations in Section 6.2 can also have some fun.

The rules for effective vertices are in the 't Hooft–Feynman gauge for the $W^\pm$ propagator as follows:

$$\text{Box}(\Delta S = 2) = \lambda_i^2 \frac{G_F^2}{16\pi^2} M_W^2 S_0(x_i)(\bar{s}d)_{V-A}(\bar{s}d)_{V-A}, \tag{6.1}$$

$$\text{Box}(T_3 = 1/2) = \lambda_i \frac{G_F}{\sqrt{2}} \frac{\alpha}{2\pi \sin^2\vartheta_W}[-4B_0(x_i)](\bar{s}d)_{V-A}(\bar{\nu}\nu)_{V-A}, \tag{6.2}$$

$$\text{Box}(T_3 = -1/2) = \lambda_i \frac{G_F}{\sqrt{2}} \frac{\alpha}{2\pi \sin^2\vartheta_W} B_0(x_i)(\bar{s}d)_{V-A}(\bar{\mu}\mu)_{V-A}, \tag{6.3}$$

$$\bar{s}Zd = i\lambda_i \frac{G_F}{\sqrt{2}} \frac{e}{2\pi^2} M_Z^2 \frac{\cos\vartheta_W}{\sin\vartheta_W} C_0(x_i)\bar{s}\gamma_\mu(1-\gamma_5)d, \tag{6.4}$$

$$\bar{s}\gamma d = -i\lambda_i \frac{G_F}{\sqrt{2}} \frac{e}{8\pi^2} D_0(x_i)\bar{s}(q^2\gamma_\mu - q_\mu \not{q})(1-\gamma_5)d, \tag{6.5}$$

$$\bar{s}G^a d = -i\lambda_i \frac{G_F}{\sqrt{2}} \frac{g_s}{8\pi^2} E_0(x_i)\bar{s}_\alpha(q^2\gamma_\mu - q_\mu \not{q})(1-\gamma_5)t^a_{\alpha\beta}d_\beta, \tag{6.6}$$

$$\bar{s}\gamma' b = i\bar{\lambda}_i^* \frac{G_F}{\sqrt{2}} \frac{e}{8\pi^2} D_0'(x_i)\bar{s}[i\sigma_{\mu\lambda}q^\lambda[m_b(1+\gamma_5)]]b, \tag{6.7}$$

$$\bar{s}G'^a b = i\bar{\lambda}_i^* \frac{G_F}{\sqrt{2}} \frac{g_s}{8\pi^2} E_0'(x_i)\bar{s}_\alpha[i\sigma_{\mu\lambda}q^\lambda[m_b(1+\gamma_5)]]t^a_{\alpha\beta}b_\beta, \tag{6.8}$$

where we simplified the notation for CKM factors

$$\lambda_i \equiv \lambda_i^{(K)} = V_{is}^* V_{id}, \qquad \bar{\lambda}_i \equiv \lambda_i^{(s)} = V_{ib}^* V_{is}. \tag{6.9}$$

The first six rules are relevant for K meson physics. For B meson physics only external flavors in the operators should be changed. The functions $F(x_i)$ are the same. The last two rules are relevant for $b \to s$ transitions. The generalization to $b \to d$ transitions should be obvious. These two rules are less relevant in K physics because these vertices are suppressed by $m_{s,d}$ in this case.

In these rules q_μ is the *outgoing* gluon or photon momentum, and T_3 indicates whether $\nu\bar{\nu}$ or $\ell^+\ell^-$ leaves the box diagram. The last two rules involve on-shell photon and gluon. We have set $m_s = 0$ in these rules.

Downloaded from https://www.cambridge.org/core. UNIVERSIDAD AUTONOMA METROPOLITANA, on 18 Nov 2026 at 18:06:35, subject to the Cambridge Core terms of use, available at https://www.cambridge.org/core/terms. https://doi.org/10.1017/9781139524100.011

These rules for effective vertices together with the rules for the propagators of the gauge boson involved allow the calculation of the effective Hamiltonians for FCNC processes, albeit without the inclusion of QCD corrections. The way these rules should be used requires some care:

- The penguin vertices should be used in the same manner as the elementary Feynman rules, which follow from $i\mathcal{L}$. Once a mathematical expression corresponding to a given diagram has been found, the contribution of this diagram to the relevant effective Hamiltonian is obtained by multiplying this mathematical expression by "i."
- Our conventions for the box vertices are such that they directly give the contributions to the effective Hamiltonians.

We will give an example later by calculating the internal top-quark contributions to $K^+ \to \pi^+\nu\bar{\nu}$. First, however, let us make a few general remarks emphasizing the new features of these effective vertices as compared to the elementary ones.

- They are higher order in the gauge couplings and consequently suppressed relative to the elementary transitions. This is consistent with experimental findings, which show very strong suppression of FCNC transitions relative to tree-level processes.
- Because of the internal $W^\pm$ exchanges, all penguin vertices in Figure 6.2 are purely $V-A$, i.e., the effective vertices involving γ and G are parity violating as opposed to their elementary interactions in Figure 6.1! Also, the Dirac structure of the flavor-violating Z coupling generated at one-loop level differs from the elementary one because now only $V-A$ couplings are involved. The box vertices are of the $(V-A)\otimes(V-A)$ type.
- The effective vertices depend on the masses of internal quarks or leptons and consequently are calculable functions of

$$x_i = \frac{m_i^2}{M_W^2}, \qquad i = u, c, t. \tag{6.10}$$

  The masses of leptons except for the τ in internal charm contributions are set to zero, as this is an excellent approximation. A set of basic universal functions can be found. These functions govern the physics of all FCNC processes in the SM. They are given subsequently.
- The effective vertices depend on the elements of the CKM matrix, and this dependence can be found directly from the diagrams of Figures 6.2 and 6.4.
- The dependences of a given vertex on the CKM factors and the masses of internal fermions govern the strength of the vertex in question.
- Another new feature of the effective vertices as compared to the elementary ones is their dependence on the gauge used for the $W^\pm$ propagator. We will return to this point soon.

Basic Functions

The basic functions present in (6.1)–(6.8) were calculated by various authors, in particular by Inami and Lim [132]. We will present some of these calculations using our methods in Section 6.2. They are given explicitly as follows:

Downloaded from https://www.cambridge.org/core. UNIVERSIDAD AUTONOMA METROPOLITANA, on 18 Nov 2026 at 18:06:35, subject to the Cambridge Core terms of use, available at https://www.cambridge.org/core/terms. https://doi.org/10.1017/9781139524100.011

$$B_0(x_t) = \frac{1}{4}\left[\frac{x_t}{1-x_t} + \frac{x_t \ln x_t}{(x_t-1)^2}\right], \tag{6.11}$$

$$C_0(x_t) = \frac{x_t}{8}\left[\frac{x_t-6}{x_t-1} + \frac{3x_t+2}{(x_t-1)^2}\ \ln x_t\right], \tag{6.12}$$

$$D_0(x_t) = -\frac{4}{9}\ln x_t + \frac{-19x_t^3+25x_t^2}{36(x_t-1)^3} + \frac{x_t^2(5x_t^2-2x_t-6)}{18(x_t-1)^4}\ln x_t, \tag{6.13}$$

$$E_0(x_t) = -\frac{2}{3}\ln x_t + \frac{x_t^2(15-16x_t+4x_t^2)}{6(1-x_t)^4}\ln x_t + \frac{x_t(18-11x_t-x_t^2)}{12(1-x_t)^3}, \tag{6.14}$$

$$D_0'(x_t) = -\frac{(8x_t^3+5x_t^2-7x_t)}{12(1-x_t)^3} + \frac{x_t^2(2-3x_t)}{2(1-x_t)^4}\ln x_t, \tag{6.15}$$

$$E_0'(x_t) = -\frac{x_t(x_t^2-5x_t-2)}{4(1-x_t)^3} + \frac{3}{2}\frac{x_t^2}{(1-x_t)^4}\ln x_t, \tag{6.16}$$

$$S_0(x_t) = \frac{4x_t-11x_t^2+x_t^3}{4(1-x_t)^2} - \frac{3x_t^3\ln x_t}{2(1-x_t)^3}, \tag{6.17}$$

$$S_0(x_c) = x_c, \tag{6.18}$$

$$S_0(x_c,x_t) = x_c\left[\ln\frac{x_t}{x_c} - \frac{3x_t}{4(1-x_t)} - \frac{3x_t^2\ln x_t}{4(1-x_t)^2}\right]. \tag{6.19}$$

We would like to make a few comments:

- In the last two expressions we have kept only linear terms in $x_c \ll 1$, but of course all orders in x_t. The last function generalizes $S_0(x_t)$ in (6.17) to include box diagrams with simultaneous top-quark and charm-quark exchanges.
- The subscript "0" indicates that these functions do not include QCD corrections to the relevant penguin and box diagrams. These corrections will be discussed in detail in subsequent sections.
- In writing the expressions in (6.11)–(6.19), we have omitted x_t-independent terms, which do not contribute to decays due to the GIM mechanism. We will discuss this issue in more detail later. Moreover,

$$S_0(x_t) \equiv F(x_t,x_t) + F(x_u,x_u) - 2F(x_t,x_u) \tag{6.20}$$

and

$$S_0(x_i,x_j) = F(x_i,x_j) + F(x_u,x_u) - F(x_i,x_u) - F(x_j,x_u), \tag{6.21}$$

where $F(x_i,x_j)$ is the true function corresponding to a given box diagram with i and j quark exchanges. These particular combinations can be found by drawing all possible box diagrams (also those with u-quark exchanges), setting $m_u = 0$, and using unitarity of the CKM-matrix, which implies in particular the relations:

$$\lambda_u^{(i)} + \lambda_c^{(i)} + \lambda_t^{(i)} = 0, \qquad i = K,s,d \tag{6.22}$$

Downloaded from https://www.cambridge.org/core. UNIVERSIDAD AUTONOMA METROPOLITANA, on 18 Nov 2026 at 18:06:35, subject to the Cambridge Core terms of use, available at https://www.cambridge.org/core/terms. https://doi.org/10.1017/9781139524100.011

for K, B_s^0 and B_d^0 systems with explicit expressions for CKM factors given in (6.9) and (6.41). In this way the effective Hamiltonians for FCNC transitions can be directly obtained by summing only over t and c quarks.

- The expressions given for $B_0(x_t)$, $C_0(x_t)$, and $D_0(x_t)$ correspond to the 't Hooft–Feynman gauge ($\xi = 1$). In an arbitrary R_ξ gauge they look different. In phenomenological applications it is therefore useful to work instead with the following gauge independent combinations [133]:

$$C_0(x_t,\xi) - 4B_0(x_t,\xi,1/2) = C_0(x_t) - 4B_0(x_t) = X_0(x_t), \tag{6.23}$$

$$C_0(x_t,\xi) - B_0(x_t,\xi,-1/2) = C_0(x_t) - B_0(x_t) = Y_0(x_t), \tag{6.24}$$

$$C_0(x_t,\xi) + \frac{1}{4}D_0(x_t,\xi) = C_0(x_t) + \frac{1}{4}D_0(x_t) = Z_0(x_t). \tag{6.25}$$

- $X_0(x_t)$ and $Y_0(x_t)$ are linear combinations of the $V-A$ components of Z^0-penguin and box diagrams with final quarks or leptons having weak isospin T_3 equal to 1/2 and – 1/2, respectively.
- $Z_0(x_t)$ is a linear combination of the vector component of the Z^0-penguin and the γ-penguin.
- These new functions are given explicitly as follows:

$$X_0(x_t) = \frac{x_t}{8}\left[\frac{x_t+2}{x_t-1} + \frac{3x_t-6}{(x_t-1)^2}\ln x_t\right], \tag{6.26}$$

$$Y_0(x_t) = \frac{x_t}{8}\left[\frac{x_t-4}{x_t-1} + \frac{3x_t}{(x_t-1)^2}\ln x_t\right], \tag{6.27}$$

$$Z_0(x_t) = -\frac{1}{9}\ln x_t + \frac{18x_t^4 - 163x_t^3 + 259x_t^2 - 108x_t}{144(x_t-1)^3} + \frac{32x_t^4 - 38x_t^3 - 15x_t^2 + 18x_t}{72(x_t-1)^4}\ln x_t. \tag{6.28}$$

Thus the set of gauge independent basic functions that govern the FCNC processes in the SM is given by:

$$S_0(x_t), \quad X_0(x_t), \quad Y_0(x_t), \quad Z_0(x_t), \quad E_0(x_t), \quad D_0'(x_t), \quad E_0'(x_t). \tag{6.29}$$

For numerical calculations one should, of course, use the exact expressions just given but to get an idea on the size of these functions and for derivation of analytical formulas one can use the following approximate but simple expressions

$$S_0(x_t) = 0.784\, x_t^{0.76}, \quad X_0(x_t) = 0.660\, x_t^{0.575}, \tag{6.30}$$

$$Y_0(x_t) = 0.315\, x_t^{0.78}, \quad Z_0(x_t) = 0.175\, x_t^{0.93}, \quad E_0(x_t) = 0.564\, x_t^{-0.51}, \tag{6.31}$$

$$D_0'(x_t) = 0.244\, x_t^{0.30}, \quad E_0'(x_t) = 0.145\, x_t^{0.19}. \tag{6.32}$$

Downloaded from https://www.cambridge.org/core. UNIVERSIDAD AUTONOMA METROPOLITANA, on 18 Nov 2026 at 18:06:35, subject to the Cambridge Core terms of use, available at https://www.cambridge.org/core/terms. https://doi.org/10.1017/9781139524100.011

In the range $160\,\text{GeV} \le m_t(m_t) \le 165\,\text{GeV}$, these approximations reproduce the exact expressions to an accuracy better than 0.2%, which is sufficient for deriving analytic formulas. We have then

$$S_0(x_t) = 2.31 \left(\frac{m_t(m_t)}{163\,\text{GeV}}\right)^{1.52}, \tag{6.33}$$

$$X_0(x_t) = 1.49 \left(\frac{m_t(m_t)}{163\,\text{GeV}}\right)^{1.15}, \qquad Y_0(x_t) = 0.95 \left(\frac{m_t(m_t)}{163\,\text{GeV}}\right)^{1.56}, \tag{6.34}$$

$$Z_0(x_t) = 0.66 \left(\frac{m_t(m_t)}{163\,\text{GeV}}\right)^{1.86}, \qquad E_0(x_t) = 0.27 \left(\frac{m_t(m_t)}{163\,\text{GeV}}\right)^{-1.02}, \tag{6.35}$$

$$D_0'(x_t) = 0.37 \left(\frac{m_t(m_t)}{163\,\text{GeV}}\right)^{0.60}, \qquad E_0'(x_t) = 0.19 \left(\frac{m_t(m_t)}{163\,\text{GeV}}\right)^{0.38}. \tag{6.36}$$

These formulas will allow us to exhibit elegantly the m_t dependence of various branching ratios in the phenomenological sections of this book. But as m_t is in 2020 rather precisely known, such representation of the m_t dependence of various observables does not play as important role as it played in 1990, that is, before the top-quark discovery, when the basic gauge independent functions were introduced.

An Example

With the help of the elementary Feynman rules for gauge boson propagators and the effective rules in (6.2) and (6.4), it is an easy matter to construct the effective Hamiltonian for the decay $K^+ \to \pi^+ \bar{\nu}_e \nu_e$ to which the diagrams in Figure 6.5 contribute.

We show this for the top-quark contribution. Neglecting the momentum in the Z^0 propagator in the first diagram, that is, replacing it by $ig_{\mu\nu}/M_Z^2$, multiplying it by the vertex in (6.4) and by "i," we find Z^0-penguin contribution. Subsequently adding the box diagram in (6.2), we find the well-known result for the top contribution to this decay:

$$\mathcal{H}_{\text{eff}}(K^+ \to \pi^+ \nu_e \bar{\nu}_e) = \frac{G_{\text{F}}}{\sqrt{2}} \frac{\alpha}{2\pi \sin^2 \vartheta_{\text{W}}} V_{ts}^* V_{td}\, X_0(x_t)\, (\bar{s}d)_{V-A} (\bar{\nu}_e \nu_e)_{V-A}. \tag{6.37}$$

Here we have expressed the combination $C_0(x_t) - 4B_0(x_t)$ through the function $X_0(x_t)$.

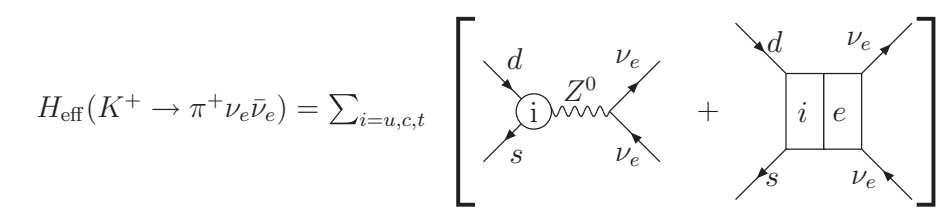


Figure 6.5 Calculation of $\mathcal{H}_{\text{eff}}(K^+ \to \pi^+ \nu_e \bar{\nu}_e)$. From [29].

Downloaded from https://www.cambridge.org/core. UNIVERSIDAD AUTONOMA METROPOLITANA, on 18 Nov 2026 at 18:06:35, subject to the Cambridge Core terms of use, available at https://www.cambridge.org/core/terms. https://doi.org/10.1017/9781139524100.011

Penguin-Box Expansion

One can generalize this calculation to other processes in which other basic effective vertices are present. For decays involving photonic and/or gluonic penguin vertices, the $1/q^2$ in the propagator cancels the q^2 in the vertex, and the resulting effective Hamiltonian can again be written in terms of local four-fermion operators. Thus generally an effective Hamiltonian for any decay considered can be written in the absence of QCD corrections as

$$\mathcal{H}_{\text{eff}}^{\text{FCNC}} = \sum_k C_k O_k, \tag{6.38}$$

where O_k denote local operators such as $(\bar{s}d)_{V-A}(\bar{s}d)_{V-A}$, $(\bar{s}d)_{V-A}(\bar{u}u)_{V-A}$, etc. The coefficients C_k of these operators are simply linear combinations of the functions in (6.29) times the corresponding CKM factors, which can be read from our rules. Consequently, it is possible to write down the SM amplitudes for all FCNC decays and transitions as linear combinations of the basic, process-independent m_t-dependent functions $F_r(x_t)$ in (6.29) with corresponding coefficients P_r characteristic for the decay under consideration. This "Penguin-Box-Expansion" (PBE) [133] takes the following general form:

$$\boxed{A(\text{decay}) = P_0(\text{decay}) + \sum_r P_r(\text{decay})\, F_r(x_t),} \tag{6.39}$$

where the sum runs over all possible functions contributing to a given amplitude. P_0 summarizes contributions stemming from internal quarks other than the top, in particular the charm quark. It will be evident from our presentation that the general expansion in (6.39) can be derived from the OPE and is valid also in the presence of QCD corrections with the dominant ones present in coefficients P_0 and P_r. At higher orders in gauge couplings new basic functions can enter, but we will leave them aside for now.

We will encounter many examples of the expansion (6.39) in this book, and generally several basic functions contribute to a given decay. In particular, in the SM we have:

$K^0 - \bar{K}^0$-mixing	$S_0(x_t)$, $S_0(x_c, x_t)$
$B^0 - \bar{B}^0$-mixing	$S_0(x_t)$
$K \to \pi\nu\bar{\nu}$, $B \to K(K^*)\nu\bar{\nu}$	$X_0(x_t)$
$K_{\text{L}} \to \mu\bar{\mu}$, $B_{s,d} \to \ell^+\bar{\ell}^-$	$Y_0(x_t)$
$K_{\text{L}} \to \pi^0 e^+ e^-$	$Y_0(x_t)$, $Z_0(x_t)$, $E_0(x_t)$
ε'	$X_0(x_t)$, $Y_0(x_t)$, $Z_0(x_t)$, $E_0(x_t)$
$B \to X_{s,d}\,\gamma$	$D_0'(x_t)$, $E_0'(x_t)$
$B \to K(K^*)\,\ell^+\bar{\ell}^-$	$Y_0(x_t)$, $Z_0(x_t)$, $E_0(x_t)$, $D_0'(x_t)$, $E_0'(x_t)$

In the last part of this book we will see that beyond the SM (BSM) other functions and other Dirac structures (operators) contribute to FCNCs. Moreover, the functions listed here will become in some BSM models complex quantities and the flavor independence of these functions will no longer be valid.

Downloaded from https://www.cambridge.org/core. UNIVERSIDAD AUTONOMA METROPOLITANA, on 18 Nov 2026 at 18:06:35, subject to the Cambridge Core terms of use, available at https://www.cambridge.org/core/terms. https://doi.org/10.1017/9781139524100.011

6.1.3 More about the GIM Mechanism

At this stage it is useful to return to the GIM mechanism [6], which did not allow tree-level FCNC transitions. This mechanism is also felt in the Hamiltonian of (6.38), and in fact it is fully effective when the masses of the internal quarks of a given charge in loop diagrams are set to be equal, e.g., $m_u = m_c = m_t$. Indeed, the CKM factors in any FCNC process enter in the combinations

$$C_k \propto \sum_{i=u,c,t} \lambda_i \, F(x_i) \quad \text{or} \quad \sum_{i,j=u,c,t} \lambda_i \lambda_j \, \tilde{F}(x_i, x_j), \tag{6.40}$$

where $F, \tilde{F}$ denote any of the functions of (6.29), and the λ_i are given in the case of K and $B_{s,d}$ meson decays and particle-antiparticle mixing as follows ($i = u, c, t$):

$$\lambda_i^{(K)} = V_{is}^* V_{id}, \qquad \lambda_i^{(d)} = V_{ib}^* V_{id}, \qquad \lambda_i^{(s)} = V_{ib}^* V_{is}. \tag{6.41}$$

They satisfy the unitarity relation (6.22), which implies vanishing coefficients C_k in (6.40) if $x_u = x_c = x_t$. For this reason the mass-independent terms in the calculation of the basic functions in (6.29) can always be omitted. In this limit, FCNC decays and transitions are absent. Thus beyond tree level the conditions for a complete GIM cancellation of FCNC processes are

- Unitarity of the CKM matrix.
- Horizontal flavor symmetry ensuring the equality of quark masses of a given charge.

Now in nature such a horizontal symmetry, even if it could exist at very short distance scales, is certainly broken at low energies by the disparity of masses of quarks of a given charge. This in fact is the origin of the breakdown of the GIM mechanism at the one-loop level and the appearance of FCNC transitions. The size of this breakdown, and consequently the size of FCNC transitions, depends on the disparity of masses, on the behavior of the basic functions in (6.29), and can be affected by QCD corrections as we will see in later chapters. Let us make two observations:

- For small $x_i \ll 1$, relevant for $i \neq t$, the functions (6.11)–(6.19) behave as follows:

$$S_0(x_i) \propto x_i, \quad B_0(x_i) \propto x_i \ln x_i, \quad C_0(x_i) \propto x_i \ln x_i, \tag{6.42}$$

$$D_0(x_i) \propto \ln x_i, \quad E_0(x_i) \propto \ln x_i, \quad D_0'(x_i) \propto x_i, \quad E_0'(x_i) \propto x_i. \tag{6.43}$$

  This implies "hard" (quadratic) GIM suppression of FCNC processes governed by the functions $S_0, B_0, C_0, D_0', E_0'$ provided the top-quark contributions due to small CKM factors can be neglected. In the case of $D_0(x_i)$ and $E_0(x_i)$, only "soft" (logarithmic) GIM suppression is present.
- For large x_t we have

$$S_0(x_t) \propto x_t, \quad B_0(x_t) \propto \text{const}, \quad C_0(x_t) \propto x_t \tag{6.44}$$

$$D_0(x_t) \propto \ln x_t, \quad E_0(x_t) \propto \text{const}, \quad D_0'(x_t) \propto \text{const}, \quad E_0'(x_t) \propto \text{const}. \tag{6.45}$$

Thus for FCNC processes governed by top-quark contributions, the GIM suppression is not effective at the one-loop level and in fact in the case of decays and transitions receiving contributions from $S_0(x_t)$ and $C_0(x_t)$ important enhancements of FCNCs are possible.

Downloaded from https://www.cambridge.org/core. UNIVERSIDAD AUTONOMA METROPOLITANA, on 18 Nov 2026 at 18:06:35, subject to the Cambridge Core terms of use, available at https://www.cambridge.org/core/terms. https://doi.org/10.1017/9781139524100.011

The latter property emphasizes the special role of K and $B_{s,d}$ decays with regard to FCNC transitions. In these decays the appearance of the top quark in the loops with $m_t > M_W \gg m_c, m_u$ removes the GIM suppression, making K and $B_{s,d}$ decays a particularly useful place to test FCNC transitions and to study the physics of the top quark. Of course, the hierarchy of various FCNC transitions is also determined by the hierarchy of the elements of the CKM matrix allowing in this manner to perform sensitive tests of this sector of the SM. It is remarkable that this structure is presently compatible within experimental and theoretical uncertainties with the data, although here and there some deviations from theory are observed.

The FCNC decays of D-mesons are much stronger suppressed in the SM because only d, s, and b quarks with $m_d, m_s, m_b \ll M_W$ enter the loops, and the GIM mechanism is much more effective. Also, the known structure of the CKM matrix is less favorable than in K and $B_{s,d}$ decays. For these reasons this book will be dominated by the latter, although some aspects of D decays will be discussed in Chapter 11 as well. In particular in the extensions of the SM, FCNC transitions are possible at the tree level, and the hierarchies discussed here may not apply. Moreover, the fact that FCNCs in D decays are so strongly suppressed in the SM allows in principle to see NP effects easier than in the other meson systems. Unfortunately, hadronic uncertainties in these decays are much larger than in K and $B_{s,d}$ decays so that the latter decays presently dominate flavor physics. Advances in lattice QCD could improve the status of the D meson system, but it will still take some years.

6.1.4 Final Comments

The discussion of FCNCs presented in this section left out completely QCD effects that we discussed in previous chapters in such a great detail in the case of tree-level decays. Still, we hope that this overture to FCNCs has shown the richness of the field of these processes. In the next section explicit calculations of the basic master one-loop functions will be presented. This particular section should not be skipped by students as it teaches them how to do loop calculations by hand. But it is not important for reading the subsequent sections in which using the technology of OPE and RG, developed in previous chapters, we will include QCD effects and electroweak effects to most interesting FCNC transitions and subsequently derive the relevant effective Hamiltonians that will be fundamental for more phenomenological parts of this book.

6.2 Calculations of Basic One-Loop Functions

6.2.1 Explicit Calculation of $\Delta F = 2$ Box Diagrams

The box diagrams contributing to $\Delta F = 2$ processes in the SM are given in Figure 6.6. We have specified the flavors so that these diagrams contribute to $K^0 - \bar{K}^0$ mixing, but analogous diagrams contribute to $B^0_{s,d} - \bar{B}^0_{s,d}$ mixings. There are also diagrams in which

Downloaded from https://www.cambridge.org/core. UNIVERSIDAD AUTONOMA METROPOLITANA, on 18 Nov 2026 at 18:06:35, subject to the Cambridge Core terms of use, available at https://www.cambridge.org/core/terms. https://doi.org/10.1017/9781139524100.011

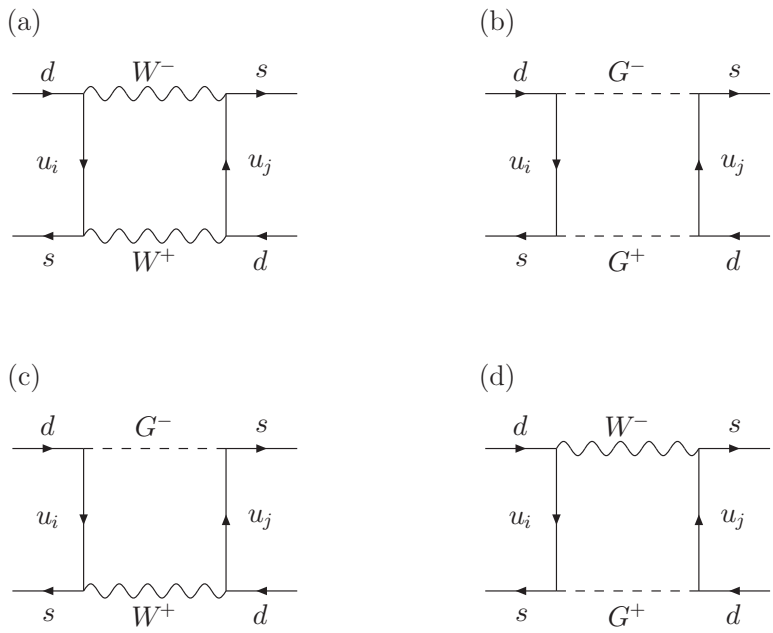


Figure 6.6 $\Delta F = 2$ Box Diagrams. From [29].

the quark lines are on horizontal propagators and W and Goldstone bosons on the vertical ones as the last diagram in the first row in Figure 6.4. But they give the same result, and it is sufficient to consider only the ones shown in Figure 6.6. In the unitary gauge only the first diagram is present, but the integrals, involving $W^{\pm}$ propagator in this gauge, although doable with the help of the list given in Appendix C.4, are not easy, and we will show here the explicit calculation in the Feynman–'t Hooft gauge $\xi = 1$. Then all diagrams contribute, but the calculation directly uses the first list of integrals in Appendix C and is straightforward. This also stresses the point that in the R_ξ gauges also diagrams with Goldstone bosons have to be included. We set the masses and momenta of external quarks to zero.

WW-Diagram

Using the rules in Appendix B, we find for a given pair of up-quarks ($i, j = u, c, t$)

$$\mathcal{D}_a = \left(\frac{g_2}{2\sqrt{2}}\right)^4 \lambda_i^{(K)} \lambda_j^{(K)} T_{\sigma\tau}^{(1)} R_1^{\sigma\tau}, \qquad \lambda_i^{(K)} = V_{is}^* V_{id}, \tag{6.46}$$

where

$$R_1^{\sigma\tau} = \int \frac{d^4k}{(2\pi)^4} \frac{k^\sigma k^\tau}{[k^2 - m_i^2][k^2 - m_j^2][k^2 - M_W^2]^2} \tag{6.47}$$

and

$$T_{\sigma\tau}^{(1)} = 4\bar{s}\gamma_\mu\gamma_\sigma\gamma_\nu(1-\gamma_5)d \otimes \bar{s}\gamma^\nu\gamma_\tau\gamma^\mu(1-\gamma_5)d. \tag{6.48}$$

Downloaded from https://www.cambridge.org/core. UNIVERSIDAD AUTONOMA METROPOLITANA, on 18 Nov 2026 at 18:06:35, subject to the Cambridge Core terms of use, available at https://www.cambridge.org/core/terms. https://doi.org/10.1017/9781139524100.011

Here the factor 4 comes after shifting $(1-\gamma_5)$ on both sides of $\otimes$ to the right end of the chain and using

$$(1-\gamma_5)^2 = 2(1-\gamma_5). \tag{6.49}$$

But $R_1^{\sigma\tau}$ is equal to the integral in (C.26)

$$R_1^{\sigma\tau} = -\frac{ig^{\sigma\tau}}{64\pi^2}\frac{1}{M_W^2}\left[\frac{x_i^2\log x_i}{(1-x_i)^2(x_i-x_j)} + \frac{x_j^2\log x_j}{(1-x_j)^2(x_j-x_i)} + \frac{1}{(1-x_i)(1-x_j)}\right], \tag{6.50}$$

where

$$x_i = \frac{m_i^2}{M_W^2}. \tag{6.51}$$

Contracting $g^{\sigma\tau}$ with $T_{\sigma\tau}$ and using the Greek method [126] explained in (5.160) and (5.161), we find

$$g^{\sigma\tau}T_{\sigma\tau}^{(1)} = 16\,(\bar{s}d)_{V-A}(\bar{s}d)_{V-A}. \tag{6.52}$$

We are now done with the calculation of $\mathcal{D}_a$ but to find its contribution to the effective Hamiltonian for $\Delta S = 2$ transitions, we have to multiply the result for $\mathcal{D}_a$ by i and divide it by a combinatoric factor 2, which takes into account both the diagram with vertical quark lines replaced by the horizontal lines and the fact that we deal with a product of two identical quark currents. The most straightforward way to find this factor is to look at a tree-level exchange of a heavy neutral particle that mediates a $\Delta F = 2$ transition and integrate it out. We will illustrate it in Section 15.4.3 on the example of a heavy Z' gauge boson.

Using

$$\left(\frac{g_2}{2\sqrt{2}}\right)^4 = \frac{1}{2}G_F^2 M_W^4, \tag{6.53}$$

we finally obtain

$$\mathcal{H}_{WW} = \frac{G_F^2}{16\pi^2}M_W^2\lambda_i^{(K)}\lambda_j^{(K)}T(x_i,x_j)(\bar{s}d)_{V-A}(\bar{s}d)_{V-A}, \tag{6.54}$$

$$T(x_i,x_j) = \left[\frac{x_i^2\log x_i}{(1-x_i)^2(x_i-x_j)} + \frac{x_j^2\log x_j}{(1-x_j)^2(x_j-x_i)} + \frac{1}{(1-x_i)(1-x_j)}\right], \tag{6.55}$$

$$T(x_i,x_i) = \left[\frac{2x_i\log x_i}{(1-x_i)^3} + \frac{1+x_i}{(1-x_i)^2}\right]. \tag{6.56}$$

Downloaded from https://www.cambridge.org/core. UNIVERSIDAD AUTONOMA METROPOLITANA, on 18 Nov 2026 at 18:06:35, subject to the Cambridge Core terms of use, available at https://www.cambridge.org/core/terms. https://doi.org/10.1017/9781139524100.011

GG-Diagram

We next calculate the diagram (b) in Figure 6.6, which contains two Goldstone bosons. We have first

$$\mathcal{D}_b = \frac{G_F^2}{2}\lambda_i^{(K)}\lambda_j^{(K)}T_{\sigma\tau}^{(2)}R_1^{\sigma\tau}, \tag{6.57}$$

with $R_1^{\sigma\tau}$ given in (6.50) and

$$T_{\sigma\tau}^{(2)} = 4m_i^2m_j^2\bar{s}\gamma_\sigma(1-\gamma_5)d\otimes\bar{s}\gamma_\tau(1-\gamma_5)d. \tag{6.58}$$

Multiplying the result by $i/2$, as explained earlier, we obtain

$$\boxed{\mathcal{H}_{GG} = \frac{G_F^2}{16\pi^2}M_W^2\lambda_i^{(K)}\lambda_j^{(K)}\left[\frac{x_ix_j}{4}\right]T(x_i,x_j)(\bar{s}d)_{V-A}(\bar{s}d)_{V-A},} \tag{6.59}$$

with $T(x_i,x_j)$ given in (6.55).

WG-Diagrams

There are two diagrams in Figure 6.6 with one W and one Goldstone boson, but they give the same result. Incorporating this factor of 2 we first have

$$\mathcal{D}_{c+d} = G_F^2M_W^2\lambda_i^{(K)}\lambda_j^{(K)}T^{(3)}R_2, \tag{6.60}$$

with

$$R_2 = \int\frac{d^4k}{(2\pi)^4}\frac{1}{[k^2-m_i^2][k^2-m_j^2][k^2-M_W^2]^2}, \tag{6.61}$$

and

$$T^{(3)} = -4m_i^2m_j^2(\bar{s}d)_{V-A}(\bar{s}d)_{V-A}. \tag{6.62}$$

But R_2 is equal to the integral in (C.20)

$$R_2 = -\frac{i}{16\pi^2}\frac{1}{M_W^4}\left[\frac{x_i\log x_i}{(1-x_i)^2(x_i-x_j)}+\frac{x_j\log x_j}{(1-x_j)^2(x_j-x_i)}+\frac{1}{(1-x_i)(1-x_j)}\right]. \tag{6.63}$$

Multiplying the result for $\mathcal{D}_{c+d}$ by $i/2$ we find

$$\mathcal{H}_{WG} = -\frac{G_F^2}{8\pi^2}M_W^2\lambda_i^{(K)}\lambda_j^{(K)}x_ix_j\tilde{T}(x_i,x_j)(\bar{s}d)_{V-A}(\bar{s}d)_{V-A}, \tag{6.64}$$

$$\tilde{T}(x_i,x_j) = \left[\frac{x_i\log x_i}{(1-x_i)^2(x_i-x_j)}+\frac{x_j\log x_j}{(1-x_j)^2(x_j-x_i)}+\frac{1}{(1-x_i)(1-x_j)}\right], \tag{6.65}$$

$$\tilde{T}(x_i,x_i) = \left[\frac{(1+x_i)\log x_i}{(1-x_i)^3}+\frac{2}{(1-x_i)^2}\right]. \tag{6.66}$$

Downloaded from https://www.cambridge.org/core. UNIVERSIDAD AUTONOMA METROPOLITANA, on 18 Nov 2026 at 18:06:35, subject to the Cambridge Core terms of use, available at https://www.cambridge.org/core/terms. https://doi.org/10.1017/9781139524100.011

Total Effective Hamiltonian

We add now the contributions in (6.54), (6.59), and (6.64) to obtain the total effective Hamiltonian for $\Delta S = 2$ transitions. We obtain first for fixed (i, j)

$$\boxed{\mathcal{H}_{\text{tot}}^{ij} = \frac{G_F^2}{16\pi^2} M_W^2 \lambda_i^{(K)} \lambda_j^{(K)} \left[\left(1 + \frac{x_i x_j}{4}\right) T(x_i, x_j) - 2 x_i x_j \tilde{T}(x_i, x_j) \right] (\bar{s}d)_{V-A} (\bar{s}d)_{V-A}.} \tag{6.67}$$

Summing over the internal up-quarks and using

$$\lambda_u^{(K)} = -\lambda_c^{(K)} - \lambda_t^{(K)}, \tag{6.68}$$

that follows from the unitarity of the CKM matrix, we find after some algebra

$$\boxed{\mathcal{H}_{\text{tot}} = \frac{G_F^2}{16\pi^2} M_W^2 \left[\lambda_c^2 S_0(x_c) + 2\lambda_c \lambda_t S_0(x_c, x_t) + \lambda_t^2 S(x_t) \right] (\bar{s}d)_{V-A} (\bar{s}d)_{V-A},} \tag{6.69}$$

where we suppressed the index (K) for artistic reasons.

The functions $S_0(x_i)$ and $S_0(x_i, x_j)$ are given in (6.17)–(6.19). They are just linear combinations in (6.20) and (6.21) with

$$F(x_i, x_j) = \left(1 + \frac{x_i x_j}{4}\right) T(x_i, x_j) - 2 x_i x_j \tilde{T}(x_i, x_j). \tag{6.70}$$

The index 0 indicates that QCD corrections have not been included.

The result in (6.67) can be extended to other meson systems by changing the quark flavors. Moreover, each term should be multiplied by QCD factors η_{cc}, η_{ct}, and η_{tt} to be given later on. We will also see that in $B_{s,d}^0$ systems only the last term in (6.69) is relevant. We will show this in the next section.

6.2.2 Explicit Calculation of $\Delta F = 1$ Box Diagrams

Let us next calculate box diagrams contributing to the transitions

$$d \to s\mu\bar{\mu}, \qquad d \to s\nu\bar{\nu}. \tag{6.71}$$

The relevant diagram for $\nu\bar{\nu}$ case is shown in Figure 6.4. We see the absence of diagrams with Goldstone bosons. They are present but can be neglected because the approximation of setting the internal lepton masses to zero is very good. An exception is the τ lepton, and we will take this into account later. Setting $m_\nu = m_\mu = 0$ the contributions of Goldstone boson exchanges $\phi^\pm$ are also set to zero, and we are left only with the $W^\pm$ exchanges.

We could proceed as in the case of $\Delta F = 2$ transitions and calculate these diagrams from scratch. But a smarter way to proceed is to get the result for these diagrams from the result in (6.54) directly. This indeed saves time.

Downloaded from https://www.cambridge.org/core. UNIVERSIDAD AUTONOMA METROPOLITANA, on 18 Nov 2026 at 18:06:35, subject to the Cambridge Core terms of use, available at https://www.cambridge.org/core/terms. https://doi.org/10.1017/9781139524100.011

$d \to s\mu\bar{\mu}$

Beginning with the first transition we note the following changes relative to the WW-case considered earlier:

- While the integral is the same, we can set $x_j = 0$.
- Next

$$T_{\sigma\tau} = 4\bar{s}\gamma_\mu\gamma_\sigma\gamma_\nu(1-\gamma_5)d \otimes \bar{\mu}\gamma^\nu\gamma_\tau\gamma^\mu(1-\gamma_5)\mu \tag{6.72}$$

  and consequently

$$g^{\sigma\tau}T_{\sigma\tau} = 16\,(\bar{s}d)_{V-A}(\bar{\mu}\mu)_{V-A}, \tag{6.73}$$

  which is exactly the result in (6.52) except that the operator is different.
- CKM factor is $\lambda_i^{(K)}$, and there is no combinatoric factor 1/2 because the second diagram with a horizontal fermion line does not exist, and the fermions in the initial and final state are all different from each other.

Taking these changes into account, we can immediately write down the effective Hamiltonian for the box contribution to the $d \to s\mu\bar{\mu}$ transition, by simply multiplying the effective Hamiltonian in (6.54) by 2, setting $x_j = 0$, removing the CKM factor $\lambda_j^{(K)}$, and changing the operator with the result:

$$\mathcal{H}_{\text{Box}}^{\mu\bar{\mu}} = \frac{G_F^2}{8\pi^2}M_W^2\sum_{i=u,c,t}\lambda_i^{(K)}T(x_i,0)(\bar{s}d)_{V-A}(\bar{\mu}\mu)_{V-A}, \tag{6.74}$$

where we took the summation over the internal up-quarks into account. We note next that

$$T(x_i,0) = 4B_0(x_i) + 1, \tag{6.75}$$

where $B_0(x_i)$ is one of the basic functions given in (6.11). Using the unitarity relation (6.68) and noting that $B_0(x_u) = 0$ to an excellent approximation, we find finally

$$\boxed{\mathcal{H}_{\text{Box}}^{\mu\bar{\mu}} = \frac{G_F^2}{2\pi^2}M_W^2\left[\lambda_c^{(K)}B_0(x_c) + \lambda_t^{(K)}B_0(x_t)\right](\bar{s}d)_{V-A}(\bar{\mu}\mu)_{V-A}.} \tag{6.76}$$

Note that the mass independent term "1" in (6.75) cancelled in the sum as a result of the GIM mechanism. We will see in later sections that in those BSM models in which the GIM mechanism is broken and $W^\pm$ is replaced by a very heavy particles with masses $O(\text{ TeV})$ only this term matters, as it is not suppressed by very small x_i in this case.

The overall factor in (6.76) can be rewritten by using the usual tree-level relations between SM parameters:

$$\boxed{\frac{G_F^2}{2\pi^2}M_W^2 = \frac{G_F}{\sqrt{2}}\frac{\alpha}{2\pi\sin^2\vartheta_W} \equiv \frac{g_{\text{SM}}^2}{4},} \tag{6.77}$$

which is useful when comparing with formulas given in the literature. g_{SM}^2 will appear frequently in the BSM part of this book.

Downloaded from https://www.cambridge.org/core. UNIVERSIDAD AUTONOMA METROPOLITANA, on 18 Nov 2026 at 18:06:35, subject to the Cambridge Core terms of use, available at https://www.cambridge.org/core/terms. https://doi.org/10.1017/9781139524100.011

$d \to s\nu\bar{\nu}$

Having the result in (6.76), we can easily obtain box diagram contribution to the effective Hamiltonian for $d \to s\nu\bar{\nu}$ transitions. We note that the momentum on the internal lepton propagator has opposite direction to the momentum k_μ. As in the WW box, the masses in the numerator of the fermion propagators do not contribute; this brings an additional overall minus sign. In addition this change implies a different order of gamma matrices so that including this sign we have

$$\tilde{T}_{\sigma\tau} = -4\bar{s}\gamma_\mu\gamma_\sigma\gamma_\nu(1-\gamma_5)d \otimes \bar{\nu}\gamma^\mu\gamma_\tau\gamma^\nu(1-\gamma_5)\nu \tag{6.78}$$

and consequently

$$g^{\sigma\tau}\tilde{T}_{\sigma\tau} = -64\,(\bar{s}d)_{V-A}(\bar{\nu}\nu)_{V-A}. \tag{6.79}$$

Concentrating first on internal e and μ leptons and setting their masses to zero, we obtain then

$$\boxed{\mathcal{H}^{\nu\bar{\nu}}_{\text{Box}} = [-4]\frac{G_F^2}{2\pi^2}M_W^2\left[\lambda_c^{(K)}B_0(x_c) + \lambda_t^{(K)}B_0(x_t)\right](\bar{s}d)_{V-A}(\bar{\nu}\nu)_{V-A}, \quad (\nu_e, \nu_\mu).} \tag{6.80}$$

In the case of τ we have to include its mass. We find then

$$\boxed{\mathcal{H}^{\nu\bar{\nu}}_{\text{Box}} = [-4]\frac{G_F^2}{2\pi^2}M_W^2\left[\lambda_c^{(K)}\tilde{B}_0(x_c) + \lambda_t^{(K)}\tilde{B}_0(x_t)\right](\bar{s}d)_{V-A}(\bar{\nu}\nu)_{V-A}, \quad (\nu_\tau),} \tag{6.81}$$

where

$$\tilde{B}_0(x_i) = T(x_i, x_\tau) - T(0, x_\tau), \qquad x_\tau = \frac{m_\tau^2}{M_W^2}, \tag{6.82}$$

with $T(x_i, x_\tau)$ given in (6.55). As the function T is symmetric in the arguments, we have using (6.75)

$$T(0, x_\tau) = 4B_0(x_\tau) + 1, \tag{6.83}$$

and again 1 cancels out in the differences in (6.81). One can check that this modification is numerically relevant only in the term involving x_c so that in the rest of this book we can set

$$\tilde{B}_0(x_t) = B_0(x_t) \tag{6.84}$$

and include the effect of m_τ only in the charm contribution.

Downloaded from https://www.cambridge.org/core. UNIVERSIDAD AUTONOMA METROPOLITANA, on 18 Nov 2026 at 18:06:35, subject to the Cambridge Core terms of use, available at https://www.cambridge.org/core/terms. https://doi.org/10.1017/9781139524100.011

6.2.3 Explicit Calculation of *Z*-Penguin Diagrams

Z-Vertex

Our first goal is the calculation of the function $C_0(x_i)$, which enters the induced flavor-violating vertex $\bar{s}Z^\mu d$

$$\boxed{\Gamma_Z^\mu \equiv i\frac{g_2^3}{16\pi^2}\frac{1}{\cos\vartheta_W}V_{id}V_{is}^* C_0(x_i)\bar{s}\gamma^\mu(1-\gamma_5)d,} \tag{6.85}$$

with $i = u, c, t$. For B_s and B_d meson systems, the flavors have to be changed, but $C_0(x_i)$ remains unchanged.

The full set of the diagrams contributing to Γ_Z^μ in the $\xi = 1$ gauge is given in Figures 6.7 and 6.8. We will see that several of these diagrams are divergent, but their sum will be finite. To regulate the divergences in the individual diagrams, we will work in $D = 4 - 2\varepsilon$ dimensions. All the integrals necessary to complete this task are collected in Appendix C so that the calculation is easy despite several contributing diagrams.

It will be useful to work with the following form of Z coupling

$$i\bar{f}Z_\mu f = i\frac{g_2}{2\cos\vartheta_W}\gamma_\mu\left[a_f(1+\gamma_5) + b_f(1-\gamma_5)\right], \tag{6.86}$$

where

$$a_f = -Q_f\sin^2\vartheta_W, \qquad b_f = T_3(f) - Q_f\sin^2\vartheta_W, \tag{6.87}$$

with f being the internal quark. In the following formulas $f = i$ represents the internal u, c, t. Moreover in the intermediate formulas we will suppress external spinors and the CKM factors, which will be exposed in the final formula for every diagram.

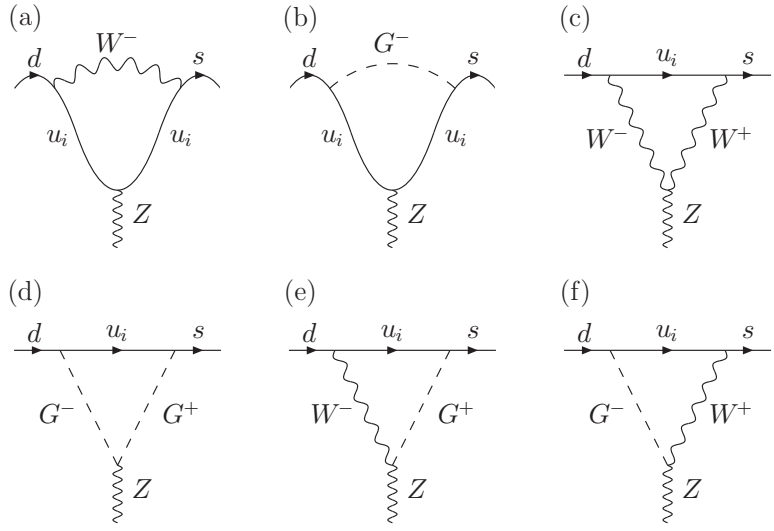


Figure 6.7 Vertex diagrams contributing to *Z*-penguin.

Downloaded from https://www.cambridge.org/core. UNIVERSIDAD AUTONOMA METROPOLITANA, on 18 Nov 2026 at 18:06:35, subject to the Cambridge Core terms of use, available at https://www.cambridge.org/core/terms. https://doi.org/10.1017/9781139524100.011

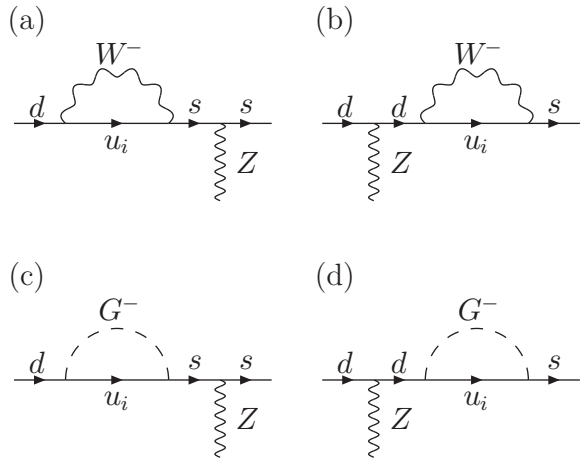


Figure 6.8 Self-energy diagrams contributing to Z-penguin.

The contribution of the diagram (a) is given by

$$\Delta_a \Gamma^\mu(Z) = \frac{g_2^3}{16\cos\vartheta_W}\int \frac{d^D k}{(2\pi)^D}\frac{k_\rho k_\lambda S_1^{\mu\rho\lambda} + m_i^2 S_2^\mu .}{[k^2 - m_i^2]^2[k^2 - M_W^2]}, \tag{6.88}$$

where after shifting $(1-\gamma_5)$ to the right of all γ_μ matrices we find

$$S_1^{\mu\rho\lambda} = 4b_i\gamma_\nu\gamma^\rho\gamma^\mu\gamma^\lambda\gamma^\nu(1-\gamma_5) \tag{6.89}$$

and

$$S_2^\mu = 4a_i\gamma_\nu\gamma^\mu\gamma^\nu(1-\gamma_5) = -8a_i(1-\varepsilon)\gamma^\mu(1-\gamma_5). \tag{6.90}$$

Note that we have dropped the terms linear in momentum k_μ as they would vanish anyway after performing the integration.

The two integrals can be found in Appendix C:

$$\int \frac{d^D k}{2\pi)^D}\frac{k_\rho k_\lambda}{[k^2 - m_i^2]^2[k^2 - M_W^2]} = I_4(m_i, m_i, M_W) = \frac{i g_{\rho\lambda}}{32\pi^2}\left[\frac{1}{\bar\varepsilon} + \frac{3}{4} + F_1(x_i)\right], \tag{6.91}$$

and

$$\int \frac{d^D k}{2\pi)^D}\frac{1}{[k^2 - m_i^2]^2[k^2 - M_W^2]} = I_3(m_i, m_i, M_W) = \frac{i}{16\pi^2}\frac{1}{M_W^2}R_1(x_i), \tag{6.92}$$

where

$$R_1(x_i) = \frac{\log x_i}{(1-x_i)^2} + \frac{1}{(1-x_i)}. \tag{6.93}$$

Now

$$g_{\rho\lambda}S_1^{\mu\rho\lambda} = 16b_i(1-2\varepsilon)\gamma^\mu(1-\gamma_5), \tag{6.94}$$

where we kept $O(\varepsilon)$ terms, as they will contribute after the multiplication by $1/\bar\varepsilon$ with $\bar\varepsilon$ defined in (C.5).

Downloaded from https://www.cambridge.org/core. UNIVERSIDAD AUTONOMA METROPOLITANA, on 18 Nov 2026 at 18:06:35, subject to the Cambridge Core terms of use, available at https://www.cambridge.org/core/terms. https://doi.org/10.1017/9781139524100.011

Inserting all these expressions into (6.88), we find

$$\boxed{\Delta_a\Gamma^\mu(Z) = i\frac{g_2^3}{32\pi^2}\frac{1}{\cos\vartheta_W}\left[b_i\left(\frac{1}{\bar{\varepsilon}} - \frac{1}{4} + F_1(x_i)\right) - a_i x_i R_1(x_i)\right] V_{id}V_{is}^*\bar{s}\gamma^\mu(1-\gamma_5)d,} \tag{6.95}$$

where we dropped terms $O(\varepsilon)$, and the functions F_1 and R_1 are defined in (C.3) and (6.93).

The contribution of the diagram (b) is given by

$$\Delta_b\Gamma^\mu(Z) = -x_i\frac{g_2^3}{16\cos\vartheta_W}\int\frac{d^Dk}{(2\pi)^D}\frac{k_\rho k_\lambda\tilde{S}_1^{\mu\rho\lambda} + m_i^2\tilde{S}_2^\mu}{[k^2-m_i^2]^2[k^2-M_W^2]}, \tag{6.96}$$

where

$$\tilde{S}_1^{\mu\rho\lambda} = 4a_i\gamma^\rho\gamma^\mu\gamma^\lambda(1-\gamma_5), \qquad \tilde{S}_2^\mu = 4b_i\gamma^\mu(1-\gamma_5). \tag{6.97}$$

The integrals to be evaluated are the same as in the first diagram and

$$g_{\rho\lambda}\tilde{S}_1^{\mu\rho\lambda} = -8a_i(1-\varepsilon)\gamma^\mu(1-\gamma_5). \tag{6.98}$$

Inserting all these expressions into (6.96), we find

$$\boxed{\Delta_b\Gamma^\mu(Z) = ix_i\frac{g_2^3}{64\pi^2}\frac{1}{\cos\vartheta_W}\left[a_i\left(\frac{1}{\bar{\varepsilon}} + \frac{1}{4} + F_1(x_i)\right) - b_i x_i R_1(x_i)\right] V_{id}V_{is}^*\bar{s}\gamma^\mu(1-\gamma_5)d.} \tag{6.99}$$

The contribution of the diagram (c) is given by

$$\Delta_c\Gamma^\mu(Z) = -\frac{g_2^3}{8}\cos\vartheta_W\int\frac{d^Dk}{(2\pi)^D}\frac{U^\mu}{[k^2-m_i^2][k^2-M_W^2]^2}, \tag{6.100}$$

where

$$U_\mu = 2k_\rho\gamma_\nu\gamma^\rho\gamma_\beta V_{\mu\beta\nu}(1-\gamma_5) \tag{6.101}$$

with the momentum dependent part of the triple gauge boson vertex listed in Appendix B and given by

$$V_{\mu\beta\nu}(0,-k,k) = k_\nu g_{\mu\beta} - 2k_\mu g_{\nu\beta} + k_\beta g_{\mu\nu}. \tag{6.102}$$

We find then

$$U_\mu = 4k^2\gamma_\mu(1-\gamma_5) + 8(1-\varepsilon)k_\mu k_\beta\gamma^\beta(1-\gamma_5). \tag{6.103}$$

The two integrals can be found in Appendix C:

$$\int\frac{d^Dk}{(2\pi)^D}\frac{k_\mu k_\beta}{[k^2-m_i^2][k^2-M_W^2]^2} = I_4(m_i,M_W,M_W) = \frac{ig_{\mu\beta}}{32\pi^2}\left[\frac{1}{\bar{\varepsilon}} + \frac{3}{4} + F_2(x_i)\right], \tag{6.104}$$

Downloaded from https://www.cambridge.org/core. UNIVERSIDAD AUTONOMA METROPOLITANA, on 18 Nov 2026 at 18:06:35, subject to the Cambridge Core terms of use, available at https://www.cambridge.org/core/terms. https://doi.org/10.1017/9781139524100.011

and

$$\int \frac{d^D k}{(2\pi)^D} \frac{k^2}{[k^2 - m_i^2][k^2 - M_W^2]^2} = \frac{i}{8\pi^2}\left[\frac{1}{\bar{\varepsilon}} + \frac{1}{2} + F_2(x_i)\right], \tag{6.105}$$

with F_2 given in (C.4).

Inserting all these expressions into (6.100), we find

$$\boxed{\Delta_c \Gamma^\mu(Z) = -i\frac{g_2^3}{32\pi^2}\cos\vartheta_W \left[\frac{3}{\bar{\varepsilon}} + \frac{5}{4} + 3F_2(x_i)\right] V_{id}V_{is}^* \bar{s}\gamma^\mu(1-\gamma_5)d.} \tag{6.106}$$

The calculation of the vertex diagram (d) is rather easy

$$\Delta_d \Gamma^\mu(Z) = \frac{g_2^3}{4}\frac{\left[\sin^2\vartheta_W - \cos^2\vartheta_W\right]}{\cos\vartheta_W} x_i \int \frac{d^D k}{(2\pi)^D} \frac{k^\mu k^\nu}{[k^2 - m_i^2][k^2 - M_W^2]^2}\gamma_\nu(1-\gamma_5). \tag{6.107}$$

The relevant integral is just the one in (6.104) so that we readily find

$$\boxed{\Delta_d \Gamma^\mu(Z) = i\frac{g_2^3}{128\pi^2}\frac{\left[\sin^2\vartheta_W - \cos^2\vartheta_W\right]}{\cos\vartheta_W} x_i \left[\frac{1}{\bar{\varepsilon}} + \frac{3}{4} + F_2(x_i)\right] V_{id}V_{is}^* \bar{s}\gamma^\mu(1-\gamma_5)dV_{id}V_{is}^*.} \tag{6.108}$$

The final two diagrams in Figure 6.7 are very simple. They give an identical result and are finite. Including a factor of two the contribution of these two diagrams is given by

$$\Delta_{e+f}\Gamma^\mu(Z) = -\frac{g_2^3}{2}\frac{\sin^2\vartheta_W}{\cos\vartheta_W}\int \frac{d^D k}{(2\pi)^D} \frac{m_i^2}{[k^2 - m_i^2][k^2 - M_W^2]^2}\gamma^\mu(1-\gamma_5). \tag{6.109}$$

The integral can be found in (C.10), but in view of other contributions, it is useful to express the result in terms of the functions F_1 and F_2 so that addition of diagrams will be easier if the calculation is done by hand. Otherwise it is irrelevant. We find

$$\boxed{\Delta_{e+f}\Gamma^\mu(Z) = -i\frac{g_2^3}{32\pi^2}\frac{\sin^2\vartheta_W}{\cos\vartheta_W} x_i \left[F_2(x_i) - F_1(x_i) - \frac{1}{2}\right] V_{id}V_{is}^* \bar{s}\gamma^\mu(1-\gamma_5)d.} \tag{6.110}$$

This completes the calculation of the vertex. It should be noted that the singularities in (6.95) and (6.106) are cancelled separately due to the unitarity of the CKM matrix when summation over internal quarks is performed. Also, the contribution in (6.110) is finite. But in (6.99) and (6.108) singularities depend on the masses of exchanged quarks, and unitarity of the CKM matrix would only remove them for $m_u = m_c = m_t$, which is clearly not the case. It is also evident that these singularities do not cancel each other so that the sum of five contributions is divergent. We will now demonstrate that these singularities disappear when contributions from the diagrams in Figure 6.8 are taken into account.

Downloaded from https://www.cambridge.org/core. UNIVERSIDAD AUTONOMA METROPOLITANA, on 18 Nov 2026 at 18:06:35, subject to the Cambridge Core terms of use, available at https://www.cambridge.org/core/terms. https://doi.org/10.1017/9781139524100.011

Self-Energy Diagrams

We first calculate only the self-energy diagram present in diagram (a) with external momentum p and denote it by

$$K_a = \frac{g_2^2}{2}(1-\varepsilon)\int \frac{d^D k}{(2\pi)^D}\frac{\not{p}+\not{k}}{[(k+p)^2-m_i^2][k^2-M_W^2]}(1-\gamma_5). \tag{6.111}$$

The integral is precisely the one in (C.2), and therefore we can right away write down the result remembering that the factor $(1-\varepsilon)$ will modify the constant term in (C.2). Including CKM factor and external spinors, we find

$$\boxed{K_a = i\frac{g_2^2}{32\pi^2}\left[\frac{1}{\bar{\varepsilon}}+\frac{1}{4}+F_2(x_i)\right]V_{id}V_{is}^*\,\bar{s}\;\not{p}(1-\gamma_5)d.} \tag{6.112}$$

This contribution is finite after summation over internal quarks, and this is also the case of self-energy diagram (b) that gives the same result $K_b = K_a$. But the rescue comes from the diagrams (c) and (d). For (c) we have

$$K_c = \frac{g_2^2}{4}x_i\int \frac{d^D k}{(2\pi)^D}\frac{\not{p}+\not{k}}{[(k+p)^2-m_i^2][k^2-M_W^2]}(1-\gamma_5). \tag{6.113}$$

The integral is as in the first self-energy diagram, but the overall factor is different and most important depends on quark masses. We find then

$$\boxed{K_c = i\frac{g_2^2}{64\pi^2}x_i\left[\frac{1}{\bar{\varepsilon}}+\frac{3}{4}+F_2(x_i)\right]V_{id}V_{is}^*\,\bar{s}\;\not{p}(1-\gamma_5)d.} \tag{6.114}$$

K_c is divergent, and this is also the case of $K_d = K_c$. We will see soon that the divergences in these diagrams remove the ones resulting from vertex diagrams. We will show this in two ways beginning with the heuristic one. We calculate the diagrams in Figure 6.8 by just inserting the results for K_a and K_c into diagrams (a) and (c), respectively. It is sufficient to calculate only these diagrams, as the result is independent of which external line is considered, and the diagram (b) gives the same result as diagram (a) and similar for (c) and (d). As we are doing some kind of renormalization like $Z_2^{1/2}$ there is a factor 1/2 that cancels the one coming from considering two diagrams.

In calculating the diagrams, the internal s and d propagators are massless, but we have to remember that the Z coupling to down-quarks differs from the one to up-quarks present in vertex diagrams.

We thus find the following additional contributions to Γ_Z^μ

$$\boxed{\Delta_{a+b}\Gamma^\mu(Z) = -i\frac{g_2^3}{32\pi^2}\frac{b_d}{\cos\vartheta_W}\left[\frac{1}{\bar{\varepsilon}}+\frac{1}{4}+F_2(x_i)\right]V_{id}V_{is}^*\bar{s}\gamma^\mu(1-\gamma_5)d,} \tag{6.115}$$

and

$$\boxed{\Delta_{c+d}\Gamma^\mu(Z) = -i\frac{g_2^3}{64\pi^2}\frac{b_d}{\cos\vartheta_W}x_i\left[\frac{1}{\bar{\varepsilon}}+\frac{3}{4}+F_2(x_i)\right]V_{id}V_{is}^*\bar{s}\gamma^\mu(1-\gamma_5)d.} \tag{6.116}$$

Downloaded from https://www.cambridge.org/core. UNIVERSIDAD AUTONOMA METROPOLITANA, on 18 Nov 2026 at 18:06:35, subject to the Cambridge Core terms of use, available at https://www.cambridge.org/core/terms. https://doi.org/10.1017/9781139524100.011

Both contributions modify the results from the vertex by finite terms, but the second one cancels in addition the divergence from the diagrams (6.99) and (6.108) so that the resulting Γ_Z^μ is finite.

Final Result for Penguin Diagrams

Adding all contributions, we find Γ_Z^μ in (6.85) with $C_0(x_i)$ given in (6.12). Having this vertex, it is now an easy matter to calculate the full Z-penguin diagram by calculating tree-level diagram with the upper vertex given simply by (6.85) and the lower by (6.86). This is a tree-level calculation that everybody can do by now. Multiplying the result by i, we find the contribution of the Z-penguin to the effective Hamiltonian:

$$\mathcal{H}_{ff}^Z = \frac{G_F^2}{2\pi^2} M_W^2 \left[\lambda_c^{(K)} C_0(x_c) + \lambda_t^{(K)} C_0(x_t)\right] (\bar{s}d)_{V-A} \times \left[2T_3(f)(\bar{f}f)_{V-A} - 4Q_f \sin^2\vartheta_W (\bar{f}f)_V\right], \tag{6.117}$$

with f being this time quark or lepton with the weak isospin $T_3(f)$ and electric charge Q_f.

It should be remarked that the overall factor in this formula found in the literature is not the preceding one but the one on the r.h.s. of (6.77). At this level both expressions give the same result, but when higher-order electroweak interactions are included and one enters the issue of definitions of $\sin^2\vartheta_W$, similar to definition of α_s, these two versions of $\mathcal{H}_{ff}^Z$ differ by a few percent with the difference cancelled by higher-order electroweak corrections. As G_F and not $\sin^2\vartheta_W$ is commonly used as input, we prefer to use in this book the overall factor as given in (6.117). Higher-order electroweak corrections have been calculated for a large m_t in [134] and for an arbitrary m_t in [135]. They will be taken into account in Section 9.5. But now let us look closer at (6.117).

In addition to the operators encountered already in (6.76) and (6.80), there is an additional operator with the vector coupling $(\bar{f}f)_V$ that is proportional to Q_f. Its Wilson coeffecient vanishes only for neutrinos but is nonzero for charged leptons and quarks. Such a vector coupling would result if the Z boson would be replaced by the photon, but then also the function C_0 would be replaced by D_0, and some factors would be changed. We will return to the calculation of the photon-penguin diagrams and of D_0 at the end of this section.

Here it is sufficient to state that the functions B_0, C_0, and D_0 are gauge dependent, where gauge dependence is related to the W propagator and only their linear combinations represented by the functions X_0, Y_0, and Z_0:

$$X_0 = C_0 - 4B_0, \qquad Y_0 = C_0 - B_0, \qquad Z_0 = C_0 + \frac{1}{4}D_0 \tag{6.118}$$

given in (6.26), (6.27), and (6.28) are gauge independent. The term involving vector coupling just discussed is represented by C_0 in Z_0. The $V-A$ part contributes to X_0 and Y_0. We will not demonstrate it here as this issue has been discussed in detail in [133], where the functions X_0, Y_0, and Z_0 were introduced. These functions are sometimes called *Inami–Lim*

Downloaded from https://www.cambridge.org/core. UNIVERSIDAD AUTONOMA METROPOLITANA, on 18 Nov 2026 at 18:06:35, subject to the Cambridge Core terms of use, available at https://www.cambridge.org/core/terms. https://doi.org/10.1017/9781139524100.011

functions, but Inami and Lim really worked with B_0, C_0, and D_0, not with X_0, Y_0, and Z_0 that have been introduced in the context of the *Penguin-Box Expansion* in [133] and are used commonly in the literature these days.

A Different Look at the Divergence in Z-Penguins

We will now consider a different approach to the issue of the removal of the singularities in the penguin diagrams. It considers only one-particle irreducible diagrams so that the diagrams in Figure 6.8 are not involved and only our results for self-energies in (6.112) and (6.114) will enter. We follow [116].

The main philosophy of this different, more sophisticated route, is as follows.

We have seen that the self-energy diagrams induce flavor nondiagonal propagation in the (s, d) sector. This propagation must be absent for the renormalized fields if we work in the flavor eigenbasis. This requirement uniquely determines electroweak counterterm that should be added to the Lagrangian resulting from the vertex calculation. Let us show this procedure in explicit terms and demonstrate that also this procedure gives the same function $C_0(x_i)$.

We begin with the kinetic term for d and s quarks in the unrenormalized Lagrangian

$$\mathcal{L}_{\text{kin}} = \bar{d}_L^0 i\partial_\mu \gamma^\mu d_L^0 + \bar{s}_L^0 i\partial_\mu \gamma^\mu s_L^0 \tag{6.119}$$

with s^0 and d^0 being unrenormalized fields.

We perform next field renormalization, allowing for nondiagonal pieces in the (d, s) sector

$$d_L^0 = Z_{11} d_L + Z_{12} s_L, \qquad s_L^0 = Z_{21} d_L + Z_{22} s_L. \tag{6.120}$$

Rewritten in terms of renormalized fields, the Lagrangian in (6.119) reads

$$\mathcal{L}_{\text{kin}} = (Z_{11}\bar{d}_L + Z_{12}\bar{s}_L) i\partial_\mu \gamma^\mu (Z_{11} d_L + Z_{12} s_L) + (Z_{21}\bar{d}_L + Z_{22}\bar{s}_L) i\partial_\mu \gamma^\mu (Z_{21} d_L + Z_{22} s_L). \tag{6.121}$$

Keeping only nondiagonal $\bar{s}d$ terms, we find

$$\mathcal{L}_{\text{kin}}^{sd} = (Z_{11}Z_{12} + Z_{22}Z_{21}) \bar{s}_L i\partial_\mu \gamma^\mu d_L \equiv \kappa \bar{s} i\partial_\mu \gamma^\mu (1-\gamma_5) d, \tag{6.122}$$

where

$$\kappa = \frac{1}{2}(Z_{11}Z_{12} + Z_{22}Z_{21}). \tag{6.123}$$

Next consider the unrenormalized neutral current Lagrangian

$$\mathcal{L}_{\text{NC}} = -\frac{g_2}{4\cos\vartheta_W}\left[1 - \frac{2}{3}\sin^2\vartheta_W\right]\left[\bar{d}^0\gamma_\mu(1-\gamma_5)d^0 + \bar{s}^0\gamma_\mu(1-\gamma_5)s^0\right] Z^\mu. \tag{6.124}$$

Rewriting it in terms of renormalized fields and using (6.123), we find for the $\bar{s}d$ term:

$$\Delta\mathcal{L}_{\text{NC}} = -2\kappa\frac{g_2}{4\cos\vartheta_W}\left[1 - \frac{2}{3}\sin^2\vartheta_W\right]\bar{s}\gamma_\mu(1-\gamma_5)d\, Z^\mu. \tag{6.125}$$

Downloaded from https://www.cambridge.org/core. UNIVERSIDAD AUTONOMA METROPOLITANA, on 18 Nov 2026 at 18:06:35, subject to the Cambridge Core terms of use, available at https://www.cambridge.org/core/terms. https://doi.org/10.1017/9781139524100.011

We have omitted right-handed fields, which do not contribute at one-loop level to Z-vertex. This shift in the Lagrangian has to be added to the result coming from the calculation of vertex diagrams and if everything works should be equal to the contribution coming from self-energy diagrams calculated by us earlier. This is in fact the case.

Indeed the expression in (6.122) is really a counter-term added to the initial Lagrangian

$$\mathcal{L}^{sd}_{\text{counter}} = \kappa \bar{s} i \partial_\mu \gamma^\mu (1-\gamma_5) d, \tag{6.126}$$

which implies the Feynman rule

$$K_{\text{counter}} = i\kappa \bar{s}\ \not{p}(1-\gamma_5) d. \tag{6.127}$$

The parameter κ can then be determined by requiring

$$K_1 + K_2 + i\kappa \bar{s}\ \not{p}(1-\gamma_5) d = 0 \tag{6.128}$$

with K_1 and K_2 given in (6.112) and (6.114), respectively. The reader may check that with κ determined in this manner, the shift in (6.125) added to the result from the vertex diagrams implies the finite expression for $C_0(x_i)$ equal to the one calculated previously.

6.2.4 Effective Hamiltonians with Boxes and Z-Penguins

Postponing the discussion of the second operator in (6.117) to the next section, we can already combine the effective Hamiltonians in (6.80) and (6.117) specified to neutrinos to obtain the effective Hamiltonian for the decays $K^+ \to \pi^+ \nu\bar{\nu}$ and $K_{\text{L}} \to \pi^0 \nu\bar{\nu}$, which with the change of flavors can also be used for $B \to K(K^*)\nu\bar{\nu}$. We have

$$\boxed{\mathcal{H}^{\nu\bar{\nu}}_{\text{eff}} = \frac{G_F^2}{2\pi^2} M_W^2 \left[\lambda_c^{(K)} X_0(x_c) + \lambda_t^{(K)} X_0(x_t)\right] (\bar{s}d)_{V-A} (\bar{\nu}\nu)_{V-A},} \tag{6.129}$$

with X_0 given in (6.26). For $B \to K(K^*)\nu\bar{\nu}$ decays, the first term is strongly suppressed relative to the second one because $X(x_t) \gg X(x_c)$, while the corresponding CKM factors are comparable.

Similarly combining the effective Hamiltonian in (6.76) and the one in (6.117) specified to muons we obtain the effective Hamiltonian for the decay $K_L \to \mu^+\mu^-$, which with the change of flavors can also be used for $B_{s,d} \to \mu^+\mu^-$ decays. We have

$$\boxed{\mathcal{H}^{\mu\mu}_{\text{eff}} = -\frac{G_F^2}{2\pi^2} M_W^2 \left[\lambda_c^{(K)} Y_0(x_c) + \lambda_t^{(K)} Y_0(x_t)\right] (\bar{s}d)_{V-A} (\bar{\mu}\mu)_{V-A},} \tag{6.130}$$

with Y_0 given in (6.27). For $B_{s,d} \to \mu^+\mu^-$ decays, the first term is strongly suppressed relative to the second one because of $Y(x_t) \gg Y(x_c)$.

Our calculation has been performed within the SM. Formulas for Z-penguin contributions in generic extensions of the SM that involve arbitrary charged fermions, scalars, and gauge bosons but similar to the SM do not generate FCNC mediated by Z at tree level, have been presented in [136]. Because of the gauge invariance also the relevant box contributions are given there. This paper is particularly important for models with RH charged currents as in this case one-loop calculations require even more care than in the

Downloaded from https://www.cambridge.org/core. UNIVERSIDAD AUTONOMA METROPOLITANA, on 18 Nov 2026 at 18:06:35, subject to the Cambridge Core terms of use, available at https://www.cambridge.org/core/terms. https://doi.org/10.1017/9781139524100.011

presence of only LH currents as illustrated earlier. It is a very useful paper. Other useful papers related to one-loop calculations will be listed in Section 14.6.2.

The inclusion of QCD and electroweak corrections to these Hamiltonians and the related phenomenology will be discussed in Chapter 9.

6.2.5 QED and QCD Penguins

General Comments

The calculation of the QED and QCD penguin diagrams and the derivation of the rules (6.5)–(6.8) is more difficult and longer because in the case of (6.5) and (6.6) one has to keep external momenta and in the case of (6.7) and (6.8) also external masses. Therefore we will not present explicit derivation of these rules but will only indicate a method that we hope will be helpful for readers that decide to do this calculation.

The result for the induced flavor-violating vertex involving photon or gluon can be written in the case of $b \to s$ transitions generally as follows

$$\Gamma_P^\mu = F_1 \bar{s}(q^2\gamma^\mu - q^\mu \not{q})P_L b + m_b F_2 \bar{s}(i\sigma^{\mu\nu}q_\nu P_R)b, \tag{6.131}$$

with

$$P_{L,R} = \frac{1}{2}(1 \mp \gamma_5), \qquad \sigma^{\mu\nu} = \frac{i}{2}[\gamma^\mu, \gamma^\nu], \qquad q^\mu = p_b^\mu - p_s^\mu. \tag{6.132}$$

p_b^μ and p_s^μ are four-momenta of the b quark and s quark, respectively. We set $m_s = 0$. We suppress t^a in the case of gluons as it does not play any role in the arguments given next.

To calculate the functions in the rules (6.5)–(6.8), it is useful to set $q^2 = 0$. Using next the identities

$$\not{p}_b\gamma^\mu = -\gamma^\mu \not{p}_b + 2p_b^\mu, \qquad \gamma^\mu \not{p}_s = -\not{p}_s\gamma^\mu + 2p_s^\mu \tag{6.133}$$

and the Dirac equation

$$\bar{s}\not{p}_s = \bar{s}m_s = 0, \qquad \not{p}_b b = m_b b, \tag{6.134}$$

the vertex Γ_P^μ can be expressed in terms of

$$O_1^\mu = 2m_b^2\gamma^\mu P_L, \qquad O_2^\mu = 2p_b^\mu m_b P_R, \qquad O_3^\mu = 2p_s^\mu m_b P_R. \tag{6.135}$$

We obtain

$$\Gamma_P^\mu = \frac{1}{2}F_1\bar{s}(O_3^\mu - O_2^\mu)b + \frac{1}{2}F_2\bar{s}(O_2^\mu + O_3^\mu - O_1^\mu)b. \tag{6.136}$$

Calculating the relevant diagrams in Figure 6.13, we find next

$$\Gamma_P^\mu = i\frac{G_F}{\sqrt{2}}\frac{g}{8\pi^2}\bar{s}(B_1O_1^\mu + B_2O_2^\mu + B_3O_3^\mu), \tag{6.137}$$

with B_i being functions of x_t.

But it turns out that B_i are related through

$$B_1 + B_3 = -(B_1 + B_2), \tag{6.138}$$

Downloaded from https://www.cambridge.org/core. UNIVERSIDAD AUTONOMA METROPOLITANA, on 18 Nov 2026 at 18:06:35, subject to the Cambridge Core terms of use, available at https://www.cambridge.org/core/terms. https://doi.org/10.1017/9781139524100.011

which constitutes a useful test of the calculation. Using this relation, we obtain

$$\Gamma_P^\mu = i\frac{G_F}{\sqrt{2}}\frac{g}{8\pi^2}\bar{s}[B_1(O_1^\mu - O_2^\mu - O_3^\mu) + (B_1 + B_2)(O_2^\mu - O_3^\mu)]b, \tag{6.139}$$

where the coupling g is either g_s for QCD or e for QED.

Comparing with (6.136), we find

$$F_1 = -\frac{G_F}{\sqrt{2}}\frac{g}{4\pi^2}(B_1 + B_2), \qquad F_2 = -\frac{G_F}{\sqrt{2}}\frac{g}{4\pi^2}B_1. \tag{6.140}$$

Calculating B_1 and B_2, we find F_1 and F_2 and

$$F_1 = -i\frac{G_F}{\sqrt{2}}\frac{g_s}{4\pi^2}E_0(x_t), \qquad F_2 = i\frac{G_F}{\sqrt{2}}\frac{g_s}{4\pi^2}E_0'(x_t), \tag{6.141}$$

in the case of the gluon penguin and

$$F_1 = -i\frac{G_F}{\sqrt{2}}\frac{e}{4\pi^2}D_0(x_t), \qquad F_2 = i\frac{G_F}{\sqrt{2}}\frac{e}{4\pi^2}D_0'(x_t), \tag{6.142}$$

in the case of the photon penguin.

Inserting these results in (6.131), we reproduce the rules in (6.5)–(6.8).

Useful Relations

The QED and QCD contributions up to color and electric charge factors differ mainly through the absence of nonabelian vertices involving $W^\pm$ and external gauge boson in the QCD case. As the color factors do not enter the function $E_0'(x_t)$, explicit calculation allows to relate the function $D_0'(x_t)$ to $E_0'(x_t)$ and the electric charges of the internal and external quark, Q_u and Q_d, respectively.

First, it is useful to decompose $D_0'(x_t)$ into contribution from abelian and nonabelian diagrams:

$$D_0'(x_t) = [D_0'(x_t)]_{\text{abelian}} + [D_0'(x_t)]_{\text{nonabelian}}. \tag{6.143}$$

We find then

$$[D_0'(x_t)]_{\text{abelian}} = (2Q_d - Q_u)\,E_0'(x_t), \tag{6.144}$$

and consequently

$$[D_0'(x_t)]_{\text{nonabelian}} = D_0'(x_t) - (2Q_d - Q_u)\,E_0'(x_t). \tag{6.145}$$

The terms involving Q_d come from the self-energy diagrams. These relations simplify the calculation of the rate for $\mu \to e\gamma$ decay, as we will see in Section 17.2.

Downloaded from https://www.cambridge.org/core. UNIVERSIDAD AUTONOMA METROPOLITANA, on 18 Nov 2026 at 18:06:35, subject to the Cambridge Core terms of use, available at https://www.cambridge.org/core/terms. https://doi.org/10.1017/9781139524100.011

6.3 $\Delta F = 2$ Transitions

6.3.1 Preliminaries

We will next investigate the structure of effective Hamiltonians for particle-antiparticle mixing like $K^0 - \bar{K}^0$ mixing and $B_q^0 - \bar{B}_q^0$ mixings with $q = d, s$. These transitions already played a crucial role in the tests of the SM and its extensions for decades. Being all FCNC transitions, they are absent at tree level in the SM and at one-loop level proceed within the SM to an excellent approximation only through box diagrams with internal $W^\pm$ and charge +2/3 quark exchanges. We have calculated these diagrams in the previous section, and we have to establish now how our results enter mixing observables.

We will begin with the presentation of $B_q^0 - \bar{B}_q^0$ mixings as the effective Hamiltonians for them have simpler structure than the one for $K^0 - \bar{K}^0$ mixing. The point is that $B_q^0 - \bar{B}_q^0$ mixings are to an excellent approximation described by box diagrams with internal top-quark exchanges. The contributions of the internal u and c quarks are only needed to remove with the help of the GIM mechanism mass-independent contributions. We have seen this explicitly in the previous section. Otherwise they can be set to zero due to the smallness of m_u and m_c relative to m_t because the relevant one-loop function increases strongly with the mass of exchanged quarks. In the case of $K^0 - \bar{K}^0$ mixing this increase is compensated partly by the size of the CKM elements and box diagrams with two charm quarks, and diagrams with one charm and one top quark have to be taken into account. We will elaborate on the size of these different contributions after a detailed presentation of $B_q^0 - \bar{B}_q^0$ mixings.

In what follows we will discuss explicitly the effective Hamiltonian for $B_d^0 - \bar{B}_d^0$ mixing. The one for $B_s^0 - \bar{B}_s^0$ mixing can then be obtained by just replacing everywhere the flavor d by s. The effective Hamiltonian for $B_d^0 - \bar{B}_d^0$ mixing, relevant for scales $\mu_b = O(m_b)$, is then given by

$$\boxed{\mathcal{H}_{\rm eff}^{\Delta B=2} = \frac{G_{\rm F}^2}{16\pi^2} M_W^2 \left(V_{tb}^* V_{td}\right)^2 C_Q(\mu_b) Q(\Delta B = 2) + h.c.,} \tag{6.146}$$

where

$$\boxed{Q(\Delta B = 2) = (\bar{b}_\alpha d_\alpha)_{V-A} (\bar{b}_\beta d_\beta)_{V-A}\,.} \tag{6.147}$$

In the absence of QCD corrections (6.146) can be easily derived by calculating the relevant box diagrams as done in Section 6.2.1. Thus the Wilson coefficient C_Q is given at $\mu_W = O(M_W)$ as follows

$$C_Q(\mu_W) = S_0(x_t), \qquad S_0(x_t) = \frac{4x_t - 11x_t^2 + x_t^3}{4(1-x_t)^2} - \frac{3x_t^3 \ln x_t}{2(1-x_t)^3}. \tag{6.148}$$

But the matrix element of the operator $Q(\Delta B = 2)$ between $\bar{B}_d^0$ and B_d^0 states is evaluated by lattice methods at scales $\mu_b = O(m_b)$, and we really need $C_Q(\mu_b)$ and not $C_Q(\mu_W)$ that serves only as the initial condition for C_Q at $\mu_W = O(M_W)$ for the RG evolution down

Downloaded from https://www.cambridge.org/core. UNIVERSIDAD AUTONOMA METROPOLITANA, on 18 Nov 2026 at 18:06:35, subject to the Cambridge Core terms of use, available at https://www.cambridge.org/core/terms. https://doi.org/10.1017/9781139524100.011

to low-energy scale μ_b. Therefore we have to include QCD corrections: first at LO and afterwards at least at NLO to reduce various scale uncertainties and have proper matching to hadronic matrix elements obtained from lattice QCD.

6.3.2 LO Analysis: $B^0_{d,s} - \bar{B}^0_{d,s}$ Mixing

From our previous studies we already know that at LO we only have to calculate the anomalous dimension of the operator $Q(\Delta B = 2)$. In fact we can calculate this anomalous dimension in no time by noting that it is equal to the anomalous dimension of the operator Q_+ considered in previous chapter. Indeed, in the case at hand the Q_1 and Q_2 operators are given by

$$Q_1(\Delta B = 2) = (\bar{b}_\alpha d_\beta)_{V-A}(\bar{b}_\beta d_\alpha)_{V-A}, \qquad Q_2(\Delta B = 2) = Q(\Delta B = 2)\,. \tag{6.149}$$

and using one of Fierz identities in Appendix A.3 we also have

$$Q_1(\Delta B = 2) = Q(\Delta B = 2). \tag{6.150}$$

Consequently

$$Q_+ = \frac{Q_2 + Q_1}{2} = Q(\Delta B = 2)\,, \qquad Q_- = \frac{Q_2 - Q_1}{2} = 0 \tag{6.151}$$

and $\gamma_Q = \gamma_+$. In particular, in LO

$$\gamma_Q = \gamma_Q^{(0)} \frac{\alpha_s}{4\pi}\,, \qquad \gamma_Q^{(0)} = \gamma_+^{(0)} = 4\,. \tag{6.152}$$

This in turn implies

$$C_Q(\mu_b) = U^{(0)}(\mu_b, \mu_W) C_Q(\mu_W), \qquad U^{(0)}(\mu_b, \mu_W) = \left[\frac{\alpha_s(\mu_W)}{\alpha_s(\mu_b)}\right]^{\frac{\gamma_Q^{(0)}}{2\beta_0}}, \tag{6.153}$$

where $\beta_0 = 23/3$ for $f = 5$. Thus in LO, with (6.148), the Wilson coefficient $C_Q(\mu_b)$ is given by

$$C_Q(\mu_b) = \left[\frac{\alpha_s(\mu_W)}{\alpha_s(\mu_b)}\right]^{6/23} S_0(x_t). \tag{6.154}$$

Before going to the NLO case, let us calculate the matrix element

$$\langle \bar{B}^0_d | \mathcal{H}_{\rm eff}^{\Delta B=2} | B^0_d \rangle = \frac{G_{\rm F}^2}{16\pi^2} M_W^2 \left(V_{tb}^* V_{td}\right)^2 C_Q(\mu_b) \langle \bar{B}^0_d | Q(\Delta B = 2)(\mu_b) | B^0_d \rangle, \tag{6.155}$$

where

$$\langle \bar{B}^0_d | Q(\Delta B = 2)(\mu_b) | B^0_d \rangle \equiv \frac{4}{3} B_{B_d}(\mu_b) F_{B_d}^2 m_{B_d} \tag{6.156}$$

and F_{B_d} is the B_d-meson decay constant. Both F_{B_d} and $B_{B_d}(\mu_b)$ have been calculated by now with good precision by means of lattice QCD. We quote their values in Table D.3.

Downloaded from https://www.cambridge.org/core. UNIVERSIDAD AUTONOMA METROPOLITANA, on 18 Nov 2026 at 18:06:35, subject to the Cambridge Core terms of use, available at https://www.cambridge.org/core/terms. https://doi.org/10.1017/9781139524100.011

The μ_b-dependent parameter $B_B(\mu_b)$ parametrizes the nonperturbative effects in the hadronic matrix element of the operator $Q(\Delta B)$. Its value is $O(1)$. In phenomenological applications it is useful to define two μ_b-independent quantities:

$$\eta_B^{(0)} = \left[\alpha_s(\mu_W)\right]^{6/23}, \qquad \hat{B}_{B_d} = B_{B_d}(\mu_b)\left[\alpha_s(\mu_b)\right]^{-6/23}. \tag{6.157}$$

Then:

$$\langle \bar{B}_d^0|\mathcal{H}_{\rm eff}^{\Delta B=2}|B_d^0\rangle = \frac{G_{\rm F}^2}{12\pi^2} M_W^2 \left(V_{tb}^* V_{td}\right)^2 \hat{B}_{B_d} F_{B_d}^2 m_{B_d} \eta_B^{(0)} S_0(x_t). \tag{6.158}$$

For B_s^0 the index d should be replaced by s, but η_B remains unchanged.

We note that there is a leftover μ_W-dependence in η_B and μ_t dependence in $S_0(x_t(\mu_t))$. The latter dependence has been suppressed until now, but we know that quark masses depend on scales and $\mu_t = O(m_t)$. To reduce these scale dependences we have to include NLO corrections.

6.3.3 NLO Analysis: $B_{d,s}^0 - \bar{B}_{d,s}^0$ Mixing

From previous chapters we know that the inclusion of NLO QCD corrections amounts in the case at hand to the calculation of $O(\alpha_s)$ corrections to the box diagrams, matching the result to the effective theory without the top quark and W boson, and finally calculating the two-loop anomalous dimension of the operator $Q(\Delta B = 2)$. Fortunately, we do not have to do the latter calculation because to all orders of perturbation theory the anomalous dimension of $Q(\Delta B = 2)$ equals the one of Q_+. Consequently, only the calculation of $O(\alpha_s)$ corrections to $C_Q(\mu_W)$ is new.

Applying the standard procedure of matching one finds [137]

$$C_Q(\mu_W) = S_0(x_t) + \frac{\alpha_s(\mu_W)}{4\pi}\left[S_1(x_t) + F(\mu_W,\mu_t) + B_t S_0(x_t)\right], \tag{6.159}$$

where

$$F(\mu_W,\mu_t) = \gamma_m^{(0)} x_t \frac{\partial S_0(x_t)}{\partial x_t} \ln\frac{\mu_t^2}{M_W^2} + \frac{\gamma_Q^{(0)}}{2} \ln\frac{\mu_W^2}{M_W^2} S_0(x_t), \tag{6.160}$$

$$B_t = 5\frac{N-1}{2N} + 3\frac{N^2-1}{2N} \qquad \text{(NDR)}, \tag{6.161}$$

$$S_1(x_t) = \text{Complicated Function}. \tag{6.162}$$

The function $S_1(x_t)$ given in (XII.12) of [111] is a result of a two-loop calculation [137] involving gluon corrections to the box diagrams. Typical diagrams are shown in Figure 6.9. The interested reader should consult the detailed analysis in [137], where a spectacular cancellation of infrared divergences and gauge dependences present in the diagrams of the full theory is achieved by the corresponding diagrams in the effective theory.

Note that in addition to the function $S_1(x_t)$, the QCD corrections in (6.159) involve one term proportional to the derivative of the leading term $S_0(x_t)$ with respect to x_t and two terms proportional to $S_0(x_t)$. This structure allows us to expect that these terms remove at

Downloaded from https://www.cambridge.org/core. UNIVERSIDAD AUTONOMA METROPOLITANA, on 18 Nov 2026 at 18:06:35, subject to the Cambridge Core terms of use, available at https://www.cambridge.org/core/terms. https://doi.org/10.1017/9781139524100.011

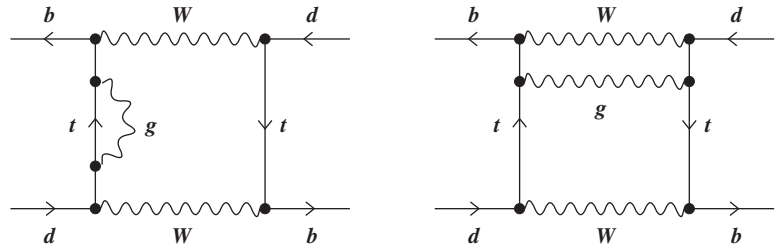


Figure 6.9 Examples of two-loop diagrams contributing to $B_d^0 - \bar{B}_d^0$ mixing. From [29].

this order some nonphysical dependences present in the LO term. Indeed the first log in $F(\mu_W, \mu_t)$ cancels the μ_t dependence in $S_0(x_t)$. The second logarithm in (6.160) cancels the μ_W dependence present in $U^{(0)}(\mu_b, \mu_W)$. For $\mu_W = \mu_t$ the formulas just given reduce to the ones given in [137] and [111]. But as discussed already there, μ_W and μ_t can differ from each other, and for pedagogical reasons we do not put them equal here. The role of the last term in (6.159) will be exhibited in a moment.

The NLO evolution function is given simply by

$$U(\mu_b, \mu_W) = \left[1 + \frac{\alpha_s(\mu_b)}{4\pi} J_5\right] U^{(0)}(\mu_b, \mu_W) \left[1 - \frac{\alpha_s(\mu_W)}{4\pi} J_5\right], \tag{6.163}$$

with

$$J_5 = J_+ = 1.627 \qquad (\text{NDR}, \ f = 5). \tag{6.164}$$

J_5 is renormalization scheme dependent, but this dependence is canceled by the one of B_t.

We can now define μ_b and μ_W independent quantities at the NLO level, which moreover are renormalization scheme independent:

$$\eta_B = \left[\alpha_s(\mu_W)\right]^{6/23} \left[1 + \frac{\alpha_s(\mu_W)}{4\pi}\left(\frac{S_1(x_t)}{S_0(x_t)} + F(\mu_W, \mu_t) + B_t - J_5\right)\right], \tag{6.165}$$

$$\boxed{\hat{B}_{B_d} = B_{B_d}(\mu_b)\left[\alpha_s^{(5)}(\mu_b)\right]^{-6/23}\left[1 + \frac{\alpha_s^{(5)}(\mu_b)}{4\pi} J_5\right].} \tag{6.166}$$

Then: [137]

$$\boxed{\mathcal{H}_{\text{eff}}^{\Delta B=2} = \frac{G_{\text{F}}^2}{16\pi^2} M_W^2 \left(V_{tb}^* V_{td}\right)^2 \eta_B S_0(x_t) Q(\Delta B = 2) + h.c.,} \tag{6.167}$$

and

$$\boxed{\langle \bar{B}_d^0 | \mathcal{H}_{\text{eff}}^{\Delta B=2} | B_d^0 \rangle = \frac{G_{\text{F}}^2}{12\pi^2} M_W^2 \left(V_{tb}^* V_{td}\right)^2 \hat{B}_{B_d} F_{B_d}^2 m_{B_d} \eta_B S_0(x_t)\,.} \tag{6.168}$$

Downloaded from https://www.cambridge.org/core. UNIVERSIDAD AUTONOMA METROPOLITANA, on 18 Nov 2026 at 18:06:35, subject to the Cambridge Core terms of use, available at https://www.cambridge.org/core/terms. https://doi.org/10.1017/9781139524100.011

It should be noted that both η_B and $S_0(x_t)$ depend on μ_t but the product $\eta_B \cdot S_0(x_t)$ is μ_t-independent in $O(\alpha_s)$ as the first logarithm in (6.160) cancels the μ_t dependence in $S_0(x_t(\mu_t))$. If one varies μ_t in the range 100 GeV $\leq \mu_t \leq$ 300 GeV, the μ_t dependence of $\langle \bar{B}^0|\mathcal{H}_{\rm eff}^{\Delta B=2}|B^0\rangle$ amounts in LO to ±9% and is reduced to ±1% in NLO.

It is customary to evaluate η_B at $\mu_t = \mu_W = m_t$, then practically η_B is independent of $m_{\rm t}$ and the full $m_{\rm t}$ dependence of $B_d^0 - \bar{B}_d^0$ mixing resides in $S_0(x_t)$ with $m_t(m_t)$. Then using these formulas one finds [137, 138]

$$\eta_B = 0.5510 \pm 0.0022, \tag{6.169}$$

where the error includes also the leftover scale uncertainties, which can only be reduced by calculating $O(\alpha_s^2)$ corrections.

6.3.4 LO and NLO Analysis: $K^0 - \bar{K}^0$ Mixing

The case of $K^0 - \bar{K}^0$ mixing is more involved. Investigating the CKM factors in the box diagrams in Figure 6.10, we observe that we cannot neglect this time the charm contributions even after the GIM mechanism has been used. Simply, the CKM factors in diagrams involving u and c quarks compensate significantly the mass suppression of these contributions relative to the top contribution that, although still enhanced by the large top-quark mass, is suppressed by small CKM factors. Indeed, after the unitarity of the CKM matrix has been used, the relevant CKM factors are

$$\lambda_c = V_{cs}^* V_{cd} = O(\lambda), \qquad V_{ts}^* V_{td} = O(\lambda^5), \tag{6.170}$$

and consequently the three terms λ_c^2, $\lambda_c \lambda_t$, and λ_t^2 have to be kept. We will see that their importance will depend on whether we will consider CP-conserving or CP-violating observables.

The second difficulty relative to $B_{d,s}^0 - \bar{B}_{d,s}^0$ mixings is the calculation of QCD corrections to the parts involving charm. The point is that the charm quark cannot be integrated out together with W or top quark at scales $O(\mu_W)$. Consequently, after W and top quark have been integrated out, the operators relevant for scales $m_c \leq \mu \leq M_W$, the so-called bilocal operators, have a more complicated structure than the operator in (6.147). Therefore, the renormalization group evolution for these scales for charm-charm and charm-top contributions is much more complicated than the one for $B_{d,s}^0 - \bar{B}_{d,s}^0$ mixings, and we

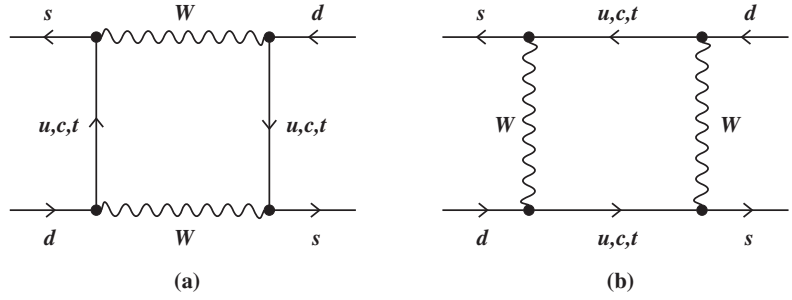


Figure 6.10 Box diagrams contributing to $K^0 - \bar{K}^0$ mixing in the SM. From [29].

Downloaded from https://www.cambridge.org/core. UNIVERSIDAD AUTONOMA METROPOLITANA, on 18 Nov 2026 at 18:06:35, subject to the Cambridge Core terms of use, available at https://www.cambridge.org/core/terms. https://doi.org/10.1017/9781139524100.011

cannot present it here. But, for scales $\mu < \mu_c = O(m_c)$, at which the charm quark is absent in the effective theory, we again find a single operator

$$\boxed{Q(\Delta S = 2) = (\bar{s}d)_{V-A}(\bar{s}d)_{V-A}.} \tag{6.171}$$

On the other hand, the renormalization group evolution in the pure top-quark part has the same structure as in $B^0_{d,s} - \bar{B}^0_{d,s}$ mixings. Only the evolution does not stop at μ_b but is continued down to $\mu < \mu_c$, implying a different value of the Wilson coefficient of $Q(\Delta S = 2)$ that in addition receives contributions from charm.

The final effective Hamiltonian for $\Delta S = 2$ transitions for $\mu < \mu_c = O(m_c)$ is given then as follows [137]

$$\begin{aligned}\mathcal{H}_{\text{eff}}^{\Delta S=2} = \frac{G_F^2}{16\pi^2} M_W^2 \left[\lambda_c^2 \eta_1 S_0(x_c) + \lambda_t^2 \eta_2 S_0(x_t) + 2\lambda_c\lambda_t \eta_3 S_0(x_c, x_t)\right] \\ \times \left[\alpha_s^{(3)}(\mu)\right]^{-2/9} \left[1 + \frac{\alpha_s^{(3)}(\mu)}{4\pi} J_3\right] Q(\Delta S = 2) + h.c.\end{aligned} \tag{6.172}$$

It contains a charm-, a top-, and a mixed charm-top contribution. This form is obtained upon eliminating λ_u by means of the unitarity of the CKM matrix and setting $x_u = 0$. The function $S_0(x_i)$ has already been given in (6.17), and $S_0(x_c, x_t)$ is given in (6.19).

Short-distance QCD effects are described through the correction factors η_1, η_2, η_3, and the explicitly α_s-dependent terms in (6.172). η_2 is the analogue of η_B discussed already. All three η_i have been evaluated at the NLO level a long time ago in [137, 139–142]. For η_1 and η_3 also NNLO corrections have been calculated in [143, 144].

η_{1-3} are defined in analogy to (6.165). This means that in $O(\alpha_s)$ they are independent of the renormalization scales and the renormalization scheme for the operator $Q(\Delta S)$. The present best values of η_i are given as follows (see however [1317])

$$\eta_1 = 1.87(76), \qquad \eta_2 = 0.5765(65), \qquad \eta_3 = 0.496(47)\,. \tag{6.173}$$

The quoted errors reflect the remaining theoretical uncertainties due to leftover μ-dependences at $O(\alpha_s^2)$ in η_2 and $O(\alpha_s^3)$ in $\eta_{1,2}$. The larger uncertainties in $\eta_{1,3}$ than η_2 reflect the fact that due to charm contribution lower scales in the process of matching are involved than in η_2.

We next define in analogy to (6.166), the renormalization group invariant parameter $\hat{B}_K$ by

$$\boxed{\hat{B}_K = B_K(\mu)\left[\alpha_s^{(3)}(\mu)\right]^{-2/9}\left[1 + \frac{\alpha_s^{(3)}(\mu)}{4\pi} J_3\right],} \tag{6.174}$$

with

$$J_3 = J_+ = 1.895 \qquad (\text{NDR},\ f = 3). \tag{6.175}$$

We will summarize the status of $\hat{B}_K$ in Chapter 7.

Downloaded from https://www.cambridge.org/core. UNIVERSIDAD AUTONOMA METROPOLITANA, on 18 Nov 2026 at 18:06:35, subject to the Cambridge Core terms of use, available at https://www.cambridge.org/core/terms. https://doi.org/10.1017/9781139524100.011

Then

$$\langle \bar{K}^0|(\bar{s}d)_{V-A}(\bar{s}d)_{V-A}|K^0\rangle \equiv \frac{4}{3}B_K(\mu)F_K^2 m_K, \tag{6.176}$$

where F_K is the K-meson decay constant and m_K the K-meson mass.

Finally, using (6.172), one finds

$$\langle \bar{K}^0|\mathcal{H}_{\rm eff}^{\Delta S=2}|K^0\rangle = \frac{G_{\rm F}^2}{12\pi^2}F_K^2\hat{B}_K m_K M_{\rm W}^2\left[\lambda_c{}^2\eta_1 S_0(x_c) + \lambda_t{}^2\eta_2 S_0(x_t) + 2\lambda_c\lambda_t\eta_3 S_0(x_c,x_t)\right]. \tag{6.177}$$

6.3.5 Summary

The most important formulas in this section are the final formulas for the matrix elements of effective Hamiltonians in (6.168) and (6.177). They will play a fundamental role in tests of the SM by means of $B_{d,s}^0 - \bar{B}_{d,s}^0$ and $K^0 - \bar{K}^0$ mixings in later steps of our expedition. But also the corresponding formulas for effective Hamiltonians in (6.167) and (6.172) will be important when we will enter the discussion of BSM physics.

6.4 The World of Penguins

6.4.1 Preliminaries

Until now we have visited in detail only the world of four-quark current-current operators Q_1 and Q_2 and just before the world of four-quark operators responsible for $B_{s,d}^0 - \bar{B}_{s,d}^0$ and $K^0 - \bar{K}^0$ mixings. We have presented effective Hamiltonians for various meson systems that involved these operators. Both LO and NLO effects in renormalization group improved perturbation theory have been taken into account, and various scale and renormalization scheme dependences including their cancelations have been discussed in detail. But as we have seen in Section 6.2.2, these operators are not the whole story, and we have to generalize the effective Hamiltonians to include many more operators already in the SM. In BSM models still more operators will be present but for the time being let us confine our discussion to the SM.

In principle the presence of new operators could have an impact on the Wilson coefficients of Q_1 and Q_2, but in fact this does not happen, and the values of $C_1(\mu)$ and $C_2(\mu)$, which we calculated in previous sections, will not be modified by the presence of new operators. This is clearly good news. But more good news is that many of the general properties related to scale and renormalization scheme dependence can be taken over to the more complicated situations where in addition to Q_1 and Q_2 other operators are present. In this and the next three sections we will discuss

Downloaded from https://www.cambridge.org/core. UNIVERSIDAD AUTONOMA METROPOLITANA, on 18 Nov 2026 at 18:06:35, subject to the Cambridge Core terms of use, available at https://www.cambridge.org/core/terms. https://doi.org/10.1017/9781139524100.011

- QCD penguin and electroweak penguin operators involving four quarks (this section), which enter the analysis not only of nonleptonic decays of mesons but through QCD effects and electroweak effects also those of semileptonic decays of mesons.
- Dipole operators relevant for $B \to X_s\gamma$ decay (Section 6.5).
- Semileptonic four-fermion operators involving a quark current and a leptonic current like $(\ell^+\ell^-)_V$ and $(\ell^+\ell^-)_A$, which enter the analyses of $B \to K(K^*)\ell^+\ell^-$, $B_{s,d} \to \ell^+\ell^-$ and $K_{L,S} \to \ell^+\ell^-$ decays (Section 6.6).
- Semileptonic operators involving a quark current and $(\nu\bar{\nu})_{V-A}$, which enter the analyses of $K \to \pi\nu\bar{\nu}$ and $B \to K(K^*)\nu\bar{\nu}$ decays (Section 6.7).

Except for an explicit calculation of one-loop anomalous dimensions of four-quark current-current and QCD penguin operators in this section, we will mainly discuss new features skipping often derivations. Indeed, these four sections should be considered as a guide to the weak effective Hamiltonians that we will use for the SM phenomenology in later chapters of this book, where further details on the physics behind them will be given. We should stress again that this and the following three sections deal exclusively with effective Hamiltonians in the SM. In the generalizations of the SM often new operators have to be included, and the effective Hamiltonians look more complicated. We will devote to them additional sections at later stages of this book stressing new features of these new operators, in particular those containing right-handed currents. Also scalar and tensor operators will sometimes play a significant role.

Finally, charged lepton flavor-violating decays involving in most cases only leptons is still another story. The relevant formulas, mostly given in the extensions of the SM, will be presented in Section 17.2. In the SM such processes are suppressed to a level that they cannot be measured even in the next decades, and an observation of any of these decays would automatically signal NP beyond the SM.

6.4.2 QCD Penguins

Operators

We will now have a close look at QCD penguin operators that contribute to nonleptonic $\Delta F = 1$ transitions. They originate in the gluon penguin diagram (a) of Figure 6.11. Evaluating this diagram one can clearly see that there are two color structures as in the case of Q_1 and Q_2. They follow simply from the decomposition

$$t^a_{\alpha\beta}t^a_{\gamma\delta} = -\frac{1}{2N}\delta_{\alpha\beta}\delta_{\gamma\delta} + \frac{1}{2}\delta_{\alpha\delta}\delta_{\gamma\beta}, \tag{6.178}$$

where t^a enters the two quark-gluon vertices. This formula is just (5.22) of Section 5.1.3, which we used to prove the existence of the operator Q_1. But as we will see soon, due to the presence of gluon and later photon exchanges and different topology of penguin diagrams, the numbers of penguin operators at the end will amount to eight: four QCD penguin operators and four electroweak penguin operators. The reason is as follows.

The upper effective FCNC vertex in the gluon penguin diagram has $V - A$ structure as can be verified by using the Feynman rules without fully calculating the diagram. This

Downloaded from https://www.cambridge.org/core. UNIVERSIDAD AUTONOMA METROPOLITANA, on 18 Nov 2026 at 18:06:35, subject to the Cambridge Core terms of use, available at https://www.cambridge.org/core/terms. https://doi.org/10.1017/9781139524100.011

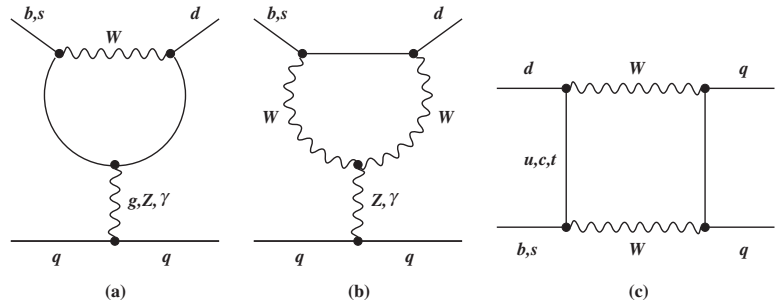


Figure 6.11 One-loop penguin and box diagrams in the full theory. From [29].

fact is related to $V - A$ structure of charged current interactions in the SM mediated by the W. The lower vertex is vectorial (V), and with the two color structures in (6.178) we have two $(V - A) \otimes V$ operators. It turns out, however, that the renormalization of these two operators requires the introduction of two new operators with the Dirac structure $(V-A)\otimes A$ and the color structures as in (6.178). Indeed, when the $(V-A)\otimes V$ operators are inserted into the one-loop diagrams of Figure 6.12 used to calculate anomalous dimensions, two new operators in question are generated. The full set of operators that closes under renormalization consists then of two current-current operators (Q_1, Q_2) and the four QCD penguin operators. It is customary to work with the $(V-A)\otimes(V-A)$ and $(V-A)\otimes(V+A)$ penguin operators rather than with the $(V - A) \otimes V$ and $(V - A) \otimes A$ structures. Then the basis of the operators necessary for the description of $\Delta B = 1$ decays with $\Delta S = 1$ is given (in the limit $\alpha \equiv \alpha_{\rm QED} = 0$) as follows:

Current-current:

$$Q_1^u = (\bar{u}_\alpha b_\beta)_{V-A}\,(\bar{s}_\beta u_\alpha)_{V-A}, \quad Q_2^u = (\bar{u}b)_{V-A}\,(\bar{s}u)_{V-A}, \tag{6.179}$$

$$Q_1^c = (\bar{c}_\alpha b_\beta)_{V-A}\,(\bar{s}_\beta c_\alpha)_{V-A}, \quad Q_2^c = (\bar{c}b)_{V-A}\,(\bar{s}c)_{V-A}. \tag{6.180}$$

QCD penguins:

$$Q_3 = (\bar{s}b)_{V-A} \sum_{q=u,d,s,c,b} (\bar{q}q)_{V-A}, \quad Q_4 = (\bar{s}_\alpha b_\beta)_{V-A} \sum_{q=u,d,s,c,b} (\bar{q}_\beta q_\alpha)_{V-A}, \tag{6.181}$$

$$Q_5 = (\bar{s}b)_{V-A} \sum_{q=u,d,s,c,b} (\bar{q}q)_{V+A}, \quad Q_6 = (\bar{s}_\alpha b_\beta)_{V-A} \sum_{q=u,d,s,c,b} (\bar{q}_\beta q_\alpha)_{V+A}. \tag{6.182}$$

The corresponding operators for other B decays and the D and K decays can be obtained from this basis by an appropriate change of flavors. We will meet these operators later on, as well as the electroweak penguin operators, and they will have to wait for us.

Downloaded from https://www.cambridge.org/core. UNIVERSIDAD AUTONOMA METROPOLITANA, on 18 Nov 2026 at 18:06:35, subject to the Cambridge Core terms of use, available at https://www.cambridge.org/core/terms. https://doi.org/10.1017/9781139524100.011

Effective Hamiltonian

The effective Hamiltonian for $\Delta B = 1$ decays with $\Delta S = 1$ is given then by

$$\mathcal{H}_{\rm eff}(\Delta B = 1) = \frac{G_F}{\sqrt{2}}\left[\lambda_u(C_1(\mu_b)Q_1^u + C_2(\mu_b)Q_2^u) + \lambda_c(C_1(\mu_b)Q_1^c + C_2(\mu_b)Q_2^c) - \lambda_t\sum_{i=3}^{6} C_i(\mu_b)Q_i\right], \qquad \lambda_q = V_{qs}^* V_{qb}, \tag{6.183}$$

where the CKM factors λ_q are just complex conjugates of the CKM factors used in $\Delta B = 2$ processes. This is merely the result of the definition of operators without any physical implications but should be kept in mind. To simplify notation we will not express λ_q in terms of the CKM factors used for $\Delta B = 2$ processes.

The reason why the operators $Q_{1,2}^q$ with $q = u, c$ have to be included is simple. The internal fermion line in the gluon penguin diagram is a quark with charge +2/3 and consequently u, c, and t quarks have to be included. But at scale $\mu < m_t$ the top quark has been integrated out and does not appear as a dynamical degree of freedom so that $Q_{1,2}^t$ are absent in the effective Hamiltonian. The presence of the top quark is signaled by the last term in (6.183), which is simply obtained by calculating, as discussed in Section 6.2, the gluon penguin diagram (a) of Figure 6.11 with internal top quark. Indeed λ_t is just the CKM factor in this diagram.

Wilson Coefficients

The calculation of the Wilson coefficients $C_i(\mu_b)$ of the QCD penguin operators proceeds as outlined in previous sections. The matching at $\mu_W = M_{\rm W}$ gives, in the presence of the penguin diagrams, the values of $\vec{C}(M_{\rm W})$. In the NDR scheme they are given by [123]:

$$C_1(M_{\rm W}) = \frac{11}{2}\,\frac{\alpha_s(M_{\rm W})}{4\pi}, \tag{6.184}$$

$$C_2(M_{\rm W}) = 1 - \frac{11}{6}\,\frac{\alpha_s(M_{\rm W})}{4\pi}, \tag{6.185}$$

$$C_3(M_{\rm W}) = -\frac{\alpha_s(M_{\rm W})}{24\pi}\widetilde{E}_0(x_t), \tag{6.186}$$

$$C_4(M_{\rm W}) = \frac{\alpha_s(M_{\rm W})}{8\pi}\widetilde{E}_0(x_t), \tag{6.187}$$

$$C_5(M_{\rm W}) = -\frac{\alpha_s(M_{\rm W})}{24\pi}\widetilde{E}_0(x_t), \tag{6.188}$$

$$C_6(M_{\rm W}) = \frac{\alpha_s(M_{\rm W})}{8\pi}\widetilde{E}_0(x_t), \tag{6.189}$$

Downloaded from https://www.cambridge.org/core. UNIVERSIDAD AUTONOMA METROPOLITANA, on 18 Nov 2026 at 18:06:35, subject to the Cambridge Core terms of use, available at https://www.cambridge.org/core/terms. https://doi.org/10.1017/9781139524100.011

where

$$\widetilde{E}_0(x_t) = E_0(x_t) - \frac{2}{3} \tag{6.190}$$

$$E_0(x_t) = -\frac{2}{3}\ln x_t + \frac{x_t(18 - 11x_t - x_t^2)}{12(1-x_t)^3} + \frac{x_t^2(15 - 16x_t + 4x_t^2)}{6(1-x_t)^4}\ln x_t, \tag{6.191}$$

with

$$x_t = \frac{m_t^2}{M_{\rm W}^2}. \tag{6.192}$$

$C_{1,2}(M_{\rm W})$ are simply obtained using (5.90) and (5.236). We will derive the QCD penguin coefficients $C_i(M_{\rm W})$ $(i = 4-6)$ soon. The constant $-2/3$ in (6.190) is characteristic for the NDR scheme. It is absent in the HV scheme. In LO $C_2(M_{\rm W}) = 1$ with all remaining coefficients set to zero. We observe that the $m_{\rm t}$-dependence in the case at hand enters first at the NLO level. It results from the gluon penguin diagram with internal top-quark propagators considered in Section 6.2.

The anomalous dimension matrix is 6×6:

$$\hat{\gamma}_s(\alpha_s) = \hat{\gamma}_s^{(0)}\frac{\alpha_s}{4\pi} + \hat{\gamma}_s^{(1)}\left(\frac{\alpha_s}{4\pi}\right)^2. \tag{6.193}$$

The one-loop coefficient $\hat{\gamma}_s^{(0)}$ is given for $N = 3$ by [145]

$$\hat{\gamma}_s^{(0)} = \begin{pmatrix} -2 & 6 & 0 & 0 & 0 & 0 \\ 6 & -2 & \frac{-2}{9} & \frac{2}{3} & \frac{-2}{9} & \frac{2}{3} \\ 0 & 0 & \frac{-22}{9} & \frac{22}{3} & \frac{-4}{9} & \frac{4}{3} \\ 0 & 0 & 6 - \frac{2f}{9} & -2 + \frac{2f}{3} & \frac{-2f}{9} & \frac{2f}{3} \\ 0 & 0 & 0 & 0 & 2 & -6 \\ 0 & 0 & \frac{-2f}{9} & \frac{2f}{3} & \frac{-2f}{9} & -16 + \frac{2f}{3} \end{pmatrix}. \tag{6.194}$$

The explicit calculation of this matrix will be presented next.

The two-loop anomalous dimension matrix $\hat{\gamma}_s^{(1)}$ in the NDR scheme looks truly horrible:

$$\begin{pmatrix} -\frac{21}{2} - \frac{2f}{9} & \frac{7}{2} + \frac{2f}{3} & \frac{79}{9} & -\frac{7}{3} & -\frac{65}{9} & -\frac{7}{3} \\ \frac{7}{2} + \frac{2f}{3} & -\frac{21}{2} - \frac{2f}{9} & -\frac{202}{243} & \frac{1354}{81} & -\frac{1192}{243} & \frac{904}{81} \\ 0 & 0 & -\frac{5911}{486} + \frac{71f}{9} & \frac{5983}{162} + \frac{f}{3} & -\frac{2384}{243} - \frac{71f}{9} & \frac{1808}{81} - \frac{f}{3} \\ 0 & 0 & \frac{379}{18} + \frac{56f}{243} & -\frac{91}{6} + \frac{808f}{81} & -\frac{130}{9} - \frac{502f}{243} & -\frac{14}{3} + \frac{646f}{81} \\ 0 & 0 & \frac{-61f}{9} & \frac{-11f}{3} & \frac{71}{3} + \frac{61f}{9} & -99 + \frac{11f}{3} \\ 0 & 0 & \frac{-682f}{243} & \frac{106f}{81} & -\frac{225}{2} + \frac{1676f}{243} & -\frac{1343}{6} + \frac{1348f}{81} \end{pmatrix}. \tag{6.195}$$

Downloaded from https://www.cambridge.org/core. UNIVERSIDAD AUTONOMA METROPOLITANA, on 18 Nov 2026 at 18:06:35, subject to the Cambridge Core terms of use, available at https://www.cambridge.org/core/terms. https://doi.org/10.1017/9781139524100.011

The corresponding matrix in the HV scheme can be found in [122, 146]. These two-loop matrices have been first calculated in the latter papers and in [124, 125]. The result in the NDR scheme has been confirmed subsequently in [147].

With all these results at hand one can now evaluate $C_i(\mu_b)$ by using

$$\vec{C}(\mu_b) = \hat{U}_5(\mu_b, M_W)\vec{C}(M_W) \tag{6.196}$$

with $\hat{U}_5(\mu_b, M_W)$ given in (5.113). With the help of Mathematica we can then find

$$C_j(\mu_b) = C_j^{(0)}(\mu_b) + \frac{\alpha_s(\mu_b)}{4\pi} C_j^{(1)}(\mu_b), \tag{6.197}$$

where

$$C_j^{(0)}(\mu_b) = \sum_{i=3}^{8} k_{ji}\eta^{a_i}, \tag{6.198}$$

$$C_j^{(1)}(\mu_b) = \sum_{i=3}^{8} [e_{ji}\eta E_0(x_t) + f_{ji} + g_{ji}\eta]\eta^{a_i} \tag{6.199}$$

with

$$\eta = \left[\frac{\alpha_s(M_W)}{\alpha_s(\mu_b)}\right] . \tag{6.200}$$

The magic numbers a_i, k_{ij}, e_{ij}, f_{ij}, and g_{ij} are collected in tables 6 and 7 of my Les Houches lectures [29], but we will not reproduce them here as eventually the calculation has to be done numerically anyway. But the structure of the preceding formulas gives us some idea about various dependences that clearly cannot be seen by performing numerical calculations.

Matching Conditions for QCD Penguins

It is instructive to derive the matching conditions for QCD penguin operators in (6.186)–(6.189). In particular it is useful to see how the scheme-dependent constant $-2/3$ is generated. After all in Chapter 2 we have briefly discussed what happens to GIM mechanism beyond the tree level. Looking at equation (2.65) it is evident that all mass independent constants in the evaluation of penguin vertices involving m_t-dependent functions like $E_0(x_t)$ can be dropped because of GIM mechanism. Yet as we will see in a moment such statements are valid only in the full theory. In the effective theory the top quark is absent as a dynamical degree of freedom, GIM is no longer valid in certain parts of the theory, and constants like $-2/3$ remain.

To demonstrate this explicitly let us consider first the tree-level Hamiltonian for $\Delta B = 1$ decays:

$$\mathcal{H}_{\text{eff}}^{(0)}(\Delta B = 1) = \frac{G_F}{\sqrt{2}} \left[\lambda_u Q_2^u + \lambda_c Q_2^c + \lambda_t Q_2^t\right], \tag{6.201}$$

in which only current-current operators Q_2^i are present. Note the appearance of the operator Q_2^t.

Downloaded from https://www.cambridge.org/core. UNIVERSIDAD AUTONOMA METROPOLITANA, on 18 Nov 2026 at 18:06:35, subject to the Cambridge Core terms of use, available at https://www.cambridge.org/core/terms. https://doi.org/10.1017/9781139524100.011

Next let us include QCD corrections and perform the matching of the full theory to an effective five-quark theory in which the top quark is no longer a dynamical degree of freedom. Because we are only interested in the penguin coefficients we can leave out the QCD corrections to Q_2^q operators and also drop the Q_1^q operators. Calculating then the usual QCD penguin diagram (a) in Figure 6.11 with full $W^\pm$ and internal u, c, t quarks and adding the result to the tree-level matrix element of the Hamiltonian (6.201), we find the amplitude in the full theory:

$$\mathcal{A}_{\text{full}} = \frac{G_F}{\sqrt{2}}\left(\lambda_u\left[\langle Q_2^u\rangle^0 - \frac{\alpha_s(M_W)}{8\pi}G_u(m_u)\langle Q_P\rangle^0\right] + \lambda_c\left[\langle Q_2^c\rangle^0 - \frac{\alpha_s(M_W)}{8\pi}G_c(m_c)\langle Q_P\rangle^0\right] + \lambda_t\left[-\frac{\alpha_s(M_W)}{8\pi}E_0(x_t)\langle Q_P\rangle^0\right]\right). \tag{6.202}$$

Note that as a preparation for the matching we have already removed the tree-level matrix element of Q_2^t in which the top-quark field is a dynamical degree of freedom. Next

$$Q_P = Q_4 + Q_6 - \frac{1}{3}(Q_3 + Q_5), \tag{6.203}$$

where Q_i with $i = 3 - 6$ are the penguin operators defined in (6.181) and (6.182).

The functions $G_i(m_i)$ result from calculating penguin diagrams with internal u and c quarks. They are given explicitly in the appendix of [122]. As we will see in a moment they will cancel out in the process of matching, and their analytic expressions are not needed here. This is the reason why in (6.186)–(6.189) the masses m_u and m_c are absent.

Now the effective theory involves only Q_2^u, Q_2^c, and Q_P. Calculating the insertions of Q_2^u and Q_2^c into QCD penguin diagrams of Figure 6.12 and adding the tree-level contributions of Q_2^q operators as in the full theory, we find

$$\mathcal{A}_{\text{eff}} = \frac{G_F}{\sqrt{2}}\left(\lambda_u\left[\langle Q_2^u\rangle^0 - \frac{\alpha_s(M_W)}{8\pi}(G_u(m_u) - r)\langle Q_P\rangle^0\right] + \lambda_c\left[\langle Q_2^c\rangle^0 - \frac{\alpha_s(M_W)}{8\pi}(G_c(m_c) - r)\langle Q_P\rangle^0\right] - \lambda_t C_P\langle Q_P\rangle^0\right), \tag{6.204}$$

where C_P is the coefficient we are looking for. The minus sign in front of λ_t is a convention that has no impact on physics. Next r is a scheme-dependent constant equal to 2/3 and 0 for NDR and HV schemes, respectively. Finally, it should be remarked that the insertions of QCD penguin operators into penguin diagrams contribute only at $O(\alpha_s^2)$ to (6.204) and do not contribute to the initial conditions for Wilson coefficients at this order. However, as we will see soon, such insertions play a role in the evaluation of the anomalous dimension matrix involving QCD penguin operators already at this order. This shows again that the RG analysis goes beyond the ordinary perturbation theory.

Comparing (6.202) and (6.204) and using the unitarity relation $\lambda_u + \lambda_c = -\lambda_t$, we determine C_P to be

$$C_P = \frac{\alpha_s(M_W)}{8\pi}[E_0(x_t) - r]. \tag{6.205}$$

Downloaded from https://www.cambridge.org/core. UNIVERSIDAD AUTONOMA METROPOLITANA, on 18 Nov 2026 at 18:06:35, subject to the Cambridge Core terms of use, available at https://www.cambridge.org/core/terms. https://doi.org/10.1017/9781139524100.011

Inserting this result into (6.204), using the expression for Q_P in (6.203) and comparing the coefficient of λ_t with the one of (6.183), we derive the matching conditions (6.186)–(6.189).

Numerical Values for $C_i(\mu_b)$

With $\Lambda^{(5)}_{\overline{\rm MS}} = 225\,\text{MeV}$ corresponding to $\alpha_s(M_Z) = 0.118$ and choosing $\mu_b = 4.40\,\text{MeV}$, we find in the NDR scheme

$$C_1(\mu_b) = -0.184, \qquad C_2(\mu_b) = 1.078, \qquad \text{(NDR)}, \tag{6.206}$$

$$C_3(\mu_b) = -0.013, \qquad C_4(\mu_b) = -0.035, \qquad \text{(NDR)}, \tag{6.207}$$

$$C_5(\mu_b) = -0.009, \qquad C_6(\mu_b) = -0.041, \qquad \text{(NDR)}. \tag{6.208}$$

Let us make just a few comments:

- Penguin coefficients are much smaller than C_1 and C_2.
- The largest penguin coefficients are C_4 and C_6.
- A numerical analysis shows that in the range $m_{\rm t} = (170 \pm 15)\,\text{GeV}$ the $m_{\rm t}$ dependence of the QCD penguin coefficients can be neglected.

Threshold Effects in the Presence of Penguin Operators

In (5.120) we have given a formula for $\vec{C}(\mu)$ in the presence of flavor thresholds. This formula implies in particular that $\vec{C}_{f-1}(\mu_f) = \vec{C}_f(\mu_f)$ where μ_f is the threshold between an effective f-flavor theory and an effective theory with $f-1$ flavors. In the presence of penguin operators the matching is more involved. One finds now

$$\vec{C}_{f-1}(\mu_f) = \hat{M}(\mu_f)\vec{C}_f(\mu_f), \tag{6.209}$$

where $\hat{M}(\mu_f)$ is a matching matrix given by

$$\hat{M}(\mu_f) = \hat{1} + \frac{\alpha_s(\mu_f)}{4\pi}\delta\hat{r}^T. \tag{6.210}$$

The matrix $\delta\hat{r}^T$ can be found in section VID of [111]. With (6.209) the formula (5.120) generalizes to

$$\vec{C}(\mu) = \hat{U}_3(\mu,\mu_c)\hat{M}(\mu_c)\hat{U}_4(\mu_c,\mu_b)\hat{M}(\mu_b)\hat{U}_5(\mu_b,\mu_W)\vec{C}(\mu_W). \tag{6.211}$$

6.4.3 Explicit Calculation of 6×6 ADM

Preliminaries

It is time to do a real climb by calculating the matrix (6.194). This involves the operator insertions into the penguin diagrams and into the current-current diagrams. Because master formulas for the latter insertions have already been derived and applied for the case of (Q_1, Q_2) in the previous section, we begin this climb by discussing the penguin insertions.

Downloaded from https://www.cambridge.org/core. UNIVERSIDAD AUTONOMA METROPOLITANA, on 18 Nov 2026 at 18:06:35, subject to the Cambridge Core terms of use, available at https://www.cambridge.org/core/terms. https://doi.org/10.1017/9781139524100.011

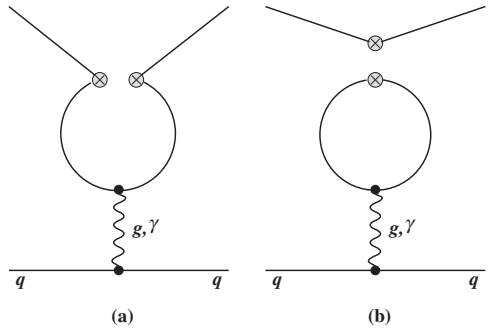


Figure 6.12 One-loop penguin diagrams in the effective theory.

Penguin Insertions: Generalities

The two diagrams contributing to the anomalous dimension matrix of $(Q_1, \ldots . Q_6)$ through the penguin insertions are given in Figure 6.12. We observe that two types of insertions of a given operator into a penguin diagram are possible. Type A insertions represented by diagram (a) are constructed by joining two quarks belonging to two different disconnected parts of an operator and attaching the gluon to the resulting internal quark line. For instance, in the case of $(\bar{c}b)_{V-A}(\bar{s}c)_{V-A}$, one can join $\bar{c}$ and c into one line. Type B insertions represented by the diagram (b) are constructed by joining two quarks belonging to the same part of a given operator and attaching the gluon to the resulting quark loop. For instance, in the case of $(\bar{c}c)_{V-A}(\bar{s}b)_{V-A}$ we have a c-quark loop. Because gluons conserve flavor, penguin insertions are only possible if a given operator contains at least two quarks with the same flavor. Note that in the case of $(\bar{s}b)_{V-A}(\bar{s}s)_{V-A}$ both types of insertions are possible and have to be taken into account. Finally, the bottom quark line attached to the lower end of the gluon represents any quark present in the effective theory. In calculating the contribution of a given diagram one has to sum over all quark flavors on this line. In this manner the penguin operators are generated from insertions of operators into penguin diagrams. It is clear from the last statement that the insertion of any operator $(Q_1, \ldots . Q_6)$ into the penguin diagrams of Figure 6.12 always results in a linear combination of penguin operators. That is, penguin operators mix under renormalization among themselves, and the current-current operators mix into penguin operators, but the mixing of penguin operators into Q_1 and Q_2 does not take place. This last feature is not affected by the insertions of penguin operators into the current-current diagrams of Figure 5.3 as we will see explicitly later. Consequently, without any calculation we can state that

$$(\hat{\gamma})_{i1} = (\hat{\gamma})_{i2} = 0 \qquad i = 3, ..6, \tag{6.212}$$

and this is also true for the electroweak penguins discussed in the last part of this section as well as other penguins discussed in the rest of this book.

After these general remarks, let us derive two master formulas for penguin insertions of type A and B, which are analogous to the three master formulas for current-current insertions given in (5.150)–(5.152).

Downloaded from https://www.cambridge.org/core. UNIVERSIDAD AUTONOMA METROPOLITANA, on 18 Nov 2026 at 18:06:35, subject to the Cambridge Core terms of use, available at https://www.cambridge.org/core/terms. https://doi.org/10.1017/9781139524100.011

As in the case of current-current insertions, we consider an arbitrary operator with the color structure $\hat{V}_1 \otimes \hat{V}_2$ and the Dirac structure $\Gamma_1 \otimes \Gamma_2$. Dropping the external spinors, the insertion of this operator into the penguin vertex in the diagram (a) of Figure 6.12 gives

$$W_\lambda = -ig\mu^\varepsilon \hat{V}_1 t^a \hat{V}_2 I^{\mu\nu} T^\lambda_{\mu\nu}, \tag{6.213}$$

where

$$T^\lambda_{\mu\nu} = \Gamma_1 \gamma_\nu \gamma_\lambda \gamma_\mu \Gamma_2, \tag{6.214}$$

and

$$I^{\mu\nu} = \int \frac{d^D k}{(2\pi)^D} \frac{k^\nu (k-q)^\mu}{k^2 (k-q)^2} = -\frac{i}{16\pi^2} \left[\frac{1}{\varepsilon}\right] \left[\frac{1}{6} q^\mu q^\nu + q^2 \frac{g^{\mu\nu}}{12}\right], \tag{6.215}$$

with q being the gluon momentum. In evaluating $I^{\mu\nu}$ we have kept only the divergent part, as we are only interested in the anomalous dimensions.

The master formula for type A insertions is then obtained by including the gluon propagator and the lower vertex in the penguin diagram (a) of Figure 6.12. We find

$$\mathcal{P}_A = -C_A \frac{\alpha_s}{4\pi} \left[\frac{1}{\varepsilon}\right] \left[\frac{1}{6} \frac{q^\mu q^\nu}{q^2} + \frac{g^{\mu\nu}}{12}\right] \Gamma_1 \gamma_\nu \gamma_\lambda \gamma_\mu \Gamma_2 \otimes \gamma^\lambda \,, \tag{6.216}$$

where the color factor is given by

$$\boxed{C_A = \hat{V}_1 t^a \hat{V}_2 \otimes t^a \,.} \tag{6.217}$$

It is understood that the Dirac and color structures on the l.h.s. of $\otimes$ are sandwiched between free spinors belonging to the inserted operator, and $\gamma^\lambda t^a$ standing on the r.h.s. of $\otimes$ are sandwiched between the spinors representing the bottom line of the penguin diagram. Formula (6.216) serves to calculate the coefficients $(b_1)_{ij}$ in the master formula (5.128). We will demonstrate this explicitly later.

The master formula for type B insertions can be derived in an analogous manner. We find

$$\mathcal{P}_B = C_B \frac{\alpha_s}{4\pi} \left[\frac{1}{\varepsilon}\right] \left[\frac{1}{6} \frac{q^\mu q^\nu}{q^2} + \frac{g^{\mu\nu}}{12}\right] \mathrm{Tr}(\Gamma_1 \gamma_\mu \gamma_\lambda \gamma_\nu) \Gamma_2 \otimes \gamma^\lambda, \tag{6.218}$$

where

$$\boxed{C_B = \mathrm{Tr}(\hat{V}_1 t^a) \hat{V}_2 \otimes t^a,} \tag{6.219}$$

with "Tr" in (6.219) standing for the trace in the color space. Note that in this formula we have closed the part $\hat{V}_1 \Gamma_1$ of the inserted operator in the loop. If the part $\hat{V}_2 \Gamma_2$ is closed instead, the indices "1" and "2" in (6.218) and (6.219) should be interchanged. The rules for the incorporation of the external spinors into (6.218) should be evident in view of the comments made after (6.217). The difference in the overall sign compared to (6.216) is a consequence of "-1" for the fermion loop.

Downloaded from https://www.cambridge.org/core. UNIVERSIDAD AUTONOMA METROPOLITANA, on 18 Nov 2026 at 18:06:35, subject to the Cambridge Core terms of use, available at https://www.cambridge.org/core/terms. https://doi.org/10.1017/9781139524100.011

Explicit Calculation of Penguin Insertions

Let us apply our master formulas to the case of the operator

$$Q_2 = (\bar{c}_\alpha b_\alpha)_{V-A}(\bar{s}_\beta c_\beta)_{V-A}, \tag{6.220}$$

for which we have

$$\hat{V}_1 \otimes \hat{V}_2 = \mathbf{1} \qquad \Gamma_1 = \Gamma_2 = \gamma_\tau(1-\gamma_5). \tag{6.221}$$

The flavor structure in (6.220) tells us that only type A insertions are possible. We use therefore the master formula (6.216). As we are only interested in the coefficient of $1/\varepsilon$, we calculate all Dirac structures in $D = 4$ dimensions. This gives

$$\left[\frac{1}{6}\frac{q^\mu q^\nu}{q^2} + \frac{g^{\mu\nu}}{12}\right]\Gamma_1\gamma_\nu\gamma_\lambda\gamma_\mu\Gamma_2 = \frac{4}{3}\left[\gamma_\lambda - \frac{q_\lambda \not{q}}{q^2}\right](1-\gamma_5), \tag{6.222}$$

where we have used the identity

$$\not{q}\gamma_\lambda \not{q} = 2q_\lambda \not{q} - q^2\gamma_\lambda. \tag{6.223}$$

The term $q_\lambda \not{q}/q^2$ does not contribute here, as using the Dirac equation one has $\bar{s} \not{q} b = 0$ for massless quarks. As discussed in Section 6.2, more care is needed when magnetic penguins corresponding to dipole operators are considered and m_b has to be kept.

Dropping then the second term on the r.h.s. of (6.222), using

$$C_A = t^a \otimes t^a = \frac{1}{2}\left[\tilde{\mathbf{1}} - \frac{1}{N}\mathbf{1}\right], \tag{6.224}$$

with $\tilde{\mathbf{1}}$ defined in (5.143) and inserting the relevant spinors we arrive at

$$\mathcal{P}_A(Q_2) = -\frac{\alpha_s}{4\pi}\left[\frac{1}{\varepsilon}\right]\left[\frac{2}{3}\right]\left[\tilde{\mathbf{1}} - \frac{1}{N}\mathbf{1}\right][\bar{s}_\alpha\gamma_\lambda(1-\gamma_5)b_\beta] \otimes \sum_q \bar{q}_\gamma\gamma^\lambda q_\delta. \tag{6.225}$$

Next we decompose γ^λ on the r.h.s. of $\otimes$ into $V-A$ and $V+A$ parts

$$\gamma^\lambda = \frac{1}{2}\gamma^\lambda(1-\gamma_5) + \frac{1}{2}\gamma^\lambda(1+\gamma_5), \tag{6.226}$$

which allows to express (6.225) in terms of the penguin operators

$$\mathcal{P}_A(Q_2) = -\frac{\alpha_s}{4\pi}\left[\frac{1}{\varepsilon}\right]\left[\frac{1}{3}\right]\left[Q_4 + Q_6 - \frac{1}{N}(Q_3 + Q_5)\right]. \tag{6.227}$$

The contribution of penguin insertions to the coefficients $(b_1)_{2j}$ relevant for the master formula (5.128) are consequently given by

$$\boxed{(b_1)^P_{23} = (b_1)^P_{25} = \frac{1}{3N}, \qquad (b_1)^P_{24} = (b_1)^P_{26} = -\frac{1}{3}.} \tag{6.228}$$

We next consider Q_1 and rewrite it using Fierz reordering as

$$Q_1 = (\bar{c}_\alpha c_\alpha)_{V-A}(\bar{s}_\beta b_\beta)_{V-A}, \tag{6.229}$$

Downloaded from https://www.cambridge.org/core. UNIVERSIDAD AUTONOMA METROPOLITANA, on 18 Nov 2026 at 18:06:35, subject to the Cambridge Core terms of use, available at https://www.cambridge.org/core/terms. https://doi.org/10.1017/9781139524100.011

so that the color and Dirac structures are again given by (6.221). This time only type B insertions are possible. However, $\mathrm{Tr}(t^a) = 0$ and consequently the color factor in (6.219) vanishes. Thus

$$\mathcal{P}_B(Q_1) = 0, \tag{6.230}$$

implying

$$\boxed{(b_1)^P_{13} = (b_1)^P_{14} = (b_1)^P_{15} = (b_1)^P_{16} = 0.} \tag{6.231}$$

In the case of Q_3, the type B insertion vanishes as in the case of Q_1, but now two type-A insertions are possible. One involves the internal b quark, the other the s quark. Because gluons are flavor-blind and Q_3 has the same color and Dirac structures as Q_2, we find immediately

$$\mathcal{P}_A(Q_3) = 2\mathcal{P}_A(Q_2). \tag{6.232}$$

Consequently, using (6.228), we find

$$\boxed{(b_1)^P_{33} = (b_1)^P_{35} = \frac{2}{3N}, \qquad (b_1)^P_{34} = (b_1)^P_{36} = -\frac{2}{3}.} \tag{6.233}$$

Next comes Q_4. Performing Fierz reordering, we have

$$Q_4 = \sum_q (\bar{s}_\alpha q_\alpha)_{V-A}(\bar{q}_\beta b_\beta)_{V-A}. \tag{6.234}$$

The type B insertions involving s and b quarks vanish as in the case of Q_1. On the other hand, we have f type A insertions involving all quark flavors. Thus

$$\mathcal{P}_A(Q_4) = f\mathcal{P}_A(Q_2) \tag{6.235}$$

and

$$\boxed{(b_1)^P_{43} = (b_1)^P_{45} = \frac{f}{3N}, \qquad (b_1)^P_{44} = (b_1)^P_{46} = -\frac{f}{3}.} \tag{6.236}$$

The penguin insertions of Q_5 vanish. The type B insertions vanish because of $\mathrm{Tr}(t^a) = 0$. The type A insertions vanish because now

$$\Gamma_1 = \gamma_\tau(1-\gamma_5)\,, \qquad \Gamma_2 = \gamma_\tau(1+\gamma_5), \tag{6.237}$$

and the Dirac structure in the master formula (6.216) vanishes. Thus

$$\boxed{(b_1)^P_{53} = (b_1)^P_{54} = (b_1)^P_{55} = (b_1)^P_{56} = 0\,.} \tag{6.238}$$

Finally, the insertions of Q_6 have to be considered. Performing Fierz reordering, we have

$$Q_6 = -2\sum_q (\bar{s}_\alpha(1+\gamma_5)q_\alpha)(\bar{q}_\beta(1-\gamma_5)b_\beta), \tag{6.239}$$

implying

$$\hat{V}_1 \otimes \hat{V}_2 = \mathbf{1}, \qquad \Gamma_1 = (1+\gamma_5), \qquad \Gamma_2 = (1-\gamma_5). \tag{6.240}$$

Downloaded from https://www.cambridge.org/core. UNIVERSIDAD AUTONOMA METROPOLITANA, on 18 Nov 2026 at 18:06:35, subject to the Cambridge Core terms of use, available at https://www.cambridge.org/core/terms. https://doi.org/10.1017/9781139524100.011

Again, as in the case of Q_4, the type B insertions vanish. The type A insertion of Q_6 is expected at first sight to give a different result than the one of Q_4 because of the different Dirac structure. However, the application of the master formula (6.216) gives

$$\mathcal{P}_A(Q_6) = \mathcal{P}_A(Q_4), \tag{6.241}$$

and consequently

$$\boxed{(b_1)^P_{63} = (b_1)^P_{65} = \frac{f}{3N}, \qquad (b_1)^P_{64} = (b_1)^P_{66} = -\frac{f}{3}.} \tag{6.242}$$

Explicit Calculation of Current-Current Insertions

In the previous chapter we calculated the 2×2 anomalous dimension matrix for the pair (Q_1, Q_2) by inserting these operators into the current-current diagrams of Figure 5.3. Using the master formulas (5.150)–(5.152) for these diagrams together with the basic formula (5.128), we have found the matrix (5.78), which as seen in the left upper corner of (6.194) constitutes a part of the 6×6 matrix we are trying to reproduce.

What remains to be done are the insertions of the penguin operators into the current-current diagrams. The case of the pair (Q_3, Q_4) is simple. From the point of view of current-current insertions the pair (Q_3, Q_4) behaves as (Q_1, Q_2), and we can write immediately

$$\boxed{(b_1)^{cc}_{33} = 2C_F + \frac{3}{N}, \qquad (b_1)^{cc}_{34} = -3,} \tag{6.243}$$

$$\boxed{(b_1)^{cc}_{43} = -3, \qquad (b_1)^{cc}_{44} = 2C_F + \frac{3}{N}.} \tag{6.244}$$

The case of Q_5 and Q_6 operators is different as they have the $(V-A)\otimes(V+A)$ structure. Let us consider Q_5 first. Using master formulas (5.150)–(5.152) for

$$\hat{V}_1 \otimes \hat{V}_2 = \mathbf{1}, \qquad \Gamma_1 = \gamma_\tau(1-\gamma_5), \qquad \Gamma_2 = \gamma_\tau(1+\gamma_5)\,, \tag{6.245}$$

we arrive at

$$\sum_i \mathcal{D}_i(Q_5) = \frac{\alpha_s}{4\pi}\frac{1}{\varepsilon}\Gamma_1 \otimes \Gamma_2 \left[C_a^{(1)} + C_a^{(2)} - (C_b^{(1)} + C_b^{(2)}) + 4(C_c^{(1)} + C_c^{(2)})\right] \tag{6.246}$$

with color factors $C_i^{(j)}$ given in (5.163) and (5.164).

To perform the reduction of Dirac structures in the master formulas (5.150)–(5.152) we had to generalize the Greek method to the $(V-A)\otimes(V+A)$ operators. In this case $\otimes$ should be replaced by 1 as otherwise the Dirac structures would identically vanish. Now the coefficients (4,16,4) in (5.157)–(5.159) are replaced by (4,4,16), respectively, which implies a different weighting of the color factors in (6.246) relative to (5.162). Noting that Q_5 is represented by $\mathbf{1}$ and Q_6 by $\tilde{\mathbf{1}}$ we obtain from (6.246)

$$\boxed{(b_1)^{cc}_{55} = 2C_F - \frac{3}{N}, \qquad (b_1)^{cc}_{56} = 3.} \tag{6.247}$$

Downloaded from https://www.cambridge.org/core. UNIVERSIDAD AUTONOMA METROPOLITANA, on 18 Nov 2026 at 18:06:35, subject to the Cambridge Core terms of use, available at https://www.cambridge.org/core/terms. https://doi.org/10.1017/9781139524100.011

Finally, we consider Q_6. Here it is useful to use the form (6.239). As Γ_i are now given by (6.240), one easily finds that the usual Greek method with $\otimes = \gamma_\tau$ applies. The master formulas (5.150)–(5.152) then give

$$\sum_i \mathcal{D}_i(Q_6) = \frac{\alpha_s}{4\pi}\frac{1}{\varepsilon}[-2\Gamma_1 \otimes \Gamma_2]\left[4(C_a^{(1)} + C_a^{(2)}) - (C_b^{(1)} + C_b^{(2)}) + (C_c^{(1)} + C_c^{(2)})\right] . \tag{6.248}$$

The weighting of color factors differs from the cases Q_2 and Q_5. In particular, using (5.164) we find that the two last terms in the square bracket cancel each other. Effectively then only the insertions of Q_6 into the diagrams (a) of Figure 5.3 and its symmetric counterpart contribute. However, contrary to the case of the operators Q_{1-5} this contribution will not be canceled by the δ_{ij} term in (5.128) as now $C_a^{(j)}$ are multiplied by 4 instead of 1. Consequently, noting that in this case Q_6 is represented by $\mathbf{1}$ and Q_5 by $\tilde{\mathbf{1}}$ we find

$$\boxed{(b_1)^{cc}_{65} = 0, \qquad (b_1)^{cc}_{66} = 8C_F.} \tag{6.249}$$

Putting Things Together

Let us add the results for penguin and current-current insertions obtained earlier and listed in white frames. Setting $N = 3$, we find the matrix $\hat{b}_1$ in (5.128):

$$\hat{b}_1 = \begin{pmatrix} 2C_F + 1 & -3 & 0 & 0 & 0 & 0 \\ -3 & 2C_F + 1 & \frac{1}{9} & -\frac{1}{3} & \frac{1}{9} & -\frac{1}{3} \\ 0 & 0 & 2C_F + \frac{11}{9} & -\frac{11}{3} & \frac{2}{9} & -\frac{2}{3} \\ 0 & 0 & -3 + \frac{f}{9} & 2C_F + 1 - \frac{f}{3} & \frac{f}{9} & -\frac{f}{3} \\ 0 & 0 & 0 & 0 & 2C_F - 1 & 3 \\ 0 & 0 & \frac{f}{9} & -\frac{f}{3} & \frac{f}{9} & 8C_F - \frac{f}{3} \end{pmatrix}. \tag{6.250}$$

Inserting this matrix into the one-loop master formula (5.128), we reproduce the full 6×6 matrix in (6.194). Fantastic! We have reproduced all the magic numbers in this matrix. This is almost like reaching the top of Monte Rosa.

We hope that this long exercise and the corresponding exercise for current-current operators in the previous chapter were useful for those readers who have never calculated anomalous dimension matrices. But there is another lesson from these exercises. The corresponding two-loop calculations of current-current and penguin insertions involving many more diagrams, more complicated color factors, and evanescent operators are truly horrible. Moreover, at two-loops we have to use, at least in NDR and HV schemes, the Dirac algebra in $D \neq 4$, and Fierz reordering is not permitted unless we introduce new evanescent operators, the so-called Fierz vanishing evanescent operators, which complicates the calculations further.

Thus two-loop calculations are not like climbing Mont Blanc but rather Mount Everest. They take several months rather than a day or two. The NNLO calculations take sometimes

Downloaded from https://www.cambridge.org/core. UNIVERSIDAD AUTONOMA METROPOLITANA, on 18 Nov 2026 at 18:06:35, subject to the Cambridge Core terms of use, available at https://www.cambridge.org/core/terms. https://doi.org/10.1017/9781139524100.011

a year or even longer and can be compared to climbing the K2 or flying to the moon. Consequently it is advisable for beginners to take an experienced guide to climb these Himalayas. Fortunately the guides in physics, as opposed to those in the real Himalayas, are doing it for free. On the other hand, the experienced guides these days as opposed to 1990s, when many two-loop calculations were done by hand, are doing such calculations entirely by Mathematica. While this certainly saves time, it prevents, in my view, to feel the details of the calculations and in this manner also to see the beauty of various structures and cancellations of various terms. Moreover, it is often easier to find an error. Yet, these comments apply only to one-loop and two-loop calculations. At three-loops, Mathematica or other computer programs have to be used.

6.4.4 Electroweak Penguins

Operators

The inclusion of the electroweak penguins and box diagrams of Figure 6.11 generates two additional operators, Q_7 and Q_9. With respect to the color structure they are analogous to Q_5 and Q_3 operators, respectively. When QCD effects are also taken into account, two additional operators, Q_8 and Q_{10}, are needed to close the system under renormalization. They are analogous to Q_6 and Q_4, respectively. The full set of operators necessary for the description of $\Delta F = 1$ nonleptonic decays including electroweak effects consists then of ten operators. The four electroweak penguin operators relevant for $\Delta B = 1$ decays with $\Delta S = 1$ are given by

$$Q_7 = \frac{3}{2}\,(\bar{s}b)_{V-A} \sum_{q=u,d,s,c,b} e_q\,(\bar{q}q)_{V+A}, \tag{6.251}$$

$$Q_8 = \frac{3}{2}\,(\bar{s}_\alpha b_\beta)_{V-A} \sum_{q=u,d,s,c,b} e_q\,(\bar{q}_\beta q_\alpha)_{V+A}, \tag{6.252}$$

$$Q_9 = \frac{3}{2}\,(\bar{s}b)_{V-A} \sum_{q=u,d,s,c,b} e_q\,(\bar{q}q)_{V-A}, \tag{6.253}$$

$$Q_{10} = \frac{3}{2}\,(\bar{s}_\alpha b_\beta)_{V-A} \sum_{q=u,d,s,c,b} e_q\,(\bar{q}_\beta q_\alpha)_{V-A}. \tag{6.254}$$

Here, α, β denote color indices. The overall factor 3/2 is introduced for convenience. The charge e_q is the charge of the quark coupled to the lower vertex of the photon or Z-propagator.

Wilson Coefficients

To generate the electroweak penguin operators Q_7–Q_{10}, it is sufficient to include the photon penguin together with the relevant QCD renormalization. However, to keep the

Downloaded from https://www.cambridge.org/core. UNIVERSIDAD AUTONOMA METROPOLITANA, on 18 Nov 2026 at 18:06:35, subject to the Cambridge Core terms of use, available at https://www.cambridge.org/core/terms. https://doi.org/10.1017/9781139524100.011

gauge invariance also Z^0-penguins and box diagrams have to be included at the NLO level. The latter two sets of diagrams involving only heavy fields $(W^\pm, Z^0, t)$ contribute only to the Wilson coefficients at $\mu = O(M_{\rm W})$ and have no impact on the renormalization group evolution down to low-energy scales, as at these scales being integrated out $(W^\pm, Z^0, t)$ do not appear as dynamical degrees of freedom. On the other hand, the inclusion of Z^0-penguins introduces a strong m_t-dependence into Wilson coefficients of the electroweak penguin operators, which in several cases has important phenomenological implications. We will discuss several of them in the phenomenological parts of this book. Here we give some information on the Wilson coefficients of electroweak penguin operators.

The matching at $\mu_W = M_{\rm W}$ gives in the presence of the electroweak penguin and box diagrams the values of $C_i(M_{\rm W})$ with $i = 1, ..10$. In the NDR scheme they are given by:

$$C_1(M_{\rm W}) = \frac{11}{2}\,\frac{\alpha_s(M_{\rm W})}{4\pi}, \tag{6.255}$$

$$C_2(M_{\rm W}) = 1 - \frac{11}{6}\,\frac{\alpha_s(M_{\rm W})}{4\pi} - \frac{35}{18}\,\frac{\alpha}{4\pi}, \tag{6.256}$$

$$C_3(M_{\rm W}) = -\frac{\alpha_s(M_{\rm W})}{24\pi}\widetilde{E}_0(x_t) + \frac{\alpha}{6\pi}\frac{1}{\sin^2\theta_W}\left[2B_0(x_t) + C_0(x_t)\right], \tag{6.257}$$

$$C_4(M_{\rm W}) = \frac{\alpha_s(M_{\rm W})}{8\pi}\widetilde{E}_0(x_t), \tag{6.258}$$

$$C_5(M_{\rm W}) = -\frac{\alpha_s(M_{\rm W})}{24\pi}\widetilde{E}_0(x_t), \tag{6.259}$$

$$C_6(M_{\rm W}) = \frac{\alpha_s(M_{\rm W})}{8\pi}\widetilde{E}_0(x_t), \tag{6.260}$$

$$C_7(M_{\rm W}) = \frac{\alpha}{6\pi}\left[4C_0(x_t) + \widetilde{D}_0(x_t)\right], \tag{6.261}$$

$$C_8(M_{\rm W}) = 0, \tag{6.262}$$

$$C_9(M_{\rm W}) = \frac{\alpha}{6\pi}\left[4C_0(x_t) + \widetilde{D}_0(x_t) + \frac{1}{\sin^2\theta_W}(10B_0(x_t) - 4C_0(x_t))\right], \tag{6.263}$$

$$C_{10}(M_{\rm W}) = 0. \tag{6.264}$$

The m_t-dependent one-loop functions are known to us from previous sections, and

$$\widetilde{D}_0(x_t) = D_0(x_t) - \frac{4}{9} \tag{6.265}$$

with the constant $-4/9$ characteristic for the NDR scheme. It is absent in the HV scheme. We note that the presence of electroweak effects modifies the values of $C_2(M_{\rm W})$ and $C_3(M_{\rm W})$ by small $O(\alpha)$ corrections. We also note that $C_8(M_{\rm W}) = C_{10}(M_{\rm W}) = 0$. For $\mu \neq M_{\rm W}$ nonvanishing C_8 and C_{10} are generated through QCD effects.

The anomalous dimension matrices are 10×10:

$$\hat{\gamma}(\alpha_s, \alpha) = \hat{\gamma}_s^{(0)}\frac{\alpha_s}{4\pi} + \hat{\gamma}_e^{(0)}\frac{\alpha}{4\pi} + \hat{\gamma}_s^{(1)}\left(\frac{\alpha_s}{4\pi}\right)^2 + \hat{\gamma}_{se}^{(1)}\frac{\alpha_s}{4\pi}\frac{\alpha}{4\pi} \tag{6.266}$$

Downloaded from https://www.cambridge.org/core. UNIVERSIDAD AUTONOMA METROPOLITANA, on 18 Nov 2026 at 18:06:35, subject to the Cambridge Core terms of use, available at https://www.cambridge.org/core/terms. https://doi.org/10.1017/9781139524100.011

with $\gamma_s^{(0)}$ and $\gamma_s^{(1)}$ being 10×10 generalizations of the corresponding 6×6 matrices considered previously. Because now $O(\alpha)$ effects are included in the coefficients at scales $O(M_W)$, the anomalous dimension matrix must also include $O(\alpha)$ contributions, which are represented by $\hat{\gamma}_e^{(0)}$ and $\hat{\gamma}_{se}^{(1)}$ at LO and NLO, respectively. The four matrices in (6.266) can be found in [111], where the references to the original literature are given. See also the review of all NLO and NNLO QCD calculations for weak decays until the summer of 2014 [77].

The calculation of the 6×6 submatrix of $\hat{\gamma}_s^{(0)}$ has been presented in detail earlier. The evaluation of $\hat{\gamma}_e^{(0)}$ proceeds in an analogous manner except that the color factors have to be properly replaced by electric charges and the closed fermion loops coupled to the photon have to be multiplied by $N = 3$. Any reader who succeeded in calculating $\hat{\gamma}_s^{(0)}$ should have no difficulty in calculating within few hours the matrix $\hat{\gamma}_e^{(0)}$. This is a very nice exercise indeed. The calculations of $\hat{\gamma}_s^{(1)}$ and $\hat{\gamma}_{se}^{(1)}$ are even nicer but take more time. Typically six months for $\hat{\gamma}_s^{(1)}$ and then a month for $\hat{\gamma}_{se}^{(1)}$ if the calculation is done by hand. This was in fact the case in 1992, but these days one can do such calculations much faster by using Mathematica.

Due to the simultaneous appearance of α and α_s, the RG analysis is more involved than the one discussed until now. In particular the evolution matrix takes now the general form

$$\hat{U}(m_1, m_2, \alpha) = \hat{U}(m_1, m_2) + \frac{\alpha}{4\pi} \hat{R}(m_1, m_2). \tag{6.267}$$

Here $\hat{U}(m_1, m_2)$ represents the pure QCD evolution matrix given in (5.113). $\hat{R}(m_1, m_2)$ describes the additional evolution in the presence of electromagnetic interactions. It includes both LO and NLO corrections. Let us recall that $\hat{U}(m_1, m_2)$ sums the logarithms $(\alpha_s t)^n$ and $\alpha_s(\alpha_s t)^n$ with $t = \ln(m_2^2/m_1^2)$. On the other hand, $\hat{R}(m_1, m_2)$ sums the logarithms $t(\alpha_s t)^n$ and $(\alpha_s t)^n$. The expression for $\hat{R}(m_1, m_2)$ is rather complicated. It can be found in [111]. The Wilson coefficients are then found by using

$$\vec{C}(\mu_b) = \hat{U}_5(\mu_b, M_W, \alpha)\vec{C}(M_W), \tag{6.268}$$

with $\vec{C}(M_W)$ given in (6.255)–(6.255).

6.4.5 Numerical Values of Wilson Coefficients

With $\Lambda_{\overline{\text{MS}}}^{(5)} = 225\,\text{MeV}$ corresponding to $\alpha_s(M_Z) = 0.118$, and choosing $\mu_b = 4.40\,\text{MeV}$ we find in the NDR scheme

$$C_7(\mu_b) = -0.002\,\alpha, \qquad C_8(\mu_b) = 0.054\,\alpha, \qquad \text{(NDR)}, \tag{6.269}$$

$$C_9(\mu_b) = -1.292\,\alpha, \qquad C_{10}(\mu_b) = 0.263\alpha, \qquad \text{(NDR)}. \tag{6.270}$$

Let us make just a few comments:

- Electroweak penguin coefficients being $O(\alpha)$ are smaller than C_{1-6} coefficients. A notable exception is the coefficient C_9, which is in the ballpark of the smallest QCD penguin coefficients C_3 and C_5. It is the operator Q_9 that is the dominant electroweak penguin in nonleptonic B decays [148]. With decreasing μ the coefficient C_8 increases

Downloaded from https://www.cambridge.org/core. UNIVERSIDAD AUTONOMA METROPOLITANA, on 18 Nov 2026 at 18:06:35, subject to the Cambridge Core terms of use, available at https://www.cambridge.org/core/terms. https://doi.org/10.1017/9781139524100.011

considerably. While its role in B-decays can be fully neglected, it plays an important role in the CP violation in $K \to \pi\pi$ decays, where also its hadronix matrix element is large. We will return to this operator in the context of the analysis of the ratio ε'/ε in Chapter 10.

- A numerical analysis shows that in contrast to $C_1, \ldots, C_6$, the additional coefficients $C_7, \ldots, C_{10}$ increase strongly with m_t. This strong m_t dependence originates in the Z^0-penguin represented by the function $C_0(x_t)$ in (6.12). Even in the range $m_t = (170 \pm 15)\,\text{GeV}$ with in/decreasing m_t there is a relative variation of $O(\pm 19\%)$ and $O(\pm 10\%)$ for the absolute values of C_8 and $C_{9,10}$, respectively. In obtaining the preceding values, we have just set $m_t = 170\,\text{GeV}$.

6.5 $B \to X_s\gamma$ Decay

6.5.1 General Remarks

The inclusive rare decay $B \to X_s\gamma$ played an important role in constraining NP in the last three decades because both the experimental data and theory have been in good shape for some time. Therefore it is important to discuss this decay in some detail in this book. In particular, we should describe the structure of QCD effects in this decay even if, as we will soon see, this structure is rather complicated. But the QCD effects, as opposed to rare K and B decays with leptons in the final state, are very large, and not including them would totally misrepresent the complete calculation. Therefore, already for almost thirty years several groups of theorists have made a big effort to calculate the branching ratio for $B \to X_s\gamma$, and as of 2020 this decay is known including NNLO corrections.

The experimentalists study the decays of B^+ and B_d^0 and using isospin symmetry quote the result summarized here. The operators given in (6.274) have an incoming b-quark, which means that the initial particle is really B^- and $\bar{B}_d^0$, and often in theoretical papers $\bar{B} \to X_s\gamma$ is found. But for the study of branching ratio in question these differences are irrelevant, and to simplify the notation we will just use B in this section. However, when discussing CP-asymmetries in other decays in later chapters, we have to be more explicit to get the correct signs of the asymmetries in question.

Before entering the details let us right away quote the present SM prediction and the most recent data. On the theory side we have a rather precise prediction within the SM [149]

$$\mathcal{B}(B \to X_s\gamma)_{\text{SM}} = (3.36 \pm 0.23) \times 10^{-4}, \tag{6.271}$$

for $E_\gamma \geq 1.6\,\text{GeV}$. A detailed historical account of NLO and NNLO calculations leading to this result can be found in [77].

Also experimentalists made impressive progress in measuring this branching ratio, reaching the accuracy of 4.5% [150]

$$\mathcal{B}(B \to X_s\gamma)_{\text{exp}} = (3.32 \pm 0.15) \times 10^{-4}, \tag{6.272}$$

Downloaded from https://www.cambridge.org/core. UNIVERSIDAD AUTONOMA METROPOLITANA, on 18 Nov 2026 at 18:06:35, subject to the Cambridge Core terms of use, available at https://www.cambridge.org/core/terms. https://doi.org/10.1017/9781139524100.011

where again $E_\gamma \geq 1.6\,\text{GeV}$ has been imposed. One expects that in this decade the SuperKEKB will reach the accuracy of 3% so that very precise tests of the SM and its extensions will be possible. In fact, comparing the theory with experiment we observe an impressive agreement of the SM with the data although with present uncertainties there is still some room for NP contributions.

To appreciate these results we will now describe some aspects of the dynamics behind the result in (6.271). We will succeed in describing the leading order in some detail. It will also be possible to present the general structure of the NLO corrections. But any useful description of the calculation of NNLO corrections, which finally lead to (6.271), is beyond the scope of this book.

6.5.2 General Structure

The inclusive decay $B \to X_s\gamma$ with an on-shell γ is governed by the operator $Q_{7\gamma}$, which originates in the photon-penguin vertex, shown on the left in Figure 6.13, with $q^2 = 0$, where q_μ is the momentum of the emitted photon. In addition, the diagrams in which the photon couples to $W^\pm$ are present. They are analogous to the ones involved in the calculation of Z-penguins and are shown in Figure 6.7. To obtain a nonvanishing result, one has to keep the external b-quark mass as well as external momenta. This *mass insertion* together with the expansion to second-order in external momenta generates $Q_{7\gamma}$, which due to the appearance of $\sigma^{\mu\nu}$ is known under the name of *the magnetic photon penguin.* The corresponding gluon-penguin vertex with $q^2 = 0$, shown on the right in Figure 6.13, results in *the magnetic gluon penguin operator* Q_{8G}, which plays the dominant role in the inclusive $B \to X_s$ gluon decay. This operator plays a subleading role in the $B \to X_s\gamma$ decay, but it has to be taken into account when QCD corrections are included.

The renormalization group analysis of $B \to X_s\gamma$ involves in addition to $Q_{7\gamma}$ and Q_{8G} also the operators $Q_1 \ldots Q_6$ discussed previously and given in (6.179)–(6.182). Consequently, the effective Hamiltonian for $B \to X_s\gamma$ at scales $\mu_b = O(m_b)$ reads

$$\mathcal{H}_{\text{eff}}(b \to s\gamma) = -\frac{4G_{\text{F}}}{\sqrt{2}} V_{ts}^* V_{tb} \left[\sum_{i=1}^{6} C_i(\mu_b) Q_i + C_{7\gamma}(\mu_b) Q_{7\gamma} + C_{8G}(\mu_b) Q_{8G} \right], \quad (6.273)$$

where in view of $| V_{us}^* V_{ub} / V_{ts}^* V_{tb} | < 0.02$ we have neglected the term proportional to $V_{us}^* V_{ub}$.

The magnetic-penguin operators are given as follows[1]

$$\boxed{Q_{7\gamma} = \frac{e}{16\pi^2} m_b \bar{s}_\alpha \sigma^{\mu\nu} P_R b_\alpha F_{\mu\nu}, \qquad Q_{8G} = \frac{g_s}{16\pi^2} m_b \bar{s}_\alpha \sigma^{\mu\nu} P_R t^a_{\alpha\beta} b_\beta G^a_{\mu\nu}.} \quad (6.274)$$

[1] In some papers a different normalization of these operators is used. It is compensated by the change in Wilson coefficients relative to ours or by changing the overall factor in (6.273).

Downloaded from https://www.cambridge.org/core. UNIVERSIDAD AUTONOMA METROPOLITANA, on 18 Nov 2026 at 18:06:35, subject to the Cambridge Core terms of use, available at https://www.cambridge.org/core/terms. https://doi.org/10.1017/9781139524100.011

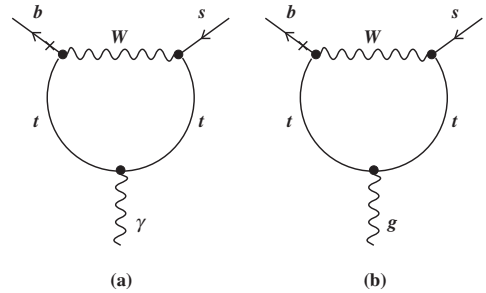


Figure 6.13 Magnetic photon (a) and gluon (b) penguins. The cross on the b signals that m_b has to be kept. The diagrams with photon coupling to $W^{\pm}$ are not shown. They are obtained from Z-penguin diagrams in Figure 6.7 by replacing Z with γ. We show them in Figure 17.1. From [29].

To derive the contribution of $Q_{7\gamma}$ to the Hamiltonian in (6.273), in the absence of QCD corrections, one multiplies the result of the first diagram in Figure 6.13 by "i" and makes the replacement (q_μ is the four-momentum of the emitted photon)

$$2i\sigma_{\mu\nu}q^\nu \to -\sigma^{\mu\nu}F_{\mu\nu}. \tag{6.275}$$

Analogous procedure gives the contribution of Q_{8G}.

It is the magnetic γ-penguin that plays the crucial role in this decay. However, the role of the dominant current-current operator Q_2 should not be underestimated. Indeed, the short-distance QCD effects involving in particular the mixing between Q_2 and $Q_{7\gamma}$ are very important in this decay. They are known [151, 152] to enhance $C_{7\gamma}(\mu_b)$ substantially, so that the resulting branching ratio $\mathcal{B}(B \to X_s\gamma)$ turns out to be by a factor of 3 higher than it would be without QCD effects.

A peculiar feature of the renormalization group analysis in $B \to X_s\gamma$ is that the mixing under infinite renormalization between the set $(Q_1 \dots Q_6)$ and the operators $(Q_{7\gamma}, Q_{8G})$ vanishes at the one-loop level. Consequently, to calculate the coefficients $C_{7\gamma}(\mu_b)$ and $C_{8G}(\mu_b)$ in the leading logarithmic approximation, two-loop calculations of $O(eg_s^2)$ and $O(g_s^3)$ are necessary. The corresponding NLO analysis requires the evaluation of the mixing in question at the three-loop level and four-loop contributions at the NNLO level. This peculiar feature caused that the first fully correct calculation of the leading anomalous dimension matrix relevant for this decay has been obtained only in 1993 [153, 154]. It has been confirmed subsequently in [155–157]. But the result exhibited a very large μ_b dependence in the branching ratios [158], which made the calculation of the NLO corrections mandatory.

The outline of such a calculation has been presented in 1993 [159], but only in 2002 the NLO corrections to $B \to X_s\gamma$ have been completed and summarized in [160]. Many different groups contributed to this result:

- The $O(\alpha_s)$ corrections to $C_{7\gamma}(\mu_W)$ and $C_{8G}(\mu_W)$, involving the gluon corrections to the diagrams in Figure 6.13, have been calculated in [117, 118, 128, 161, 162].

Downloaded from https://www.cambridge.org/core. UNIVERSIDAD AUTONOMA METROPOLITANA, on 18 Nov 2026 at 18:06:35, subject to the Cambridge Core terms of use, available at https://www.cambridge.org/core/terms. https://doi.org/10.1017/9781139524100.011

- The two-loop mixing in the sector $(Q_{7\gamma}, Q_{8G})$ has been calculated in [163, 164] and the three-loop mixing between the set $(Q_1 \dots Q_6)$ and the operators $(Q_{7\gamma}, Q_{8G})$ in [147, 164, 165].
- One-loop matrix elements $\langle s\gamma \text{gluon}|Q_i|b\rangle$ have been calculated in [166, 167], and the dominant contributions to the very difficult two-loop corrections to $\langle s\gamma|Q_i|b\rangle$ have been presented in [168, 169]. Only in 2002 has this result been confirmed in [170, 171], where the evaluation of additional small corrections from QCD penguin operators completed the NLO story.

But then it has been pointed out in [172] that the uncertainty in the scale of the charm-quark mass entering the evaluation of the matrix elements $\langle s\gamma|Q_i|b\rangle$ was significant at the NLO level implying the necessity of NNLO calculations. This means increasing the complexity of each of the three difficult parts just listed by much. In particular the four-loop mixing between the set $(Q_1 \dots Q_6)$ and the operators $(Q_{7\gamma}, Q_{8G})$ had to be calculated. This heroic effort was basically completed in 2006 in [173], and some refinements have been made since then. We refer to the historical review in [77] and to [149], where further references can be found.

We will now discuss some of these achievements in explicit terms. To demonstrate the importance of higher-order QCD calculations for this decay, it is instructive to discuss first the leading logarithmic approximation.

6.5.3 The Decay $B \to X_s\gamma$ in the Leading Log Approximation

Anomalous Dimension Matrix

In the presence of the magnetic penguin operators the 6×6 anomalous dimension matrix $\hat{\gamma}_s^{(0)}$ involving the operators $Q_1, \dots, Q_6$ is extended to a 8×8 matrix. The part of this matrix involving $Q_1, \dots, Q_6$ has been already discussed in Section 6.4. We will therefore concentrate our presentation on the remaining entries in this matrix.

We begin with the mixing between the sets $Q_1, \dots, Q_6$ and $Q_{7\gamma}, Q_{8G}$ in $\hat{\gamma}_s^{(0)}$. This mixing resulting from two-loop diagrams is generally regularization scheme dependent. This is certainly disturbing because the matrix $\hat{\gamma}_s^{(0)}$, being the first term in the expansion for $\hat{\gamma}_s$, is usually scheme independent. As we will show soon, there is a simple way to circumvent this difficulty [159].

As noticed in [153, 154] the regularization scheme dependence of $\hat{\gamma}_s^{(0)}$ in the case of $b \to s\gamma$ and $b \to sg$ is signaled in the finite parts of the one-loop matrix elements of $Q_1, \dots, Q_6$ for on-shell photons or gluons. They vanish in any four-dimensional regularization scheme and in the HV scheme, but some of them are nonzero in the NDR scheme. One has

$$\langle Q_i \rangle^{\gamma}_{\text{one-loop}} = y_i \, \langle Q_{7\gamma} \rangle_{\text{tree}}, \qquad i = 1, \dots, 6 \tag{6.276}$$

and

$$\langle Q_i \rangle^{G}_{\text{one-loop}} = z_i \, \langle Q_{8G} \rangle_{\text{tree}}, \qquad i = 1, \dots, 6. \tag{6.277}$$

Here $\langle Q_{7\gamma} \rangle_{\text{tree}}$ and $\langle Q_{8G} \rangle_{\text{tree}}$ denote the operators itself.

Downloaded from https://www.cambridge.org/core. UNIVERSIDAD AUTONOMA METROPOLITANA, on 18 Nov 2026 at 18:06:35, subject to the Cambridge Core terms of use, available at https://www.cambridge.org/core/terms. https://doi.org/10.1017/9781139524100.011

In the HV scheme all the y_i and z_i vanish, while in the NDR scheme

$$\vec{y} = \left(0, 0, 0, 0, -\frac{1}{3}, -1\right), \qquad \vec{z} = (0, 0, 0, 0, 1, 0). \tag{6.278}$$

But we know from previous sections that generally the finite parts in one-loop diagrams combined with the coefficients of $1/\varepsilon$ terms in two-loop diagrams give a scheme independent result. Indeed, as first demonstrated in [153, 154], the regularization scheme dependence of y_is and z_is cancels the corresponding regularization scheme dependence found in the mixing of $Q_1, \ldots, Q_6$ and $Q_{7\gamma}, Q_{8G}$ in $\hat{\gamma}_s^{(0)}$. It should be stressed that the numbers y_i and z_i come from purely short-distance parts of the one-loop integrals. So no reference to the hadronic matrix elements is necessary here.

In view of all this it is convenient in the leading order to introduce the so-called effective coefficients [159] for the operators $Q_{7\gamma}$ and Q_{8G}, which are regularization scheme independent. They are given as follows:

$$C_{7\gamma}^{(0)eff}(\mu_b) = C_{7\gamma}^{(0)}(\mu_b) + \sum_{i=1}^{6} y_i C_i^{(0)}(\mu_b) \tag{6.279}$$

and

$$C_{8G}^{(0)eff}(\mu_b) = C_{8G}^{(0)}(\mu_b) + \sum_{i=1}^{6} z_i C_i^{(0)}(\mu_b). \tag{6.280}$$

One can then introduce a scheme-independent vector

$$\vec{C}^{(0)eff}(\mu_b) = \left(C_1^{(0)}(\mu_b), \ldots, C_6^{(0)}(\mu_b), C_{7\gamma}^{(0)eff}(\mu_b), C_{8G}^{(0)eff}(\mu_b)\right). \tag{6.281}$$

From the RGE for $\vec{C}^{(0)}(\mu)$ it is straightforward to derive the RGE for $\vec{C}^{(0)eff}(\mu)$. It has the form

$$\mu\frac{d}{d\mu}C_i^{(0)eff}(\mu) = \frac{\alpha_s}{4\pi}\gamma_{ji}^{(0)eff}C_j^{(0)eff}(\mu), \tag{6.282}$$

where

$$\gamma_{ji}^{(0)eff} = \begin{cases} \gamma_{j7}^{(0)} + \sum_{k=1}^{6} y_k\gamma_{jk}^{(0)} - y_j\gamma_{77}^{(0)} - z_j\gamma_{87}^{(0)} & \text{i=7, j=1,...,6} \\ \gamma_{j8}^{(0)} + \sum_{k=1}^{6} z_k\gamma_{jk}^{(0)} - z_j\gamma_{88}^{(0)} & \text{i=8, j=1,...,6} \\ \gamma_{ji}^{(0)} & \text{otherwise.} \end{cases} \tag{6.283}$$

The matrix $\hat{\gamma}^{(0)eff}$ is a scheme-independent quantity. It equals the matrix that one would directly obtain from two-loop diagrams in the HV scheme. To simplify the notation we will omit the label "eff" in the expressions for the elements of this effective one-loop anomalous dimension matrix given later and keep it only in the Wilson coefficients of the operators $Q_{7\gamma}$ and Q_{8G}.

After the clarification of this rather subtle point we can now write down the leading anomalous dimension matrix relevant for the calculation of the $B \to X_s\gamma$ rate in the LO approximation. The 6×6 submatrix of $\hat{\gamma}^{(0)}$ involving the operators $Q_1, \ldots, Q_6$ is given in (6.194). Here we only give the remaining nonvanishing entries of $\hat{\gamma}^{(0)}$ [153, 154].

Downloaded from https://www.cambridge.org/core. UNIVERSIDAD AUTONOMA METROPOLITANA, on 18 Nov 2026 at 18:06:35, subject to the Cambridge Core terms of use, available at https://www.cambridge.org/core/terms. https://doi.org/10.1017/9781139524100.011

The elements $\gamma_{i7}^{(0)}$ with $i = 1, \ldots, 6$ are

$$\gamma_{17}^{(0)} = 0, \quad \gamma_{27}^{(0)} = \frac{104}{27} C_F, \tag{6.284}$$

$$\gamma_{37}^{(0)} = -\frac{116}{27} C_F, \quad \gamma_{47}^{(0)} = \left(\frac{104}{27} u - \frac{58}{27} d\right) C_F, \tag{6.285}$$

$$\gamma_{57}^{(0)} = \frac{8}{3} C_F, \quad \gamma_{67}^{(0)} = \left(\frac{50}{27} d - \frac{112}{27} u\right) C_F, \tag{6.286}$$

where u and d denote the number of quarks with charge $+2/3$ and $-1/3$, respectively.

The elements $\gamma_{i8}^{(0)}$ with $i = 1, \ldots, 6$ are

$$\gamma_{18}^{(0)} = 3, \quad \gamma_{28}^{(0)} = \frac{11}{9} N - \frac{29}{9} \frac{1}{N}, \tag{6.287}$$

$$\gamma_{38}^{(0)} = \frac{22}{9} N - \frac{58}{9} \frac{1}{N} + 3f, \quad \gamma_{48}^{(0)} = 6 + \left(\frac{11}{9} N - \frac{29}{9} \frac{1}{N}\right) f, \tag{6.288}$$

$$\gamma_{58}^{(0)} = -2N + \frac{4}{N} - 3f, \quad \gamma_{68}^{(0)} = -4 - \left(\frac{16}{9} N - \frac{25}{9} \frac{1}{N}\right) f. \tag{6.289}$$

Finally, the 2×2 one-loop anomalous dimension matrix in the sector $Q_{7\gamma}, Q_{8G}$ is given by [174]

$$\gamma_{77}^{(0)} = 8C_F, \qquad \gamma_{78}^{(0)} = 0, \tag{6.290}$$

$$\gamma_{87}^{(0)} = -\frac{8}{3} C_F \qquad \gamma_{88}^{(0)} = 16C_F - 4N.$$

Renormalization Group Evolution

The coefficients $C_i(\mu_b)$ in (6.273) can be calculated by using

$$\vec{C}(\mu_b) = \hat{U}_5(\mu_b, \mu_W) \vec{C}(\mu_W). \tag{6.291}$$

Here $\hat{U}_5(\mu_b, \mu_W)$ is the 8×8 evolution matrix, which is given in general terms in (5.113) with $\hat{\gamma}$ being this time an 8×8 anomalous dimension matrix. In the leading order $\hat{U}_5(\mu_b, \mu_W)$ is to be replaced by $\hat{U}_5^{(0)}(\mu_b, \mu_W)$ and the initial conditions by $\vec{C}^{(0)}(\mu_W)$ with [174]

$$C_2^{(0)}(\mu_W) = 1, \qquad C_{7\gamma}^{(0)}(\mu_W) = -\frac{1}{2} D_0'(x_t), \qquad C_{8G}^{(0)}(\mu_W) = -\frac{1}{2} E_0'(x_t). \tag{6.292}$$

In LO all remaining coefficients are set to zero at $\mu = \mu_W$. The two master functions $D_0'(x_t)$ and $E_0'(x_t)$ are given in (6.15) and (6.16): $D_0'(x_t) \approx 0.37$ and $E_0'(x_t) \approx 0.19$.

Using the techniques developed in Section 6.4, the leading order results for the Wilson coefficients of all operators entering the effective Hamiltonian in (6.273) can be written in

Downloaded from https://www.cambridge.org/core. UNIVERSIDAD AUTONOMA METROPOLITANA, on 18 Nov 2026 at 18:06:35, subject to the Cambridge Core terms of use, available at https://www.cambridge.org/core/terms. https://doi.org/10.1017/9781139524100.011

Table 6.1 Magic numbers.

i	1	2	3	4	5	6	7	8
a_i	$\frac{14}{23}$	$\frac{16}{23}$	$\frac{6}{23}$	$-\frac{12}{23}$	0.4086	−0.4230	−0.8994	0.1456
h_i	2.2996	−1.0880	$-\frac{3}{7}$	$-\frac{1}{14}$	−0.6494	−0.0380	−0.0185	−0.0057
$\bar{h}_i$	0.8623	0	0	0	−0.9135	0.0873	−0.0571	0.0209

an analytic form. They are [159]

$$C_j^{(0)}(\mu_b) = \sum_{i=1}^{8} k_{ji}\eta^{a_i}, \qquad (j = 1, \ldots, 6) \tag{6.293}$$

$$C_{7\gamma}^{(0)eff}(\mu_b) = \eta^{\frac{16}{23}} C_{7\gamma}^{(0)}(\mu_W) + \frac{8}{3}\left(\eta^{\frac{14}{23}} - \eta^{\frac{16}{23}}\right) C_{8G}^{(0)}(\mu_W) + C_2^{(0)}(\mu_W) \sum_{i=1}^{8} h_i \eta^{a_i}, \tag{6.294}$$

$$C_{8G}^{(0)eff}(\mu_b) = \eta^{\frac{14}{23}} C_{8G}^{(0)}(\mu_W) + C_2^{(0)}(\mu_W) \sum_{i=1}^{8} \bar{h}_i \eta^{a_i}, \tag{6.295}$$

with

$$\eta = \frac{\alpha_s(\mu_W)}{\alpha_s(\mu_b)} \tag{6.296}$$

and $C_{7\gamma}^{(0)}(\mu_W)$ and $C_{8G}^{(0)}(\mu_W)$ given in (6.292). The numbers a_i, h_i, and $\bar{h}_i$ necessary for the calculation of $C_{7\gamma}^{(0)eff}(\mu_b)$ and $C_{8G}^{(0)eff}(\mu_b)$ are given in Table 6.1. k_{ji} have been already discussed in Section 6.4.

It is instructive to perform a quick numerical analysis of (6.294) and (6.295). We use the leading order expression

$$\alpha_s(\mu_b) = \frac{\alpha_s(M_Z)}{1 - \beta_0 \frac{\alpha_s(M_Z)}{2\pi} \ln(M_Z/\mu_b)}. \tag{6.297}$$

We find the results in Table 6.2, where we choose a significantly larger range for $\alpha_s^{(5)}(M_Z)$ than presently known to exhibit the dependence on this important parameter. The central value is close to the present one.

Three features of these results should be emphasized:

- The strong enhancement of the coefficient $C_{7\gamma}^{(0)\text{eff}}$ by short-distance QCD effects, which we illustrate by the relative numerical importance of the three terms in expression (6.294). For instance, for $m_t = 170\,\text{GeV}$, $\mu_b = 5\,\text{GeV}$, and $\alpha_s^{(5)}(M_Z) = 0.118$ one obtains

$$\begin{aligned} C_{7\gamma}^{(0)\text{eff}}(\mu_b) &= 0.695\; C_{7\gamma}^{(0)}(\mu_W) + 0.085\; C_{8G}^{(0)}(\mu_W) - 0.158\; C_2^{(0)}(\mu_W) \\ &= 0.695\;(-0.193) + 0.085\;(-0.096) - 0.158 = -0.300. \end{aligned} \tag{6.298}$$

  In the absence of QCD we would have $C_{7\gamma}^{(0)\text{eff}}(\mu_b) = C_{7\gamma}^{(0)}(\mu_W)$ (in that case one has $\eta = 1$). Therefore, the dominant term in the preceding expression (the one proportional

Downloaded from https://www.cambridge.org/core. UNIVERSIDAD AUTONOMA METROPOLITANA, on 18 Nov 2026 at 18:06:35, subject to the Cambridge Core terms of use, available at https://www.cambridge.org/core/terms. https://doi.org/10.1017/9781139524100.011

Table 6.2 Wilson coefficients $C_{7\gamma}^{(0)\text{eff}}$ and $C_{8G}^{(0)\text{eff}}$ for $m_t = 163\text{GeV}$ and various values of $\alpha_s^{(5)}(M_Z)$ and μ.

	$\alpha_s^{(5)}(M_Z) = 0.113$		$\alpha_s^{(5)}(M_Z) = 0.118$		$\alpha_s^{(5)}(M_Z) = 0.123$	
μ[GeV]	$C_{7\gamma}^{(0)\text{eff}}$	$C_{8G}^{(0)\text{eff}}$	$C_{7\gamma}^{(0)\text{eff}}$	$C_{8G}^{(0)\text{eff}}$	$C_{7\gamma}^{(0)\text{eff}}$	$C_{8G}^{(0)\text{eff}}$
2.5	−0.328	−0.155	−0.336	−0.158	−0.344	−0.161
5.0	−0.295	−0.142	−0.300	−0.144	−0.306	−0.146
7.5	−0.277	−0.134	−0.282	−0.136	−0.286	−0.138
10.0	−0.265	−0.130	−0.269	−0.131	−0.273	−0.133

to $C_2^{(0)}(\mu_W)$) is the additive QCD correction that causes the enormous QCD enhancement of the $B \to X_s\gamma$ rate [151, 152]. It originates solely from the two-loop diagrams. On the other hand, the multiplicative QCD correction (the factor 0.695) tends to suppress the rate, but fails in the competition with the additive contributions.

In the case of $C_{8G}^{(0)\text{eff}}$ a similar enhancement is observed

$$\begin{aligned} C_{8G}^{(0)\text{eff}}(\mu_b) &= 0.727\, C_{8G}^{(0)}(\mu_W) - 0.074\, C_2^{(0)}(\mu_W) \\ &= 0.727\, (-0.096) - 0.074 = -0.144. \end{aligned} \tag{6.299}$$

- A strong μ_b-dependence of both coefficients as first stressed by Ali and Greub [158] and confirmed in [159]. Because $B \to X_s\gamma$ is dominated by QCD effects, it is not surprising that this scale uncertainty in the leading order is particularly large. We will investigate this scale uncertainty in a moment.
- Relatively small uncertainty in the values of the coefficients from the one in $\alpha_s(M_Z)$, even for the range shown, which is practically negligible in 2020.

Scale Uncertainties at LO

To illustrate the scale uncertainty at LO in $\mathcal{B}(B \to X_s\gamma)$ we just use the spectator model in which the inclusive decay $B \to X_s\gamma$ is approximated by the partonic decay $b \to s\gamma$. In fact, this is the leading term in the heavy quark expansion, an expansion in $1/m_\text{b}$, discussed briefly in Chapter 7 with the first corrections appearing at $O(1/m_\text{b}^2)$.

We have then the following approximate equality:

$$\frac{\Gamma(B \to X_s\gamma)}{\Gamma(B \to X_c e\bar{\nu}_e)} \simeq \frac{\Gamma(b \to s\gamma)}{\Gamma(b \to ce\bar{\nu}_e)} \equiv R_\text{quark}, \tag{6.300}$$

where the quantities on the r.h.s. are calculated in the spectator model corrected for short-distance QCD effects. The normalization to the semileptonic rate is usually introduced to reduce the uncertainties due to the CKM matrix elements and factors of m_b^5 in the r.h.s. of (6.300).

The leading logarithmic calculations can be summarized in a compact form as follows:

$$R_\text{quark} = \frac{\mathcal{B}(B \to X_s\gamma)}{\mathcal{B}(B \to X_c e\bar{\nu}_e)} = \frac{|V_{ts}^* V_{tb}|^2}{|V_{cb}|^2} \frac{6\alpha}{\pi f(z)} |C_7^{(0)\text{eff}}(\mu_b)|^2, \tag{6.301}$$

Downloaded from https://www.cambridge.org/core. UNIVERSIDAD AUTONOMA METROPOLITANA, on 18 Nov 2026 at 18:06:35, subject to the Cambridge Core terms of use, available at https://www.cambridge.org/core/terms. https://doi.org/10.1017/9781139524100.011

where

$$f(z) = 1 - 8z + 8z^3 - z^4 - 12z^2 \ln z \quad \text{with} \quad z = \frac{m_{c,pole}^2}{m_{b,pole}^2}, \tag{6.302}$$

is the phase space factor in $\mathcal{B}(B \to X_c e \bar{\nu}_e)$ and $\alpha = e^2/4\pi$. To find (6.301) only the tree-level matrix element $< s\gamma|Q_{7\gamma}|B >$ has to be computed. We leave the derivation of (6.301) to motivated readers.

There are three scale uncertainties present in (6.301):

- The low-energy scale $\mu_b = O(m_b)$ at which the Wilson Coefficient $C_7^{(0)\text{eff}}(\mu_b)$ is evaluated.
- The high-energy scale $\mu_W = O(M_\text{W})$ at which the full theory is matched with the effective five-quark theory. In LO this scale enters only η in (6.296). $C_7^{(0)}(\mu_W)$ and $C_8^{(0)}(\mu_W)$ serve in LO as initial conditions to the renormalization group evolution from μ_W down to μ_b. As seen in (6.292), they do not depend on μ_W.
- The scale $\mu_t = O(m_t)$ at which the running top-quark mass is defined. In LO it enters only through $x_t(\mu_t)$. As we stressed in connection with $B^0 - \bar{B}^0$ mixing in Section 6.3, μ_W and μ_t do not have to be equal. Initially when the top quark and the W-boson are integrated out, it is convenient in the process of matching to keep $\mu_t = \mu_W$. Yet one has always the freedom to redefine the top-quark mass and to work with $m_t(\mu_t)$ where $\mu_t \neq \mu_W$.

It is evident from the preceding formulas that in LO the variations of μ_b, μ_W, and μ_t remain uncompensated, which results in potential theoretical uncertainties in the predicted branching ratio. We have seen this feature already in the case of $\Delta F = 2$ transitions. But here this problem is really serious, as far as μ_b uncertainty is concerned, because the renormalization group effects are larger. This is related to the fact that the elements of the anomalous dimension matrix entering $B \to X_s\gamma$ are significantly larger than in the case of $\Delta F = 2$ transitions.

It is customary to estimate the uncertainties due to μ_b by varying it in the range $m_\text{b}/2 \leq \mu_b \leq 2m_\text{b}$. Similarly one can vary μ_W and μ_t in the ranges $M_\text{W}/2 \leq \mu_W \leq 2M_\text{W}$ and $m_\text{t}/2 \leq \mu_t \leq 2m_\text{t}$, respectively. Specifically in our numerical analysis we will consider the ranges

$$2.5 \text{ GeV} \leq \mu_b \leq 10 \text{ GeV} \tag{6.303}$$

and

$$40 \text{ GeV} \leq \mu_W \leq 160 \text{ GeV} \qquad 80 \text{ GeV} \leq \mu_t \leq 320 \text{ GeV}. \tag{6.304}$$

In the LO analysis we use the leading order formula for $\alpha_s(\mu_b)$ in (6.297) with $\alpha_s(M_Z) = 0.118$, set $m_t(m_\text{t}) = 163.0$ GeV, and use

$$m_t(\mu_t) = m_t(m_t)\left[\frac{\alpha_s(\mu_t)}{\alpha_s(m_\text{t})}\right]^{\frac{4}{\beta_0}}, \qquad \beta_0 = 23/3. \tag{6.305}$$

Downloaded from https://www.cambridge.org/core. UNIVERSIDAD AUTONOMA METROPOLITANA, on 18 Nov 2026 at 18:06:35, subject to the Cambridge Core terms of use, available at https://www.cambridge.org/core/terms. https://doi.org/10.1017/9781139524100.011

Varying μ_b, μ_W, and μ_t in the ranges (6.303) and (6.304), we find the following uncertainties in the branching ratio:

$$\Delta\mathcal{B}(B\to X_s\gamma)=\begin{cases}\pm 22\% & (\mu_b)\\ \pm 13\% & (\mu_W)\\ \pm 3\% & (\mu_t)\end{cases}. \tag{6.306}$$

The fact that the μ_W-uncertainty is smaller than the μ_b uncertainty is entirely due to $\alpha_s(\mu_W) < \alpha_s(\mu_b)$. Still this uncertainty is rather disturbing, as it introduces an error of approximately $\pm 0.40\cdot 10^{-4}$ in the branching ratio. The smallness of the μ_t-uncertainty is related to the weak x_t dependence of $C_7^{(0)}(\mu_W)$ and $C_8^{(0)}(\mu_W)$, which in the range of interest can be well approximated by

$$C_7^{(0)}(\mu_W)=-0.185\left(\frac{m_t(m_t)}{163\,\text{GeV}}\right)^{0.60},\qquad C_8^{(0)}(\mu_W)=-0.095\left(\frac{m_t(m_t)}{163\,\text{GeV}}\right)^{0.38}. \tag{6.307}$$

Thus this uncertainty is much smaller than in $B^0_{d,s}-\bar{B}^0_{d,s}$ mixings (±9%), already considered in Section 6.3 and also in rare decays $B_{s,d}\to\mu^+\mu^-$ (±13%) and $K_L\to\pi^0\nu\bar{\nu}$ (±10%), which we will study in next sections.

A critical analysis of theoretical and experimental uncertainties present in the prediction for $\mathcal{B}(B\to X_s\gamma)$, based on the formula (6.301), was made in [159] with the result that the error in the SM prediction in the LO approximation is dominated by the scale ambiguities. The final result of the LO analysis in [159], which omitted the μ_t and μ_W uncertainties, was

$$\mathcal{B}(B\to X_s\gamma)_{\text{LO}}=(2.8\pm 0.8)\times 10^{-4}. \tag{6.308}$$

A similar result has been found in [158]. The central value given here is out of date but what is important is the large uncertainty, roughly by a factor of four larger than in the present result in (6.271).

These findings made it clear already in 1993 that a complete NLO analysis of $B\to X_s\gamma$ was mandatory to have a useful test of the SM on the basis of this decay. Such a complete NLO calculation was outlined in [159] in general terms demonstrating formally there, that the cancellation of the dominant μ_b-dependence in the leading order can then be achieved in this manner. In 1998 this program has been realized except for the matrix elements of QCD penguin operators, calculated in 2001 [170, 171], but their contributions, as expected, turned out to be small. Let us then have a look at the NLO analysis in explicit terms. It is more complicated than for $B^0_{d,s}-\bar{B}^0_{d,s}$ mixing.

6.5.4 $B\to X_s\gamma$ beyond Leading Logarithms

Master Formulas

The formula (6.301) modifies after the inclusion of NLO corrections as follows [147]:

$$R_{\text{quark}}=\frac{|V_{ts}^*V_{tb}|^2}{|V_{cb}|^2}\frac{6\alpha}{\pi f(z)}F\left(|D|^2+A\right), \tag{6.309}$$

Downloaded from https://www.cambridge.org/core. UNIVERSIDAD AUTONOMA METROPOLITANA, on 18 Nov 2026 at 18:06:35, subject to the Cambridge Core terms of use, available at https://www.cambridge.org/core/terms. https://doi.org/10.1017/9781139524100.011

where

$$F = \frac{1}{\kappa(z)}\left(\frac{\overline{m}_b(\mu = m_b)}{m_{b,\text{pole}}}\right)^2 = \frac{1}{\kappa(z)}\left(1 - \frac{8}{3}\frac{\alpha_s(m_b)}{\pi}\right), \tag{6.310}$$

$$D = C_{7\gamma}^{(0)\text{eff}}(\mu_b) + \frac{\alpha_s(\mu_b)}{4\pi}\left\{C_{7\gamma}^{(1)\text{eff}}(\mu_b) + \sum_{i=1}^{8} C_i^{(0)\text{eff}}(\mu_b)\left[r_i + \gamma_{i7}^{(0)\text{eff}}\ln\frac{m_b}{\mu_b}\right]\right\}, \tag{6.311}$$

and A is discussed soon. Further refinements in the overall factor relevant for NNLO calculations can be found [172, 173].

Let us explain the origin of various new contributions:

- First $\kappa(z)$ is the QCD correction to the semileptonic decay [175]. To a good approximation it is given by [176]

$$\kappa(z) = 1 - \frac{2\alpha_s(\bar{\mu}_b)}{3\pi}\left[\left(\pi^2 - \frac{31}{4}\right)(1-z)^2 + \frac{3}{2}\right]. \tag{6.312}$$

  An exact analytic formula for $\kappa(z)$ can be found in [177]. Here $\bar{\mu}_b = O(m_b)$ is a scale in the calculation of QCD corrections to the semileptonic rate, which is generally different from the one used in the $b \to s\gamma$ transition. Therefore the "bar."
- The second factor in (6.310) originates as follows. The $B \to X_s\gamma$ rate is proportional to $m_{b,\text{pole}}^3$ present in the two-body phase space and to $m_b^2(\mu = m_b)$ resulting from $\langle s\gamma|Q_{7\gamma}|B\rangle^2$. On the other hand, the semileptonic rate is is proportional to $m_{b,\text{pole}}^5$ present in the three-body phase space. Thus the m_b^5 factors present in both rates differ by an $O(\alpha_s)$ correction, which has been consistently omitted in the leading logarithmic approximation but has to be included now.
- For similar reasons the variable z entering $f(z)$ and $\kappa(z)$ can be more precisely specified at the NLO level to be [147, 168, 169]:

$$z = \frac{m_{c,\text{pole}}}{m_{b,\text{pole}}} = 0.29 \pm 0.02, \tag{6.313}$$

  which is obtained from $m_{b,\text{pole}} = 4.8 \pm 0.15$ GeV and $m_{b,\text{pole}} - m_{c,\text{pole}} = 3.40$ GeV. This gives

$$\kappa(z) = 0.879 \pm 0.002 \approx 0.88, \qquad f(z) = 0.54 \pm 0.04. \tag{6.314}$$

- The amplitude D in (6.311) includes two types of new contributions. The first α_s-correction originates in the NLO correction to the Wilson coefficients of $Q_{7\gamma}$:

$$C_{7\gamma}^{\text{eff}}(\mu_b) = C_{7\gamma}^{(0)\text{eff}}(\mu_b) + \frac{\alpha_s(\mu_b)}{4\pi}C_{7\gamma}^{(1)\text{eff}}(\mu_b). \tag{6.315}$$

  It is this correction that requires the calculation of the three-loop anomalous dimensions [147]. An explicit formula for $C_{7\gamma}^{(1)\text{eff}}(\mu_b)$ has been given for the first time in the latter paper. We will give a generalization of this formula in a moment.

  The two remaining corrections in (6.311) come from one-loop matrix elements $< s\gamma|Q_{7\gamma}|B >$ and $< s\gamma|Q_{8G}|B >$ and from two-loop matrix elements $< s\gamma|Q_i|B >$ of the remaining operators. The ones with $i = 1, 2$ have been calculated in [168, 169] and

Downloaded from https://www.cambridge.org/core. UNIVERSIDAD AUTONOMA METROPOLITANA, on 18 Nov 2026 at 18:06:35, subject to the Cambridge Core terms of use, available at https://www.cambridge.org/core/terms. https://doi.org/10.1017/9781139524100.011

confirmed in [170, 171], where also the matrix elements of penguin operators ($i = 3 - 6$) have been calculated. The imporant point is that r_i being renormalization scheme dependent cancel the scheme dependence of $C_{7\gamma}^{(1)\text{eff}}(\mu_b)$. Finally, the coefficients of the logarithm are the relevant elements in the leading anomalous dimension matrix. The explicit logarithmic μ_b dependence in the last term in D will soon play an important role.

- The term A in (6.309) originates from the bremsstrahlung corrections and the necessary virtual corrections needed for the cancellation of the infrared divergences. These were calculated in [166, 167] and are also considered in [147, 168, 169] in the context of the full analysis. Because the virtual corrections are also present in the terms r_i in D, care must be taken to avoid double counting. This is discussed in detail in [147], where an explicit formula for A can be found. It is the equation (32) of that paper.

  Actually A depends on the lower cut on the photon energy

$$E_\gamma > (1-\delta)E_\gamma^{\max} \equiv (1-\delta)\frac{m_b}{2} \tag{6.316}$$

  and is divergent in the limit $\delta \to 1$. While this divergence can be in principle cancelled in the sum of $B \to X_s\gamma$ and $b \to X_s$ decay rates, it is customary to give the theoretical and experimental results making a lower cut on the photon energy. See the beginning of this section: $E_\gamma \geq 1.6\,\text{GeV}$.

- Finally the values of $\alpha_s(\mu_b)$ in all the preceding formulas are calculated with the use of the NLO expression for the strong coupling constant:

$$\alpha_s(\mu) = \frac{\alpha_s(M_Z)}{v(\mu)}\left[1 - \frac{\beta_1}{\beta_0}\frac{\alpha_s(M_Z)}{4\pi}\frac{\ln v(\mu)}{v(\mu)}\right], \tag{6.317}$$

  where

$$v(\mu) = 1 - \beta_0\frac{\alpha_s(M_Z)}{2\pi}\ln\left(\frac{M_Z}{\mu}\right), \qquad \beta_0 = \frac{23}{3}, \qquad \beta_1 = \frac{116}{3}. \tag{6.318}$$

This completes the discussion of various pieces of the NLO calculation. Certainly a rather advanced project. But as we already succeeded to make all these steps, let us write down the final result, as this is still possible at the NLO level but certainly not at NNLO.

Generalizing the formula (21) of [147] to include μ_t and μ_W dependences one finds [128]

$$\begin{aligned} C_7^{(1)eff}(\mu_b) = {} & \eta^{\frac{39}{23}} C_7^{(1)eff}(\mu_W) + \frac{8}{3}\left(\eta^{\frac{37}{23}} - \eta^{\frac{39}{23}}\right) C_8^{(1)eff}(\mu_W) \\ & + \left(\frac{297664}{14283}\eta^{\frac{16}{23}} - \frac{7164416}{357075}\eta^{\frac{14}{23}} + \frac{256868}{14283}\eta^{\frac{37}{23}} - \frac{6698884}{357075}\eta^{\frac{39}{23}}\right) C_8^{(0)}(\mu_W) \\ & + \frac{37208}{4761}\left(\eta^{\frac{39}{23}} - \eta^{\frac{16}{23}}\right) C_7^{(0)}(\mu_W) + \sum_{i=1}^{8}(e_i\eta E_0(x_t) + f_i + g_i\eta)\eta^{a_i} \\ & + \Delta C_7^{(1)eff}(\mu_b), \end{aligned} \tag{6.319}$$

Downloaded from https://www.cambridge.org/core. UNIVERSIDAD AUTONOMA METROPOLITANA, on 18 Nov 2026 at 18:06:35, subject to the Cambridge Core terms of use, available at https://www.cambridge.org/core/terms. https://doi.org/10.1017/9781139524100.011

Table 6.3 Magic numbers.

i	1	2	3	4	5	6	7	8
a_i	$\frac{14}{23}$	$\frac{16}{23}$	$\frac{6}{23}$	$-\frac{12}{23}$	0.4086	−0.4230	−0.8994	0.1456
e_i	$\frac{4661194}{816831}$	$-\frac{8516}{2217}$	0	0	−1.9043	−0.1008	0.1216	0.0183
f_i	−17.3023	8.5027	4.5508	0.7519	2.0040	0.7476	−0.5385	0.0914
g_i	14.8088	−10.8090	−0.8740	0.4218	−2.9347	0.3971	0.1600	0.0225
l_i	0.5784	− 0.3921	−0.1429	0.0476	−0.1275	0.0317	0.0078	−0.0031

where in the $\overline{\text{MS}}$ scheme

$$C_7^{(1)eff}(\mu_W) = C_7^{(1)eff}(M_W) + 8x_t \frac{\partial C_7^{(0)}(\mu_W)}{\partial x_t} \ln\left(\frac{\mu_t^2}{M_W^2}\right) + \left(\frac{16}{3}C_7^{(0)}(\mu_W) - \frac{16}{9}C_8^{(0)}(\mu_W) + \frac{\gamma_{27}^{(0)\text{eff}}}{2}\right)\ln\left(\frac{\mu_W^2}{M_W^2}\right), \tag{6.320}$$

$$C_8^{(1)eff}(\mu_W) = C_8^{(1)eff}(M_W) + 8x_t \frac{\partial C_8^{(0)}(\mu_W)}{\partial x_t} \ln\left(\frac{\mu_t^2}{M_W^2}\right) + \left(\frac{14}{3}C_8^{(0)}(\mu_W) + \frac{\gamma_{28}^{(0)\text{eff}}}{2}\right)\ln\left(\frac{\mu_W^2}{M_W^2}\right), \tag{6.321}$$

$$\Delta C_7^{(1)eff}(\mu_b) = \sum_{i=1}^{8}\left(\frac{2}{3}e_i + 6l_i\right)\eta^{a_i+1}\ln\left(\frac{\mu_W^2}{M_W^2}\right). \tag{6.322}$$

Here $C_7^{(1)eff}(M_W)$ and $C_8^{(1)eff}(M_W)$ are rather complicated functions of x_t with explicit expressions given in (12.53) and (12.54) of [29]. $E_0(x)$ is one of the master functions encountered already in previous sections.

The formulas for $C_{7,8}^{(1)eff}(M_W)$ were given earlier where first presented in [147] using the general formulas for the effective coefficient functions in (6.279) and (6.280). We have put back the superscript "eff" in (6.320) and (6.321) to emphasize that the effective anomalous dimensions should be used here.

The numbers e_i–g_i and l_i are given in Table 6.3. These numbers as well as the numerical coefficients in (6.319) can be confirmed easily by using the anomalous dimension matrices in [147] and the techniques developed in Section 6.4.

For completeness we give here some information on the relevant NLO anomalous dimension matrix $\gamma_s^{(1)}$. The 6×6 two-loop submatrix of $\gamma_s^{(1)}$ involving the operators $Q_1, \ldots, Q_6$ is given in (6.195). The two-loop generalization of (6.290) has been calculated in [163, 164]. It is given for both NDR and HV schemes as follows

$$\gamma_{77}^{(1)} = C_F\left(\frac{548}{9}N - 16C_F - \frac{56}{9}f\right),$$
$$\gamma_{78}^{(1)} = 0, \tag{6.323}$$

Downloaded from https://www.cambridge.org/core. UNIVERSIDAD AUTONOMA METROPOLITANA, on 18 Nov 2026 at 18:06:35, subject to the Cambridge Core terms of use, available at https://www.cambridge.org/core/terms. https://doi.org/10.1017/9781139524100.011

$$\gamma_{87}^{(1)} = C_F\left(-\frac{404}{27}N + \frac{32}{3}C_F + \frac{56}{27}f\right),$$
$$\gamma_{88}^{(1)} = -\frac{458}{9} - \frac{12}{N^2} + \frac{214}{9}N^2 + \frac{56}{9}\frac{f}{N} - \frac{13}{9}fN.$$

The generalization of (6.284)–(6.289) to next-to-leading order requires three-loop calculations. The result can be found in [147].

The constants r_i resulting from the calculations of NLO corrections to decay matrix elements [147, 168, 169] are collected in [147]. It should be stressed that the basis of the operators with $i = 1 - 6$ used in [147] differs from the standard basis used in [168, 169] and here. The basis used in [147] has been chosen to avoid γ_5 problems in the three-loop calculations performed in the NDR scheme. This has to be remembered when using formulas of this paper. In particular the constants r_i calculated in [168, 169] have to be transformed to the basis of [147]. We refer to the hep-ph-version of the latter paper and to [164, 178].

For the following discussion it will be useful to have [153]

$$\gamma_{27}^{(0)\text{eff}} = \frac{416}{81}, \qquad \gamma_{28}^{(0)\text{eff}} = \frac{70}{27}, \tag{6.324}$$

which enter (6.320) and (6.321), respectively. They can be obtained from (6.284) and (6.287).

Reduction of Scale Uncertainties at NLO

Let us investigate how much the uncertainties in (6.306) are reduced after including NLO corrections. We begin this discussion by demonstrating analytically that the μ_b, μ_W, and μ_t dependences present in $C_7^{(0)\text{eff}}(\mu_b)$ are indeed cancelled at $O(\alpha_s)$ by the explicit scale-dependent terms in (6.311) and (6.320). The scale-dependent terms in (6.321) do not enter this cancellation at this order in α_s in $B \to X_s\gamma$. On the other hand, they are responsible for the cancellation of the scale dependences in $C_8^{(0)\text{eff}}(\mu_b)$ relevant for the $b \to s$ gluon transition.

Expanding the three terms in (6.294) in α_s and keeping the leading logarithms, we find:

$$\eta^{\frac{16}{23}} C_7^{(0)}(\mu_W) = \left(1 + \frac{\alpha_s}{4\pi}\frac{16}{3}\ln\frac{\mu_b^2}{\mu_W^2}\right) C_7^{(0)}(\mu_W), \tag{6.325}$$

$$\frac{8}{3}\left(\eta^{\frac{14}{23}} - \eta^{\frac{16}{23}}\right) C_8^{(0)}(\mu_W) = -\frac{\alpha_s}{4\pi}\frac{16}{9}\ln\frac{\mu_b^2}{\mu_W^2} C_8^{(0)}(\mu_W), \tag{6.326}$$

$$\sum_{i=1}^{8} h_i \eta^{a_i} = \frac{\alpha_s}{4\pi}\frac{23}{3}\ln\frac{\mu_b^2}{\mu_W^2} \sum_{i=1}^{8} h_i a_i = \frac{208}{81}\frac{\alpha_s}{4\pi}\ln\frac{\mu_b^2}{\mu_W^2}, \tag{6.327}$$

respectively. In (6.327) we have used $\sum h_i = 0$. Inserting these expansions into (6.311), we observe that the μ_W dependences in (6.325), (6.326), and (6.327) are precisely cancelled by the three explicit logarithms in (6.320) involving μ_W, respectively. Similarly, one can convince oneself that the μ_t-dependence of $C_7^{(0)\text{eff}}(\mu_b)$ is cancelled at $O(\alpha_s)$ by the $\ln \mu_t^2/M_W^2$ term in (6.320). Finally and most important, the μ_b dependences in (6.325),

Downloaded from https://www.cambridge.org/core. UNIVERSIDAD AUTONOMA METROPOLITANA, on 18 Nov 2026 at 18:06:35, subject to the Cambridge Core terms of use, available at https://www.cambridge.org/core/terms. https://doi.org/10.1017/9781139524100.011

(6.326), and (6.327) are cancelled by the explicit logarithms in (6.311) that result from the calculation of the one-loop matrix elements $< s\gamma|Q_{7\gamma}|B >$ and $< s\gamma|Q_{8G}|B >$ and the two-loop matrix element $< s\gamma|Q_2|B >$ as discussed previously. Interestingly the scale-dependent term in (6.322) does not contribute to any cancellation of the μ_W dependence at this order in α_s due to the relation

$$\sum_{i=1}^{8}\left(\frac{2}{3}e_i + 6l_i\right) = 0. \tag{6.328}$$

This can be verified by using Table 6.3.

Clearly there remain small μ_b, μ_W, and μ_t dependences in (6.309), which can only be reduced by going beyond the NLO approximation. They constitute the theoretical uncertainty, which should be taken into account in estimating the error in the prediction for $\mathcal{B}(B \to X_s\gamma)$. For this reason also the term $\Delta C_7^{(1)eff}(\mu_b)$ in (6.319) has to be kept as pointed out in [179].

Using the two-loop generalization of (6.305) in (4.153) and varying μ_b, μ_W, and μ_t in the ranges (6.303) and (6.304), one finds [128] the following respective uncertainties in the branching ratio after the inclusion of NLO corrections:

$$\Delta\mathcal{B}(B \to X_s\gamma) = \begin{cases} \pm 4.3\% & (\mu_b) \\ \pm 1.1\% & (\mu_W) \\ \pm 0.4\% & (\mu_t) \end{cases}. \tag{6.329}$$

This reduction of the μ_b-uncertainty by roughly a factor of seven relative to ±22% in LO is impressive. The remaining μ_W and μ_t uncertainties are negligible.

6.5.5 Final Remarks on NLO

We hope that this rather technical part of this book has shown that already the NLO calculations of $\mathcal{B}(B \to X_s\gamma)$ are very involved. It should also be emphasized that there are other uncertainties like the parametric ones related to the elements of the CKM matrix and corrections to the relation (6.300). The latter ones can be calculated using Heavy Quark Expansion (HQE) so that at NLO one finds [147]

$$\mathcal{B}(B \to X_s\gamma) = \mathcal{B}(B \to X_c e\bar{\nu}_e) \cdot R_{\text{quark}}\left(1 - \frac{\delta_{sl}^{NP}}{m_b^2} + \frac{\delta_{rad}^{NP}}{m_b^2}\right), \tag{6.330}$$

where $\delta_{\text{sl}}^{\text{NP}}$ and $\delta_{\text{rad}}^{\text{NP}}$ parametrize nonperturbative corrections to the semileptonic and radiative B-meson decay rates, respectively.

Next, to improve the accuracy also electroweak $O(\alpha)$ corrections to R_{quark} have to be included. In this context an important point has been made by Czarnecki, and Marciano [180] already in 1998 when they made the first analysis of these corrections. It is related to the scale μ in $\alpha_{\text{em}} \equiv e^2(\mu)/4\pi$, which is rather arbitrary if corrections $O(\alpha)$ are not considered. In all calculations prior to their paper $m_{\text{b}} \le \mu \le M_{\text{W}}$ has been used, giving $1/\alpha_{\text{em}} = 130.3 \pm 2.3$. The inclusion of fermion loop contributions in the photon propagator indicates [180], however, that α renormalized at $q^2 = 0$, i.e., $\alpha = 1/137.036$ is more appropriate. This reduces the branching ratio by roughly 5%. The fermion loops in the

Downloaded from https://www.cambridge.org/core. UNIVERSIDAD AUTONOMA METROPOLITANA, on 18 Nov 2026 at 18:06:35, subject to the Cambridge Core terms of use, available at https://www.cambridge.org/core/terms. https://doi.org/10.1017/9781139524100.011

W-propagator bring a reduction of 2%. Two other reductions, each of roughly 1%, come from short-distance photonic corrections to $b \to s\gamma$ and $b \to ce\nu$. The total reduction of R_{quark} found in [180] amounted then to $(9 \pm 2)\%$. With this reduction and all the NLO corrections discussed by us these authors gave in 1998 the SM prediction

$$\mathcal{B}(B \to X_s\gamma) = (3.28 \pm 0.30) \times 10^{-4}\,, \tag{6.331}$$

not far from the present NNLO result in (6.271).

There have been other analyses at the end of the previous millennium that addressed other small effects contributing to $\mathcal{B}(B \to X_s\gamma)$. They are discussed in Section 12 in [29], and we will not review them here. These analyses made it clear that to convincingly reduce the error in the branching ratio below 10% and possibly even below 5% a complete calculation of NNLO QCD corrections and NLO electroweak corrections is necessary.

In fact, presently such corrections are known. It is out of the question that we could present the NNLO analysis at the level we have done until now. Therefore we refer to original literature, to the extensive list of references in [77], and to various reports by Mikolaj Misiak.

6.6 $b \to s\ell^+\ell^-$ and $d \to s\ell^+\ell^-$ Transitions

6.6.1 $b \to s\ell^+\ell^-$

General Remarks

The FCNC transitions $b \to s\ell^+\ell^-$ play a very important role in flavor physics. They are responsible for several important decays like $B_d \to K\ell^+\ell^-$, $B_d \to K^*\ell^+\ell^-$, $B \to X_s\mu^+\mu^-$, and $B_s \to \mu^+\mu^-$. Therefore, we will devote this section to the fundamental effective Hamiltonian governing these decays in the SM. The expressions for the branching ratios and in particular for various angular observables related to $B_d \to K^*\ell^+\ell^-$ will be presented in Section 9.1. In fact the formulas presented there are quite general and valid also beyond the SM. But here to get familiar with these decays in a simpler setting we will confine our discussion to the SM.

The starting point in any analysis of $b \to s\ell^+\ell^-$ transitions is the effective Hamiltonian at scales $\mu = O(m_b)$. It is obtained by calculating Z-penguin and photon-penguin diagrams and box diagrams that we discussed at the beginning of this chapter. Subsequently renormalization group effects have to be included to obtain the Wilson coefficients of contributing operators at $\mu = O(m_b)$.

There are different conventions for operators contributing to $b \to s\ell^+\ell^-$ transitions. The effective Hamiltonian used in this book and in many recent publications is given as follows:

$$\mathcal{H}_{\text{eff}}(b \to s\ell\bar{\ell}) = \mathcal{H}_{\text{eff}}(b \to s\gamma) - \frac{4G_{\text{F}}}{\sqrt{2}}\frac{\alpha}{4\pi}V_{ts}^*V_{tb}\left[C_9(\mu)Q_9 + C_{10}(\mu)Q_{10}\right], \tag{6.332}$$

Downloaded from https://www.cambridge.org/core. UNIVERSIDAD AUTONOMA METROPOLITANA, on 18 Nov 2026 at 18:06:35, subject to the Cambridge Core terms of use, available at https://www.cambridge.org/core/terms. https://doi.org/10.1017/9781139524100.011

where we have again neglected the term proportional to $V_{us}^* V_{ub}$ and $\mathcal{H}_{\rm eff}(b \to s\gamma)$ is given in (6.273). In addition to the operators relevant for $B \to X_s\gamma$, there are two new operators:

$$\boxed{Q_9 = (\bar{s}\gamma_\mu P_L b)(\bar{\ell}\gamma^\mu \ell), \qquad Q_{10} = (\bar{s}\gamma_\mu P_L b)(\bar{\ell}\gamma^\mu\gamma_5 \ell).} \tag{6.333}$$

In some papers the factor $\alpha/4\pi$ is included in the definition of these two operators in analogy to what is done in the case of $B \to X_s\gamma$ decay in (6.273), and this difference has to be remembered when calculating the matrix elements of operators and relevant branching ratios. Therefore it is crucial to always check which normalization is used in a given paper. We will stress it whenever for strategical reasons we will make some rescalings of normalization in Wilson coefficients in later chapters of this book. It should also be noticed that using the same notation, namely Q_9 and Q_{10}, for these semileptonic operators and nonleptonic operators in $\Delta B = 1$ transitions is not a good idea, and possibly the notation in (6.339) in the case of $K_L \to \pi^0\ell^+\ell^-$, as done originally also in the case of $b \to s\ell^+\ell^-$ in [127], would be better. But presently the literature is dominated by the notation in (6.333), and we will use it here as well with the hope that this will not confuse some readers.

While we do not show explicitly the four-quark operators in (6.332), they play an important role in the calculation of QCD and electroweak corrections as we will see soon.

The Wilson coefficients at $\mu_b = O(m_b)$ are given as follows

$$\sin^2\vartheta_W C_9(\mu_b) = \sin^2\vartheta_W P_0^{\rm NDR} + [\eta_{\rm eff} Y_0(x_t) - 4\sin^2\vartheta_W Z_0(x_t)], \tag{6.334}$$

$$\sin^2\vartheta_W C_{10}(\mu_b) = -\eta_{\rm eff} Y_0(x_t) \tag{6.335}$$

with functions $Y_0(x_t)$ and $Z_0(x_t)$ calculated already in Section 6.2. The entries $P_0^{\rm NDR}$ and $\eta_{\rm eff}$ are QCD and electroweak corrections, which we will now discuss in some detail.

QCD and Electroweak Corrections

Wilson Coefficient C_{10}

We begin the discussion with C_{10}, which is simpler because the operator Q_{10} does not renormalize under QCD so that C_{10} has no μ dependence related to the RG evolution to the low scales.[2] But it does not mean that the calculations are simple if one wants to achieve sufficient precision. Indeed, QCD corrections to the relevant penguin and box diagrams have to be included and also electroweak corrections. We will collect all these effects in $\eta_{\rm eff}$, which equals unity without these corrections.

The NLO QCD corrections to $\eta_{\rm eff}$ were calculated a long time ago in [181, 182] with the result $\eta_{\rm eff} = 1.012$ for $m_t = m_t(m_t)$. Over several years electroweak corrections have been calculated [134, 183–185], but they were incomplete, implying dependence on the renormalization scheme used for electroweak parameters as analyzed in detail in [185, 186]. The complete NLO electroweak corrections have been calculated in [187] and QCD corrections up to NNLO in [188]. The inclusion of these higher-order corrections reduced

[2] We write $C_{10}(\mu_b)$ to stress that it can be used at the low scale.

Downloaded from https://www.cambridge.org/core. UNIVERSIDAD AUTONOMA METROPOLITANA, on 18 Nov 2026 at 18:06:35, subject to the Cambridge Core terms of use, available at https://www.cambridge.org/core/terms. https://doi.org/10.1017/9781139524100.011

significantly various scale uncertainties so that nonparametric uncertainties in C_{10} have been reduced below 1%.

The calculations performed in [187, 188] are very involved and in analogy to the QCD factors, like η_B and η_{1-3} in $\Delta F = 2$ processes, we find it useful to include all QCD and electroweak corrections into $\eta_{\rm eff}$ introduced in (6.335) that without these corrections would be equal to unity. Inspecting the analytic formulas in [189] one finds then [190]

$$\eta_{\rm eff} = 0.9882 \pm 0.0024\,. \tag{6.336}$$

One could ask the question whether there was a point in doing such complicated calculations finding at the end such a small correction. But it should be emphasized that it was crucial to perform such involved calculations as these small corrections are only valid for particular definitions of the top-quark mass and of other electroweak parameters involved. In particular one has to use in $Y_0(x_t)$ the $\overline{\rm MS}$-renormalized top-quark mass $m_t(m_t)$ with respect to QCD but on-shell one with respect to electroweak interactions. This means $m_t(m_t) = 163.5\,{\rm GeV}$ as calculated in [189]. Moreover, in using (6.336) to calculate observables like branching ratios, it is important to have the same normalization of the effective Hamiltonian as in the latter paper. There this normalization is expressed in terms of G_F and M_W only. Needless to say one can also use directly the formulas in [189].

On the other hand, if one follows the normalization of an effective Hamiltonian that uses G_F, $\alpha(M_Z)$ and $\sin^2\vartheta_W$, the consistency with [189] would require $\eta_{\rm eff} = 0.991$ with $m_t(m_t) = 163.0\,{\rm GeV}$. It should be remarked that presently only in the case of the $B_{s,d} \to \mu^+\mu^-$ decays discussed here and $K^+ \to \pi^+\nu\bar\nu$ and $K_{\rm L} \to \pi^0\nu\bar\nu$ decays discussed in the next section one has to take such a care about the definition of m_t with respect to electroweak corrections. In most cases such corrections are not known or hadronic uncertainties are too large to worry about such small corrections. But the discussion here shows that at a certain level of precision one has to take into account such small effects.

Wilson Coefficient C_9

While the QCD corrections to C_{10} did not involve any renormalization group running, the case of C_9 is more profound. In particular the structure of these corrections differs from the ones encountered in previous sections. This is related to the appearance of a large logarithm represented by $1/\alpha_s$ in P_0 given in (6.337). Consequently, the renormalization group improved perturbation theory for C_9 has the structure $O(1/\alpha_s) + O(1) + O(\alpha_s)+$ higher-order terms, whereas the corresponding series for $C_{7\gamma}(\mu)$ and C_{10} are $O(1) + O(\alpha_s)+$ higher-order terms. Therefore, to find the next-to-leading $O(1)$ term in various branching ratios the full two-loop renormalization group analysis has to be performed to find C_9, but the coefficients of the remaining operators should be taken in the leading logarithmic approximation. In particular at the NLO level one should include in these decays only the leading term $C_{7\gamma}^{(0)\rm eff}(\mu)$ in $C_{7\gamma}(\mu)$. The scheme-dependent correction $C_{7\gamma}^{(1)\rm eff}(\mu)$ should be omitted in a consistent NLO calculation as it is a part of NNLO correction.

The QCD corrections to $C_9(\mu)$ have been calculated over many years with increasing precision by several groups, and presently LO, NLO, and NNLO corrections are known. Here, as in previous sections, we can only discuss the structure of LO and NLO corrections.

Downloaded from https://www.cambridge.org/core. UNIVERSIDAD AUTONOMA METROPOLITANA, on 18 Nov 2026 at 18:06:35, subject to the Cambridge Core terms of use, available at https://www.cambridge.org/core/terms. https://doi.org/10.1017/9781139524100.011

This should already give a good idea what is going on. Very motivated readers can study the NNLO analyses listed in table 8 in [77], in particular [183, 184] and references therein.

Collecting NLO corrections into the factor $P_0^{\rm NDR}$ one finds [127] in the NDR scheme

$$P_0^{\rm NDR} = \frac{\pi}{\alpha_s(M_W)}\left(-0.1875 + \sum_{i=1}^{8} p_i \eta^{a_i+1}\right) + 1.2468 + \sum_{i=1}^{8} \eta^{a_i}[r_i^{\rm NDR} + s_i\eta]. \qquad (6.337)$$

The powers a_i are the same as in Table 6.1. The coefficients p_i, $r_i^{\rm NDR}$, and s_i can be found in Table 6.4. In the HV scheme only the coefficients r_i are changed. They are given in the last row of Table 6.4.

In Table 6.5 we show the constant P_0 in (6.337) for different μ and $\Lambda_{\overline{\rm MS}}$ in the leading order corresponding to the first term in (6.337) and for the NDR as given by (6.337). In the last row we show the results in the HV scheme. In Table 6.6 we show the corresponding values for $C_9(\mu)$. To this end we set $m_t = 170\,\text{GeV}$ and vary $\Lambda^{(5)}_{\overline{\rm MS}}$ in a larger range than presently known to better exhibit this dependence.

Table 6.4 Additional magic numbers.

i	1	2	3	4	5	6	7	8
p_i	0,	0,	$-\frac{80}{203}$,	$\frac{8}{33}$,	0.0433	0.1384	0.1648	−0.0073
$r_i^{\rm NDR}$	0	0	0.8966	−0.1960	−0.2011	0.1328	−0.0292	−0.1858
s_i	0	0	−0.2009	−0.3579	0.0490	−0.3616	−0.3554	0.0072
$r_i^{\rm HV}$	0	0	−0.1193	0.1003	−0.0473	0.2323	−0.0133	−0.1799

Table 6.5 The coefficient P_0 of C_9 for various values of $\Lambda^{(5)}_{\overline{\rm MS}}$ and μ.

	$\Lambda^{(5)}_{\overline{\rm MS}} = 160\,\text{MeV}$			$\Lambda^{(5)}_{\overline{\rm MS}} = 225\,\text{MeV}$			$\Lambda^{(5)}_{\overline{\rm MS}} = 290\,\text{MeV}$		
μ[GeV]	LO	NDR	HV	LO	NDR	HV	LO	NDR	HV
2.5	2.022	2.907	2.787	1.933	2.846	2.759	1.857	2.791	2.734
5.0	1.835	2.616	2.402	1.788	2.591	2.395	1.748	2.568	2.390
7.5	1.663	2.386	2.127	1.632	2.373	2.127	1.605	2.361	2.128
10.0	1.517	2.201	1.913	1.494	2.194	1.917	1.475	2.185	1.920

Table 6.6 Wilson coefficient C_9 for $m_t = 170\text{GeV}$ and various values of $\Lambda^{(5)}_{\overline{\rm MS}}$ and μ.

	$\Lambda^{(5)}_{\overline{\rm MS}} = 160\,\text{MeV}$			$\Lambda^{(5)}_{\overline{\rm MS}} = 225\,\text{MeV}$			$\Lambda^{(5)}_{\overline{\rm MS}} = 290\,\text{MeV}$		
μ[GeV]	LO	NDR	HV	LO	NDR	HV	LO	NDR	HV
2.5	2.022	4.472	4.352	1.933	4.410	4.323	1.857	4.355	4.298
5.0	1.835	4.182	3.968	1.788	4.156	3.961	1.748	4.134	3.955
7.5	1.663	3.954	3.694	1.632	3.940	3.694	1.605	3.928	3.695
10.0	1.517	3.769	3.481	1.494	3.761	3.485	1.475	3.754	3.487

Downloaded from https://www.cambridge.org/core. UNIVERSIDAD AUTONOMA METROPOLITANA, on 18 Nov 2026 at 18:06:35, subject to the Cambridge Core terms of use, available at https://www.cambridge.org/core/terms. https://doi.org/10.1017/9781139524100.011

Let us briefly discuss these numerical results. We observe:

- The NLO corrections to P_0 enhance this constant relatively to the LO result by roughly 45% and 35% in the NDR and HV schemes, respectively.
- The NLO corrections to C_9, which include also the m_t-dependent contributions, are large as seen in Table 6.6. The results in HV and NDR schemes are by more than a factor of two larger than the leading order result $C_9 = P_0^{\rm LO}$, which consistently should not include m_t-contributions. This demonstrates very clearly the necessity of NLO calculations, which allow a consistent inclusion of the important m_t-contributions.
- The μ dependence of C_9 is sizable: ~15% in the range of μ considered. On the other hand, its $\Lambda^{(5)}_{\overline{\rm MS}}$ dependence is weak and can be neglected with the 2020 precision for α_s. Also the m_t dependence of C_9 is weak. Finally, the difference between $C_9^{\rm NDR}$ and $C_9^{\rm HV}$ is small and amounts to roughly 5%.

The phenomenology of $b \to s\ell^+\ell^-$ transitions will be discussed in Section 9.1.

6.6.2 $d \to s\ell^+\ell^-$

The decays $K_{\rm L} \to \pi^0 e^+ e^-$, $K_{\rm L,S} \to \pi^0\mu^+\mu^-$, and $K_{L,S} \to \mu^+\mu^-$ are the counterparts of the transitions just discussed, but in the K meson system. Presently, they do not play as big role in the phenomenology as the decays governed by $b \to s\ell^+\ell^-$ transitions. There are two reasons for this

- $K_{\rm L} \to \pi^0 e^+ e^-$ and $K_{\rm L} \to \pi^0\mu^+\mu^-$ have not been observed and there are presently no plans for a dedicated experiment to measure them. $K_L \to \mu^+\mu^-$ has been measured, but only a small fraction of it can be predicted in the SM, the so-called *short-distance* part. For $K_S \to \mu^+\mu^-$ only a weak experimental result from LHCb exists.
- All four decays contain significant *long-distance* contributions so that presently precise tests of the SM and of its extensions are not possible. But as we will see in later chapters they still provide useful rough upper bounds on possible new physics contributions. $K_{\rm L} \to \pi^0\ell^+\ell^-$ and $K_S \to \mu^+\mu^-$ bound in particular new CP-violating contributions while $K_L \to \mu^+\mu^-$ the corresponding CP-conserving ones. We will see several examples in BSM chapters.

In what follows we will summarize the effective Hamiltonian for the decays in question postponing the phenomenology and the discussion of long-distance contributions to Section 9.7.

The effective Hamiltonian for $d \to s\ell^+\ell^-$ transitions, relevant for the four decays in question, is given at scales $\mu < m_c$ in the SM as follows:

$$\mathcal{H}_{\rm eff}(d \to \bar{s}\ell^+\ell^-) = 4\frac{G_{\rm F}}{\sqrt{2}}\frac{\alpha}{4\pi}V_{us}^*V_{ud}\left[\sum_{i=1}^{6,7V}\Big[z_i(\mu) + \tau y_i(\mu)\Big]Q_i + \tau y_{7A}(M_W)Q_{7A}\right], \tag{6.338}$$

Downloaded from https://www.cambridge.org/core. UNIVERSIDAD AUTONOMA METROPOLITANA, on 18 Nov 2026 at 18:06:35, subject to the Cambridge Core terms of use, available at https://www.cambridge.org/core/terms. https://doi.org/10.1017/9781139524100.011

where $Q_1, \ldots Q_6$ are the current-current and QCD penguin operators discussed previously, and the new operators Q_{7V} and Q_{7A} are given by

$$\boxed{Q_{7V} = (\bar{s}\gamma_\mu P_L d)(\bar{\ell}\gamma^\mu \ell), \qquad Q_{7A} = (\bar{s}\gamma_\mu P_L d)(\bar{\ell}\gamma^\mu \gamma_5 \ell).} \tag{6.339}$$

At this stage we should warn readers that in the literature these two operators are sometimes denoted by Q_9 and Q_{10}, respectively. Indeed as seen in (6.333), only the flavor-changing current differs from the one in $b \to s\ell\bar{\ell}$. But as the contributions of the dipole operators Q_7 and Q_8 can be neglected due to the suppression by $m_{s,d}$ in these decays, it appears to be useful to use the notation in (6.339).

As only the coefficients y_i will be of interest to us in this book, we only give the results for them. The renormalization group analysis proceeds as in $b \to s\ell^+\ell^-$ transitions, except that now the evolution has to be continued down to $\mu < m_c$. One finds including NLO corrections [131]

$$y_{7V} = P_0 + \frac{Y_0(x_t)}{\sin^2\vartheta_W} - 4Z_0(x_t) + P_E E_0(x_t), \qquad y_{7A} = -\frac{1}{\sin^2\vartheta_W} Y_0(x_t), \tag{6.340}$$

with Y_0, Z_0 and E_0 given in (6.27), (6.28), and (6.14), respectively. P_E is $O(10^{-2})$, and consequently the last term in (6.340) can be neglected. The next-to-leading QCD corrections to these coefficients enter only P_0. They have been calculated in [131] reducing certain ambiguities present in leading order analyses [191, 192]. It is not possible to show an analytic expression for P_0 as the additional renormalization group evolution from $\mu = m_b$ down to $\mu \leq m_c$ complicates the expressions. We refer to [111, 131] for further details and quote the value of P_0 in the NDR scheme for $\mu = 1.0 \pm 0.2\,\text{GeV}$ using 2019 input parameters

$$P_0 = 2.88 \pm 0.06, \tag{6.341}$$

which is sufficient for our purposes. The error includes also uncertainty in α_s.

6.7 $d \to s\nu\bar{\nu}$ and $b \to s\nu\bar{\nu}$ Transitions

6.7.1 $d \to s\nu\bar{\nu}$

We will now move to discuss the transition $d \to s\nu\bar{\nu}$ that governs the semileptonic rare decays $K^+ \to \pi^+\nu\bar{\nu}$ and $K_L \to \pi^0\nu\bar{\nu}$. $K^+ \to \pi^+\nu\bar{\nu}$ is CP conserving while $K_L \to \pi^0\nu\bar{\nu}$ is governed by CP violation. Within the SM these decays are loop-induced semileptonic FCNC processes receiving only contributions from Z^0-penguin and box diagrams and are governed by the single-function $X_0(x_t)$ given in (6.26). This function has been calculated in Section 6.2. A particular and very important virtue of $K \to \pi\nu\bar{\nu}$ decays is their clean theoretical character. This is related to the fact that the low-energy hadronic matrix elements required for the calculations of their branching ratios are just the matrix elements

Downloaded from https://www.cambridge.org/core. UNIVERSIDAD AUTONOMA METROPOLITANA, on 18 Nov 2026 at 18:06:35, subject to the Cambridge Core terms of use, available at https://www.cambridge.org/core/terms. https://doi.org/10.1017/9781139524100.011

of quark currents between hadron states, which can be extracted from the leading (nonrare) semileptonic decays.

The investigation of these low-energy rare decay processes, in conjunction with their theoretical cleanliness, allows to probe, albeit indirectly, high-energy scales of the theory, far beyond the reach of the LHC. They are also very sensitive to the values of the CKM parameters, in particular to V_{td} and $\mathrm{Im}\lambda_t = \mathrm{Im}V_{ts}^* V_{td}$ so that the latter could in principle be extracted from precise measurements of the decay rates for $K^+ \to \pi^+\nu\bar{\nu}$ and $K_\mathrm{L} \to \pi^0\nu\bar{\nu}$, respectively. Moreover, the combination of these two decays offers one of the cleanest measurements of $\sin 2\beta$ [193]. However, the very fact that these processes are based on higher-order electroweak effects implies that their branching ratios are expected to be very small and not easy to access experimentally.

As of 2020 one can look back at four decades of theoretical efforts to calculate the branching ratios for these two decays within the SM. Among early calculations are [5, 132] in which QCD corrections were not considered. The first LO QCD corrections have been calculated in [194, 195] and the NLO ones in the 1990s [181, 182, 196, 197]. Already the NLO calculations reduced significantly various renormalization scale uncertainties present at LO. Yet, in the last twenty years further progress has been made through the following calculations:

- NNLO QCD corrections to the charm contributions: [198–200].
- Isospin breaking effects and nonperturbative effects: [201, 202].
- Complete NLO electroweak corrections to the charm-quark contribution to $K^+ \to \pi^+\nu\bar{\nu}$: [203].
- Complete NLO electroweak corrections to the top-quark contribution to $K^+ \to \pi^+\nu\bar{\nu}$ and $K_\mathrm{L} \to \pi^0\nu\bar{\nu}$: [135].

On the experimental side the NA62 experiment at CERN is presently running and is expected to measure the $K^+ \to \pi^+\nu\bar{\nu}$ branching ratio with the precision of 10% by 2021, as described in [204], that would improve the accuracy of the previous measurement by a factor of five. The expected measurement of $K_\mathrm{L} \to \pi^0\nu\bar{\nu}$ by KOTO at J-PARC, [205, 206], should reach the SM level by 2022. Experimental reviews of these two decays can be found in [205, 207–210] and the power of these decays in testing energy scales as high as several hundreds of TeV has been demonstrated in [211]. We will return to this in Chapter 19.

But before we come to discuss all this we have to take a closer look at the effective Hamiltonians for these decays first within the SM.

The effective Hamiltonian for $K^+ \to \pi^+\nu\bar{\nu}$ can be written as

$$\mathcal{H}_{\mathrm{eff}}(K^+ \to \pi^+\nu\bar{\nu}) = \frac{G_\mathrm{F}}{\sqrt{2}} \frac{\alpha}{2\pi \sin^2 \vartheta_W} \sum_{l=e,\mu,\tau} \left(V_{cs}^* V_{cd} X_{\mathrm{NNL}}^l + V_{ts}^* V_{td} X(x_t) \right) (\bar{s}d)_{V-A} (\bar{\nu}_l \nu_l)_{V-A}. \tag{6.342}$$

The index l=e, μ, τ denotes the lepton flavor. The dependence on the charged lepton mass resulting from the box diagram is negligible for the top contribution. In the charm sector this is the case only for the electron and the muon but not for the τ-lepton. We have discussed it and even calculated it in Section 6.2.2.

Downloaded from https://www.cambridge.org/core. UNIVERSIDAD AUTONOMA METROPOLITANA, on 18 Nov 2026 at 18:06:35, subject to the Cambridge Core terms of use, available at https://www.cambridge.org/core/terms. https://doi.org/10.1017/9781139524100.011

The function $X(x_t)$ relevant for the top part is given by

$$X(x_t) = X_0(x_t) + \frac{\alpha_s}{4\pi} X_1(x_t) = \eta_X \cdot X_0(x_t), \qquad \eta_X = 0.994 \tag{6.343}$$

with the QCD correction

$$X_1(x_t) = \tilde{X}_1(x_t) + 8x_t \frac{\partial X_0(x_t)}{\partial x_t} \ln x_\mu. \tag{6.344}$$

Here $x_\mu = \mu_t^2/M_W^2$ with $\mu_t = O(m_t)$ and $\tilde{X}_1(x_t)$ is a complicated function given in [181, 182].

The μ_t-dependence of the last term in (6.344) cancels to the considered order the μ_t-dependence of the leading term $X_0(x_t(\mu_t))$. The leftover μ_t-dependence in $X(x_t)$ is below 1%. The factor η_X summarizes the NLO corrections represented by the second term in (6.343). With $m_t \equiv m_t(m_t)$ the QCD factor η_X is practically independent of m_t and α_s and is very close to unity. Moreover, complete NLO electroweak corrections to this function have been calculated in [135]. They reduced significantly the dependence on the definition of electroweak parameters, in particular $\sin^2 \vartheta_W$.

Including all these corrections the present best value is given by [212]

$$\boxed{X(x_t) = 1.481 \pm 0.005_{\text{th}} + 0.008_{\text{exp}} = 1.481 \pm 0.009.} \tag{6.345}$$

The contribution corresponding to $X(x_t)$ in the charm sector is represented by the functions X^l_{NNL} that are known, including QCD NLO [181, 197] and NNLO corrections [198, 199]. They also include complete two-loop electroweak contributions [203].

The expressions for X^l_{NNL} are very complicated. For our purposes it will be sufficient to collect these results in a parameter that directly enters the branching ratio, which we will derive in Section 9.5. It is

$$P_c(X) = P_c^{\text{SD}}(X) + \delta P_{c,u}, \qquad \delta P_{c,u} = 0.04 \pm 0.02, \tag{6.346}$$

with the short-distance part given by

$$P_c^{\text{SD}}(X) = \frac{1}{\lambda^4} \left[\frac{2}{3} X^e_{\text{NNL}} + \frac{1}{3} X^\tau_{\text{NNL}} \right], \tag{6.347}$$

and the long-distance contributions $\delta P_{c,u}$ calculated in [201]. Future lattice calculations could reduce the present error in this part [213], and in fact first steps in this direction have been made in [214, 1337].

An excellent approximation for $P_c^{\text{SD}}(X)$, including QCD and electroweak corrections listed earlier, is given as a function of $\alpha_s(M_Z)$ and $m_c(m_c)$ in (50) of [203]. Using this formula for the most recent input parameters [35, 215]:

$$\lambda = 0.2252(9), \qquad m_c(m_c) = 1.279(13)\,\text{GeV}, \qquad \alpha_s(M_Z) = 0.1181(6), \tag{6.348}$$

one finds [212]

$$P_c^{\text{SD}}(X) = 0.365 \pm 0.012. \tag{6.349}$$

Downloaded from https://www.cambridge.org/core. UNIVERSIDAD AUTONOMA METROPOLITANA, on 18 Nov 2026 at 18:06:35, subject to the Cambridge Core terms of use, available at https://www.cambridge.org/core/terms. https://doi.org/10.1017/9781139524100.011

Adding the long-distance contribution in (6.346), we finally find

$$P_c(X) = 0.405 \pm 0.024, \tag{6.350}$$

where we have added the errors in quadratures. We will use this value in this book.

The effective Hamiltonian for $K_L \to \pi^0 \nu\bar{\nu}$ is given as follows:

$$\mathcal{H}_{\rm eff}(K_L \to \pi^0 \nu\bar{\nu}) = \frac{G_F}{\sqrt{2}} \frac{\alpha}{2\pi \sin^2 \vartheta_W} \sum_{l=e,\mu,\tau} V_{ts}^* V_{td} X(x_t) (\bar{s}d)_{V-A} (\bar{\nu}_l \nu_l)_{V-A} + h.c., \tag{6.351}$$

where the function $X(x_t)$, present already in $K^+ \to \pi^+ \nu\bar{\nu}$, is given in (6.345).

The branching ratios for both decays using the Hamiltonians (6.342) and (6.351) will be calculated in Section 9.5, where also the phenomenology of these decays within the SM will be presented in detail. But the most important role of these two decays is in the search for NP. We will witness it in the last part of this book.

6.7.2 $b \to s\nu\bar{\nu}$

These decays are governed in the SM by the penguin and box diagrams considered in the case of $d \to s\nu\bar{\nu}$ except that b has to be replaced by d. The calculation of these loop diagrams is not modified, and as the relevant operators have no anomalous dimensions, also QCD corrections in the effective Hamiltonian are the same. Therefore the effective Hamiltonian for $b \to s\nu\bar{\nu}$ transitions can be easily obtained from the one for $d \to s\nu\bar{\nu}$ by simply changing $b \to d$ both in operators and the CKM factors.

Now these factors are

$$V_{cs}^* V_{cb} \approx V_{ts}^* V_{tb} = 4 \cdot 10^{-2}, \tag{6.352}$$

and consequently the hierarchy of charm and top contributions is governed by the values of the loop functions. These functions to first approximation are given by $X_0(x_c)$ and $X_0(x_t)$, implying that the charm contribution is irrelevant for $b \to s\nu\bar{\nu}$ transitions.

The effective Hamiltonian in the SM is then given by

$$\mathcal{H}_{\rm eff}(b \to s\nu\bar{\nu}) = \frac{G_F}{\sqrt{2}} \frac{\alpha}{2\pi \sin^2 \vartheta_W} \sum_{l=e,\mu,\tau} V_{ts}^* V_{tb} X(x_t) (\bar{s}b)_{V-A} (\bar{\nu}_l \nu_l)_{V-A}, \tag{6.353}$$

and the decays to be studied in this case are

$$B \to K\nu\bar{\nu}, \qquad B \to K^*\nu\bar{\nu}, \qquad B \to X_s\nu\bar{\nu}. \tag{6.354}$$

As the function $X(x_t)$, including QCD corrections, is precisely the same as the one in (6.345), there are strong correlations between the latter decays and $K \to \pi\nu\bar{\nu}$ in the SM [216]. We will return to this correlation and its breakdown in the BSM part of this book.

The branching ratios of the decays in (6.354), based on the effective Hamiltonian (6.353), will be presented in Section 9.6 where phenomenological virtues of these decays will be discussed in detail.

Downloaded from https://www.cambridge.org/core. UNIVERSIDAD AUTONOMA METROPOLITANA, on 18 Nov 2026 at 18:06:35, subject to the Cambridge Core terms of use, available at https://www.cambridge.org/core/terms. https://doi.org/10.1017/9781139524100.011